Potential of unmanned aerial vehicle-based remote sensing to detect water stress and estimate yield in pecan

by

Muhammad Uthman Pandor

Submitted in partial fulfilment of the requirements for the degree
MSc (Agric) Horticulture
In the Department of Plant and Soil Sciences
Faculty of Natural and Agricultural Sciences
University of Pretoria

Supervisor: Dr NJ Taylor

April 2023

TABLE OF CONTENTS

Acknowledgements ..... **iv**

Declaration ..... **v**

Abstract ..... **vi**

List of Tables ..... **ix**

List of Figures ..... **x**

LIST OF ABBREVIATIONS AND SYMBOLS ..... **xiii**

Dissertation Outline ..... **xvi**

1 General introduction **1**

1.1 Hypotheses 4
1.2 Aims 5
1.3 Objectives 5

2 Literature Review **6**

2.1 Background 6
2.2 Leaf Spectral Response 7
2.3 Pre-processing of raw reflectance data 10
2.3.1 Removing Background Pixels 11
2.4 Data Available from Corrected Canopy Images 13
2.5 Water Stress Detection by Vegetation Indices 13
2.6 Water Stress Detection by Thermal Indices 15
2.6.1 The Non-Water-Stressed-Baseline 19
2.6.2 Artificial Reference Surfaces 24
2.6.3 Reference Temperature from Cold Pixels 25
2.6.4 The Upper Limit 25
2.6.5 Empirical Upper Limit 27
2.7 Application of the Crop Water Stress Index 28
2.8 Yield Estimation by Remote Sensing 29

3 General Materials and Methods **32**

3.1 Study Site Description 32
3.2 Remote Sensing Data Collection 34
3.3 Remote Sensing Data Processing 37
3.4 Field Water Stress Data Collection 43

4 Water stress detection by vegetation indices **44**

4.1 Introduction 44
4.2 Materials and Methods 45
4.3 Results and Discussion 45
4.4 Conclusions 53
5 Water Stress Detection by thermal remote sensing 55
5.1 Introduction 55
5.2 Materials and Methods 57
5.2.1 Finding the lower limit of the CWSI 57
5.2.2 Finding the Upper Limit of the CWSI 58
5.2.3 Testing the CWSI 60
5.3 Results and Discussion 61
5.3.1 T_c-T_a 61
5.3.2 The Non-Water-Stressed-Baseline (NWSB) 63
5.3.3 The Crop Water Stress Index 68
5.4 Conclusion 72
6 Yield Estimation 73
6.1 Introduction 73
6.2 Materials and Methods 74
6.3 Results and Discussion 75
6.3.1 Canopy size as a predictor of yield 75
6.3.2 Yield Estimation by Vegetation Indices 84
6.4 Conclusion 89
7 General conclusion 91
8 References 95

ACKNOWLEDGEMENTS

I would like to express my gratitude and thanks to my supervisor Dr N.J. Taylor for the support, encouragement, and much-needed guidance throughout my study.

I thank the Water Research Commission of South Africa and the South African Pecan Producers Association for funding this project.

I would like to thank the University of Pretoria, the Faculty of Natural and Agricultural Science and the Department of Plant and Soil Sciences for affording me the opportunity to study at the institution.

My thanks are also extended to Marnus Groenewald for allowing access to commercial pecan orchards for data collection.

I would also like to thank Ronnie, Lesego and her team, and my colleagues Robert, Ncamsile, Seluleko, Mhlonishwa and Aidan for their assistance during data collection, without which the study could not have been completed, as well as everyone who contributed towards the success of this study.

Finally, and with due importance given to their contribution, I would like to thank my parents, family and friends who supported and encouraged me throughout this study.

DECLARATION

I, Muhammad Uthman Pandor hereby declare that this dissertation is my own work, except where duly acknowledged. I also certify that there was no plagiarism committed in writing this thesis.

Muhammad Uthman Pandor

ABSTRACT

Three potential uses for UAV remote sensing in pecan were tested in this study over two seasons, the 2020/21 and 2021/22 seasons. The use of vegetation indices (VIs) to detect water stress, the use of remotely sensed canopy temperature to detect water stress, and the use of remote sensing to estimate yield were all tested. Vegetation indices were of absolute importance in the processing of raw images by allowing the separation of pecan canopy from background soil and vegetation The Simple Ratio Index (SRI) was found to be the best suited of all the VIs tested for this purpose, due to ease of calculation and the large range of values. Vegetation indices were found to have a weak relationship with water stress. The best relationship found between a VI and midday stem water potential (ψ_{midday}) during the 2020/21 season was an R^2 of 0.122 with normalised difference vegetation index (NDVI). Most other VIs tested had an R^2 an order of magnitude smaller. During the 2021/22 season, the Green NDVI (GNDVI) had the best relationship of all the VIs with ψ_{midday} (R^2 = 0.183). GNDVI also had the best relationship (R^2 = 0.248) of all the VIs tested with stomatal conductance (g_s). However, these relationships were far too weak to conclude that VIs can be used to detect or quantify water stress. It is suspected that variability in the conditions during different remote data collection flights contributed to the poor relationships between VIs and water stress, due to variability in both intercepted and reflected radiation from the canopy. When data from a single flight was tested against ψ_{midday}, to eliminate variability in conditions, the relationship did not improve (R^2 < 0.1), this suggests that VIs are inherently poor at detecting water stress.

The stress degree day (T_c-T_a) and the crop water stress index (CWSI) were the thermal indices tested to allow water stress detection using remotely sensed canopy temperature (T_c), while adjusting for the effects of air temperature (T_a) and vapour pressure deficit (VPD). A weak relationship was found between T_c and ψ_{midday} (R^2 = 0.186), adjusting for T_a using the stress degree day did not improve the relationship (R^2 = 0.16). This proved the necessity of adjusting for VPD as well, through the CWSI. The baselines of the CWSI were calculated using the non-water-stressed baseline (NWSB), reference surfaces and the warmest and coldest pixels of the orchard canopy-only thermal image. Destructive measurement of the non-transpiring baseline was attempted, but the resulting data was never used due to extreme variability observed in leaf-scale measurements. The equation of the NWSB was (T_c-T_a) = -0.8086VPD + 0.509 for the 2020/21 season, and (T_c-T_a) = -0.7312VPD – 0.3315 for the 2021/22 season. The differences in intercept are the result of the prevailing conditions during each season, with regards to factors other than T_a and VPD, and include radiation and windspeed. The combined NWSB using data from both seasons was (T_c-T_a) = -0,7549VPD + 0,0482. Water stress data was regressed against the CWSI from each season's own NWSB and the combined NWSB.

The importance of using T_c data from a full canopy only during the hours either side of midday was also shown. Data collected during the early morning and late evening, and from a porous canopy yielded a NWSB that differed greatly in both slope and intercept from one collected using the accepted methodology. these also differed greatly from any published NWSB for pecan.

All the methods of obtaining the CWSI baselines yielded a CWSI that did not correlate well with ψ_{midday} (NWSB and 6˚C constant upper limit: $R^2 = 0.157$, wet reference surface and 6˚C constant upper limit: $R^2 = 0.0026$, warmest and coolest pixels: $R^2 = 0.07$). Unexpectedly the NWSB method performed the best, while the methods that relied on the extraction of the CWSI limits from the thermal image performed exceptionally poorly. This is evidence that the fault lies not in the method, but in some aspect of the thermal data itself, or the extraction of the reference data from the thermal data. The poor performance of the NWSB method relative to examples in the literature may have been as a result of inaccurate T_c from the thermal camera used. More work will need to be done, with accurate equipment, before the CWSI can be used to quantify water stress in pecans.

Yield estimation was performed by finding the relationship between yield and canopy fractional cover, change in canopy size over the season and % change in canopy size over the season. Canopy fractional cover gave a relationship strong enough to estimate yield, but only in an “on”, or heavy bearing, year of an alternate bearing cycle, and performed better in a high yielding cultivar in the area (‘Western Schley’ $R^2 = 0.603$) than a low yielding one (‘Wichita’ $R^2 = 0.497$). Both of these relationships were observed at the beginning of March of the season when each cultivar had an “on” year. A good relationship between yield and canopy fractional cover was also observed early in the second measurement season (November) when ‘Wichita’ trees were in an “on” year ($R^2 = 0.535$), no data was available for the first half of the first measurement season. Both the absolute change in fractional canopy cover and the % change in canopy cover performed poorly ($R^2 < 0.3$) relative to fractional canopy cover on its own for both cultivars during the second season, when data was available for both the start and the end of the season, enabling the calculation of change in canopy cover.

Reasonable relationships between VIs and yield were primarily observed in the last two months of the season (March and April) during the 2021/22 season, while only data from these months was available for the 2020/21 season. The VIs that performed best were RDVI, MCARI and OSAVI. All three VIs correlated best ($0.35 < R^2 < 0.5$) with the yield of the cultivar that was “on” during each season. It is likely that these VIs are sensitive to differences in some aspect of canopy structure that is related to yield. Specific VIs seem to be best able to estimate yield for specific crop conditions at specific times of the year. Large datasets will be required to

determine the exact relationships present and the best time to use them, before VIs can be used to estimate yield in pecans.

LIST OF TABLES

Table 3.1. Wavelength bands available from the Micasense Altum Multispectral and thermal sensor with band centres and bandwidth (https://support.micasense.com/hc/en-us/articles/360010025413-Altum-Integration-Guide#h.5ow085yb2oll) 35
Table 3.2 UAV data collection flights, and available plant water stress measurements. Rows highlighted in grey indicate the days selected for data analysis 36
Table 3.3 Vegetation Indices created using the multispectral images of the UP Pecan orchard 37
Table 5.1 Methods used to calculate the CWSI 60
Table 6.1Average yield per tree (kg) of the two cultivars, ‘Wichita’ and ‘Western Schley’ in the UP pecan orchard during the two measurement seasons, and the percentage change in yield between the seasons 79
Table 6.2 Correlation coefficients (R^2) between the yield of individual trees (kg) during the 2020/2021 season and the vegetation index value of their canopies on four dates during the season for all the vegetation indices tested. The two cultivars, ‘Wichita’ and ‘Western Schley’ are shown separately. 85
Table 6.3 Correlation coefficients (R^2) between the yield of individual trees (kg) during the 2021/2022 season and the vegetation index value of their canopies on 10 dates throughout the season for all the vegetation indices tested. The two cultivars, ‘Wichita’ and ‘Western Schley’ are shown separately. 86

LIST OF FIGURES

Figure 2.1 The reflectance spectrum of a plant leaf (tobacco) over the visible and near-infrared wavelength range (Knipling, 1970)..... 8
Figure 2.2 The various energy fluxes (W m^{-2}) influencing leaf temperature, the net effect of which determines the actual leaf temperature (T_{leaf}) (Muir, 2019)..... 17
Figure 2.3 Visual illustration of the components of the energy balance equation as it applies to a leaf (Muir, 2019)..... 18
Figure 2.4 Non Water Stressed Baseline (NWSB) plot (the difference between canopy and air temperature (T_c-T_a)as a function of vapour pressure deficit) showing both the lower limit of the Crop Water Stress Index from the canopy temperature(T_c) of a well-watered crop and the upper limit calculated using the negative VPD method, as well as the effect of stomatal opening and closing and the effect of temperature on the upper limit (Idso et al., 1981)..... 20
Figure 3.1 The pecan orchard at Innovation Africa@UP, showing both high density (5 x 10 m) and industry standard (10 x 10 m) orchards 32
Figure 3.2 Classified Simple ratio index (SRI) classified orchard image used to separate pecan canopies from background soil and vegetation 38
Figure 3.3 Raster histogram of the simple ratio index (SRI) used to decide on a background-separation threshold value, showing a large background spike and normal distribution for the canopy. The threshold in this case is an SRI value of approximately 5. 38
Figure 3.4 Normalised difference vegetation index (NDVI) Image of pecan orchard showing little differentiation between shadows and the pecan canopy..... 39
Figure 3.5 Simple ratio index (SRI) image of the pecan orchard showing clear differentiation between pecan canopy and the background..... 39
Figure 3.6 Threshold raster created using threshold value of the SRI 40
Figure 3.7 Individual canopy polygons created using threshold value of simple ratio index (SRI)..... 41
Figure 3.8 Normalised difference vegetation index (NDVI) orchard image with all non-canopy pixels removed 41
Figure 3.9 Grid aligned to individual canopies, used to extract average vegetation indices (VI) and thermal canopy values 42

Figure 4.1 Relationships between vegetation indices and midday stem water potential (ψ_{midday}) collected during the 2020/2021 season. Data was collected from 20 trees on 6 days. 46
Figure 4.2 Relationships between vegetation indices and midday stem water potential (ψ_{midday}) collected during the 2021/2022 season. Data was collected from 8 trees on 12 days 47
Figure 4.3 Relationships between vegetation indices (VIs) and stomatal conductance (g_s) collected during the 2020/2021 season. Data was collected from 20 trees on 6 days 48
Figure 4.4 Relationships between vegetation indices (VIs) and midday stem water potential (ψ_{midday}) collected on 24 February 2022 51
Figure 5.1 Raster histogram of thermal pecan canopy images, showing a normal distribution, used to derive the limits of the crop water stress index (CWSI) 58
Figure 5.2The relationship between canopy temperature (T_c) and midday stem water potential (ψ_{midday}), showing the problems with using leaf temperature alone to detect water stress. Data was collected from 18 trees over 10 days during the 2021/22 season. 61
Figure 5.3 Relationship between the difference between canopy and air temperature (T_c-T_a) and midday stem water potential (ψ_{midday}), showing that correcting for T_a alone is not sufficient for detecting water stress. Data was collected from 18 trees over 10 days during the 2021/22 season. 62
Figure 5.4 Non water stressed baseline (NWSB) plotted from data collected during the 2020/21 season at the Vaalharts site. T_c-T_a is the difference between canopy and air temperature. Canopy temperature data was measured using infrared radiometers. 63
Figure 5.5 Non water stressed baseline (NWSB) plotted from data collected during the 2021/22 season at the Vaalharts site. T_c-T_a is the difference between canopy and air temperature. Canopy temperature data was measured using infrared radiometers. 64
Figure 5.6 Combined non-water stressed baseline (NWSB) from both measurement season 65
Figure 5.7 Non-water stressed baseline (NWSB) from the 2020/21 season using only data from the two hours after sunrise and two hours before sunset 66
Figure 5.8 Non water stressed baseline (NWSB) from the 2021/22 season including data from the infrared radiometer detecting the temperature of a bare branch within the canopy (indicated by open circles) 67

Figure 5.9 Relationship between the crop water stress index (CWSI) calculated using the non-water stressed baseline (NWSB) and the static Upper Limit for each season, and the midday stem water potential (ψ_{midday}) 69
Figure 5.10 Relationship between the crop water stress index (CWSI) with a lower limit found from a wet reference surface and an upper limit of 6˚C, and midday stem water potential (ψ_{midday}) 69
Figure 5.11 Relationship between the CWSI with a lower limit found from a wet reference surface and an upper limit of 6˚C on 13 April 2022, and midday stem water potential (ψ_{midday}) 70
Figure 5.12 Relationship between the crop water stress index (CWSI) calculated using the thermal image histogram for both limits, and midday stem water potential (ψ_{midday}) 71
Figure 6.1 Relationship between individual tree yield (kg tree^{-1}) at the end of the 2020/2021 season and canopy fractional cover on four dates during the 2020/2021 season. Solid dots are for 'Western Schley' trees and open circles are for 'Wichita' trees. 75
Figure 6.2 Relationship between individual tree yield (kg.tree^{-1}) at the end of the 2021/2022 season and canopy fractional cover on 10 dates during the 2021/2022 season. Solid dots are 'Western Schley' and open circles are 'Wichita' 77
Figure 6.3 Water stage showing split and senescence, and eventual nut drop, all examples are 'Wichita' during the 2020/2021 season. 78
Figure 6.4 Yield map of the UP pecan orchard from the 2020/2021 season, rows of 'Witchita' and 'Western Schley' alternate, with the first labelled row on the right-hand side (Eastern side) of the image being 'Western Schley'. Labels are in kilograms harvested from the tree, and intensity of shading corresponds to yield. 81
Figure 6.5 Individual tree yield (kg) of the two cultivars in the UP pecan orchard as a function of the change in fractional canopy cover. The open circles, dotted trendline and R^2 at the bottom of the figure represent 'Wichita', while 'Western Schley' is shown as the solid dots and trendline, with R^2 at the top of the figure. 83
Figure 6.6 Individual tree yield (kg) of the two cultivars in the UP pecan orchard as a function of the percentage change in fractional canopy cover. The open circles, dotted trendline and R^2 at the bottom of the figure represent 'Wichita', while 'Western Schley' is shown as the solid dots and trendline and R^2 at the top of the figure ... 83
Figure 6.7 The relationship between the individual tree yield (kg) and the RDVI value of the corresponding canopy of the two pecan cultivars on 4 March 2021, showing an exponential relationship between the variables. 'Western Schley' is represented as solid dots, and 'Wichita' as open circles. 88

LIST OF ABBREVIATIONS AND SYMBOLS

Symbol	Definition	Units
CWSI	Crop water stress index	
NWSB	Non water stressed baseline	
UAV	Unmanned aerial vehicle	
UAS	Unmanned aerial system	
VI	Vegetation index	
RGB	Red-green-blue	
NIR	Near infrared	
RE	Red-edge	
IR	Infrared	
SRI	Simple ratio index	
ReSRI	Red-edge simple ration index	
MSRI	Modified Simple ratio index	
NDVI	Normalised difference vegetation index	
GNDVI	Green normalised difference vegetation index	
RNDVI	Red-edge normalised difference vegetation index	
RDVI,	Renormalised difference vegetation index	
MCARI	Modified chlorophyll absorption ratio index	
MCARI1	Modified chlorophyll absorption ratio index 1	
OSAVI	Optimised soil adjusted vegetation index	
TCARI	Transformed chlorophyll absorption ration index	
CARI	Chlorophyll absorption ratio index	
SAVI	Soil adjusted vegetation index	
PRI	Photochemical reflectance index	

PRI_{Norm}	Normalised Photochemical reflectance index	
e_a	Vapour pressure	kPa
e_a^*	Saturated vapour pressure	kPa
$e_a^* - e_a$	Vapour pressure deficit	kPa
VPD	Vapour pressure deficit	kPa
r_a	Canopy aerodynamic resistance	s m^{-1}
r_c	Canopy diffusion resistance	s m^{-1}
ρ	Air density	kg m^{-3}
C_p	Specific heat of air at constant pressure,	
γ	Psychrometric constant	kPa °C^{-1}
R_n	Net radiation flux	W m^{-2}
VPG	Vapour pressure gradient	kPa ˚C^{-1}
Δ	Saturated vapour pressure gradient	kPa ˚C^{-1}
ET	Evapotranspiration	
K_c	Crop coefficient	
PAR	Photosynthetically active radiation	
fPAR	Fraction of absorbed photosynthetically active radiation	
LAI	Leaf area index	
GPS	Global positioning system	
IMU	Inertial motion unit	
GCP	Ground control point	
AI	Artificial Intelligence	
GIS	Geographic information system	
ψ_{midday}	Midday stem water potential	MPa

ψ_{leaf}	Leaf water potential	MPa
$\Psi_{predawn}$	Predawn stem water potential	MPa
Ψ_{stem}	Stem water potential	MPa
g_s	Stomatal conductance	$mol.m^{-2}.s^{-1}$
T_a	Air temperature	˚C
T_c	Canopy temperature	˚C
T_{leaf}	Leaf temperature	˚C
T_c-T_a	Difference between canopy and air temperature	˚C
$(T_c$-$T_a)_{LL}$	Lower limit of the NWSB at a particular VPD	˚C
$(T_c$-$T_a)_{UL}$	Upper limit of the NWSB at a particular VPD	˚C
T_{wet}	Wet reference temperature	˚C
T_{dry}	Dry reference temperature	˚C
T_{br}	Brightness temperature	K
T_{bg}	Background temperature	K
T_s	Actual surface temperature	
ε	Emissivity	
σ	Stefan-Blotzmann constant	$W. m^{-2}. K^{-4}$
$L_{emitted}$	Radiation flux density emitted	$W. m^{-2}$
$L_{reflected}$	Reflected longwave radiation	$W. m^{-2}$
L_{in}	Incoming longwave radiation	

DISSERTATION OUTLINE

This dissertation is organised into six chapters. Chapter 1 is a general introduction that provides context and justification for the use of UAV-based remote sensing in water management applications in South Africa. The hypotheses, aims and objectives of the study are also outlined. Chapter 2 is a review of the foundational and more current literature relating to the basics of remote sensing in general, as well as the specific methods that have proven successful at detecting and quantifying crop water stress, using both the spectral and thermal properties of the canopy. A review of the potential and methodologies used to estimate yield by remote sensing is also provided. Chapter 3 provides a description of the study sites, as well as the general data collection and processing methodologies relevant to all subsequent chapters. In chapter 4 and 5, the detailed methodology and findings of attempts to detect and quantify water stress using canopy spectral and thermal properties respectively are presented. Chapter 6 presents the methods used and findings of the attempts to estimate yield using both the spectral and physical properties of the canopy. The general conclusions drawn from all sections of the study, together with recommendations for further study are presented in Chapter 7.

1 GENERAL INTRODUCTION

Irrigation is well known as one of the greatest improvers of agricultural productivity, and the situation in South Africa is no different, with 30% of all agricultural production in the country coming off irrigated land (FAO, 2016), which is estimated to only account for between 9 and 13% of cultivated land (FAO, 2016; Van Niekerk et al., 2018). In the drier western regions of the country, irrigation not only improves productivity, but is a critical enabler of agricultural production, to the extent that more than half of all cultivated land in the arid to semi-arid Northern Cape province is irrigated (Van Niekerk et al., 2018).

Given the critical role that irrigation plays in ensuring food security in South Africa, adequate water availability is of utmost importance. The supply of water to agriculture is, however, already under significant pressure, with the situation only likely to deteriorate in the future. Agriculture is estimated to account for approximately 60 % of all water used in South Africa, with the requirements of all other users having to be met by the balance (FAO, 2016; Hedden and Cilliers, 2014). The water requirements of these other users, such as the industrial and municipal sectors, is expected to increase rapidly with population growth and urban development, resulting in the national water allocation to agriculture coming under significant threat in the future, with water being redirected to users seen as more important. Current surface water resources, the source of most irrigation water in South Africa, are fully exploited; with low rainfall years already resulting in restrictions on agricultural water withdrawal (Hedden and Cilliers, 2014). It is also unlikely that groundwater resources will ever be fully exploited (Hedden and Cilliers, 2014). These water scarcity problems are already understood to be severe without even beginning to address changing rainfall patterns.

While already an existential issue, the situation for high value, predominantly horticultural crops, is particularly acute. It has been estimated that between 80 and 90 % of high value crop production relies on irrigation (Backeberg, 2005). The effects of a reduced water allocation to these crops can be well illustrated by the crop of concern to this study, pecan nuts. Mature pecan trees have been shown to require no less than 1200 mm of water per season (Ibraimo et al., 2016; Miyamoto, 1983; Sammis et al., 2004). This far exceeds the annual rainfall in most of the important pecan growing regions in South Africa, and most certainly exceeds the average annual rainfall of the country as a whole, which is approximately 450 mm according to FAO (2016). Water application below the crop requirement for the growth stage, that is; applying less water than the water lost to evapotranspiration, has the potential to have real, and significant negative effects on both yield and quality, and therefore profitability (Garrot et

al., 1993; Sepulcre-Cantó et al., 2007). During the nut filling stage in particular, greater care has to be taken to avoid water stress, which has been shown to be very difficult to do, especially with a heavy crop load (Wells, 2015). This problem can only be made worse with poor irrigation management. This is a problem that South African growers will have to learn to manage, while still maintaining a profitable level of production. Water demand outstripping supply is a real risk in the future, especially considering that one way to ensure sufficient water for human use is to reduce water allocations to agriculture (Hedden and Cilliers, 2014). The only possible solution is for growers to manage their water applications with a greater degree of accuracy to avoid wastage and increase water use efficiency, or the mass of produce harvested per unit water used, including evaporation, transpiration, runoff and drainage.

Better irrigation management depends heavily on applying water according to the needs of the crop, considering the growth stage of the crop and atmospheric conditions. The seasonal growth cycle of pecans makes it an ideal crop to achieve water savings, by irrigating according to the growth cycle if water is limited. Pecan trees do not use water uniformly throughout the season, rather, water use follows a six-stage curve (Ibraimo et al., 2016), which can be expressed using the crop coefficient (K_c) approach. There is a very low K_c early in the season, increasing unevenly to a maximum at the nut filling stage before decreasing again (Ibraimo et al., 2016; Wang et al., 2007). Importantly, water can be withheld to some degree during parts of the season without unduly heavy consequences in terms of yield or quality (Garrot et al., 1993; Wells, 2015). To avoid grossly underirrigating, it is necessary to carefully estimate, or directly measure the onset of plant stress to prevent avoidable yield loss. This should be done even if water supply is not constrained. Irrigating based on intuition or calendar date usually results in wastage and inefficiency, which are fast becoming luxuries in a water scarce country (Annandale et al., 2011).

The decision to irrigate can be based on soil water measurements, direct plant measurements, estimates of reference evapotranspiration (ET_o) used with a K_c or estimates of plant stress obtained using remote sensing tools (Abioye et al., 2020; Annandale et al., 2011; Sadler et al., 2005). Using soil water measurements and ET_o are by far the most common methods employed by growers. However, soil water measurements do not take into account water uptake by the plant according to seasonal growth stages or transpiration as a function of atmospheric demand (Abioye et al., 2020; Wells, 2015). Using crop coefficients and ET_o has the potential to become cumulatively inaccurate over the course of the season, it also makes no reference to the actual water status of the soil or plant (Abioye et al., 2020; Annandale et al., 2011). They are, however, still widely used due to convenience, requiring only the ET_o and K_c value for the crop stage. An improvement to the use of soil water status or K_c alone is to combine them in the form of mathematical models, converted to computer programs for ease

of use (Annandale et al., 2011). However, these programs tend to be highly technical and require trained professionals to use correctly because both soil and weather parameters need to be understood and entered correctly, this is in addition to the actual collection of weather data and maintenance of the weather station equipment. The models also have to be calibrated for individual crops. Remote sensing can potentially overcome the issues with these scheduling methods by providing a real-time “image” of the water status of the crop, integrating all factors affecting the plant at a single point in time.

Irrigating based on direct plant measurements, such as stem or leaf water potential, or leaf temperature, can potentially mean irrigating based directly on the water status of the plant (Abioye et al., 2020; Annandale et al., 2011; Jackson et al., 1981; Othman et al., 2014; Sadler et al., 2005). There are, however, very significant challenges to using this approach. Water potential measurements are time consuming and require specialised equipment. In addition, the relationships between the measured water potential and actual tree water status may also become distorted during certain parts of the season or if they are not carried out correctly (Abioye et al., 2020; Annandale et al., 2011; Gonzalez-Dugo et al., 2013). Using leaf temperature as a true measure of plant stress involves a complicated process, as canopy or leaf temperature alone does not correlate directly to plant water status. Leaf temperature is affected by both air temperature and vapour pressure deficit (VPD). The crop water stress index (CWSI) has been devised to rationalise this, but it does involve a large amount of work to derive the baselines before it can be of any use (Idso, 1982; Jackson et al., 1981).

Both soil and direct plant measurements take no account of spatial variation unless an exceptionally large set of measurements are taken. This is highly impractical in a commercial setting, both in terms of actual measurement and data analysis, as well as the associated labour requirement and cost. Significant water savings can, however, be made using precision irrigation, that is; irrigating according to the variability in the field (Abioye et al., 2020; Gonzalez-Dugo et al., 2013; Sadler et al., 2005). A possible solution, brought about by advances in technology, is remote sensing. Remote sensing refers to detecting plant characteristics using spectral or thermal data derived from aerial imagery(Zarco-Tejada et al., 2012; Zhang and Kovacs, 2012). While highly complex, and requiring a skill set out of the realm of the average farmer, remote sensing has the potential to become a well-used tool for managing irrigation. It may be able to avoid the challenges that prevented the adoption of irrigation and water use models, by taking advantage of near ubiquitous access to the internet and, significantly for this study, the increasingly cheaply available unmanned aerial vehicles (UAVs) and associated sensors(Zhang and Kovacs, 2012; Zhao et al., 2017b). The availability of UAVs has brought widespread access to aerial imagery with a high temporal resolution, which was previously difficult and expensive to obtain, representing a significant barrier to

remote sensing (Berni et al., 2009a; Usha and Singh, 2013; Zhang and Kovacs, 2012). Farmers do not need to have the skills to analyse and interpret remote sensing data, due to the ability to move large datasets using cloud platforms. Trained professionals are now within easy reach of farmers(Abioye et al., 2020).

Easily available aerial orchard images also open the possibility of using these images to observe spatial variability or track changes over time in tree physical properties such as canopy size. Yield prediction using tree physical properties may also be possible (Robson et al., 2017b; Usha and Singh, 2013). These, together with water stress detection can greatly aid in orchard management.

The aim of this study was to develop a better understanding of the methods by which UAV-based remote sensing can be used to improve water management in pecan orchards, primarily by water stress detection for irrigation scheduling, and whether any of these methods can compare favourably with proven methods of making irrigation decisions. The data collected will also allow for a determination of the suitability of UAV-based remote sensing for other management purposes, such as yield estimation.

1.1 Hypotheses

1. Thermal indices, including the difference between canopy and air temperature (T_c-T_a) and the Crop Water Stress Index (CWSI), derived from weather station data and a UAV based thermal sensor, will be viable options for detecting water stress in pecan trees.
2. At least one of the Vegetation Indices derived from a UAV mounted multispectral camera images will correlate with water stress in pecans, by detecting changes in the average reflectance of the canopy caused by water stress.
3. Average tree Vegetation Index values from images taken at the end of the nut filling stage will correlate with tree yield for at least some of the Indices, likely those which incorporate the red edge wavelength, such as the chlorophyll sensitive indices, as unripe nuts are less green and will be easily distinguished from leaves at the stage.
4. The increase in canopy size, as quantified by fractional canopy cover, the area covered by the canopy relative to the allocated space, over the course of the season will be inversely correlated with yield, as a high crop load will reduce vegetative growth during the crop filling stage.

1.2 Aims

1. To determine whether a correlation exists between vegetation indices and widely used and accepted ground measurements of plant stress, which can then be used to determine stress thresholds to allow for meaningful field use of the thermal indices.
2. To determine whether a correlation exists between the thermal indices, T_c-T_a and CWSI, calculated using several accepted methods, and water stress, as determined by field measurements, and whether any of the relationships are strong enough to allow the use of the thermal indices as a measure of water stress on their own in pecan.
3. To test Vegetation Indices as predictors of yield, and to develop a processing methodology to predict yield using the selected vgetation index. The exact relationship between the VI and yield will also be quantified.
4. To develop a method of detecting changes or differences in physical tree properties such as canopy fractional interception that can be used to predict yield. If any correlation is found, the exact relationship between yield the physical property will be determined.

1.3 Objectives

1. To collect multispectral and thermal images of the Innovation Africa@UP pecan orchard at regular intervals, preferably weekly, during the second half of the 2020-2021 season and the entire 2021-2022 season.
2. To collect tree water stress data, including midday stem water potential and stomatal conductance within an hour of drone flights having taken place.
3. To process multispectral data to calculate vegetation indices, which will be used to separate canopies from the background and to correlate with water stress.
4. To collect the data required for the baselines of the thermal indices, including air and canopy temperatures of unstressed trees, and vapour pressure deficit.
5. To extract reference temperature values for the thermal indices from each flight's thermal image.
6. To test the various methods of determining the baselines of the Crop Water Stress Index, to find the method that best applies to pecans.

2 LITERATURE REVIEW

2.1 Background

Remote sensing can be defined as the process of obtaining relevant data about an area or land cover type without any physical contact with the surface or objects in question (Shanmugapriya et al., 2019; Usha and Singh, 2013). This is useful as it allows data to be gathered from large areas of land at a far lower cost and labour requirement than ground-based measurements (Atzberger, 2013). Remote sensing also allows the easy detection and quantification of spatial variability, both at field or orchard scale (Gonzalez-Dugo et al., 2013; Zhang and Kovacs, 2012) and at a landscape scale (Osborne et al., 2001). As in other sectors, agricultural remote sensing began with the use of visible light cameras and multispectral sensors carried aboard manned aircraft, which provided images with relatively good resolution. Later satellite remote sensing greatly increased in popularity due to the increasing availability of satellite imagery to the civilian market, as well as the cost and inconvenience of manned aircraft (Macdonald, 1984; Usha and Singh, 2013; Zhang and Kovacs, 2012). Satellite remote sensing has seen widespread and varied use in agriculture. One of the uses for which satellite-based imagery is particularly well suited is the determination of land cover type and crop area estimation (Atzberger, 2013; Shanmugapriya et al., 2019; Usha and Singh, 2013; Van Niekerk et al., 2018), this is due to the low spatial resolution inherent to satellite derived images, where an entire agricultural area may be able to fit into a single image, and changes at a landscape level can be tracked relatively easily (Atzberger, 2013). What satellite imagery is less well suited to is detecting differences or tracking changes within a single, relatively small agricultural unit, such as a single orchard or field. Besides the low spatial resolution, satellite imagery is only available at a fixed, relatively low temporal resolution due to the availability of an image of a specific area being dependent on the orbit of the satellite. Cloud cover can also render the image from a particular pass completely unusable (Gago et al., 2015). Despite these challenges, satellite imagery has been used with some success for agricultural monitoring and management applications. This includes attempts to estimate water use of crops, in the form of evapotranspiration (ET). These attempts, however, were not at the scale of the individual tree or for constant monitoring, but rather used satellite data to determine the input parameters of water use models, such as canopy cover and canopy temperature at a larger scale of several hectares per pixel (Courault et al., 2003; O'Connell et al., 2010). Satellite imagery has also been used to estimate yield, both in the form of biomass production (Prince, 1991) and fruit production in horticultural crops (Robson et al., 2017a; Robson et al., 2017b). While highly useful, these estimates generally rely on a single or small number of images per season, and do not take full advantage of the potential of remote

sensing as a management tool, where the possibility exists to have access to almost real-time monitoring of a crop at a whole farm scale (Gago et al., 2015).

This potential exists in the form of unmanned aerial vehicles (UAVs), commonly called drones. Early UAVs used for agricultural remote sensing were often fixed-wing aircraft that had to be adapted to the purpose at hand (Lelong et al., 2008). Filters were applied to commercially available cameras, and triggering mechanisms had to be built by the operator (Berni et al., 2009b). Lately, UAVs suitable for agricultural remote sensing have become available to the civilian market relatively cheaply (Puri et al., 2017), and their use, together with appropriate sensors, have become common, although RGB cameras with filters applied are still used due to their cost-effectiveness, especially if only a single extra band is required (Gago et al., 2015; Rasmussen et al., 2016; van der Merwe et al., 2020). Three types of sensors, or cameras, are commonly used for agricultural purposes: a standard visible light, or red-green-blue (RGB) camera, a multispectral or hyperspectral sensor, and a thermal infrared sensor. Hyperspectral refers to a sensor having more bands with a narrower bandwidth when compared to a multispectral sensor (Amigo and Santos, 2020). If an RGB and multispectral sensor are used together, they do overlap if the multispectral sensor also includes bands in the visible range, rendering the RGB camera redundant. However, a high resolution RGB camera is still useful for tasks that require the human eye to pick out objects manually (van der Merwe et al., 2020). Commonly used multispectral sensors include bands in the near-infrared (NIR) and the red-edge wavelength ranges (Zhang and Kovacs, 2012).

2.2 Leaf Spectral Response

When incident radiation reaches a leaf, one of three things may occur: the light may be either absorbed, reflected, or transmitted. The fate of photons interacting with healthy leaf tissue depends largely on wavelength (McCree, 1971). The wavelength range of interest for remote sensing purposes is between approximately 400 and 1300 nm. Visible light is between 400 and 700nm, whilst wavelengths between 750 and 1300 nm are known as the NIR range (Myneni et al., 1995). The wavelength band between the visible light and NIR, up to approximately 850 nm, is known as the red-edge. Photosynthetically active radiation (PAR), or the wavelengths of light that are absorbed by plant pigments to capture energy for photosynthesis roughly corresponds to visible light (Knipling, 1970). Within this range, there are pigment absorptance peaks, corresponding to the wavelength values at which the photosynthetic pigments are most efficient at capturing energy, these are found at 440, 620 and 670 nm.

Figure 2.1 shows these absorptance peaks, as the wavelengths at which a leaf reflects the least incoming radiation.

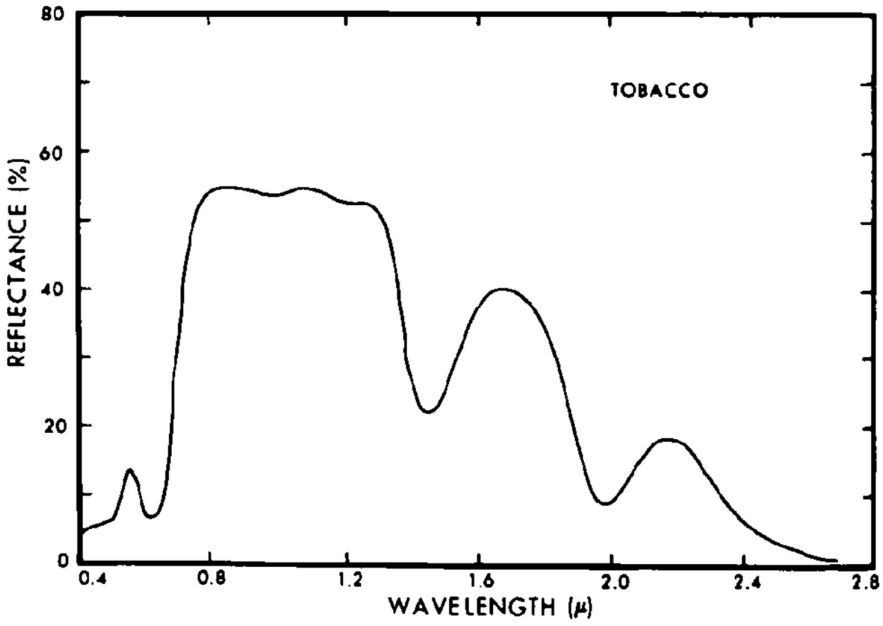

Figure 2.1 The reflectance spectrum of a plant leaf (tobacco) over the visible and near-infrared wavelength range (Knipling, 1970)

There is a noticeable decline in absorptance and, therefore, increased reflectance of light centred around 550 nm (

Figure 2.1), which is the green band. The highest absorptance, and most energy-rich wavelength band for photosynthesis is the red band, with peaks at 620 and 670 nm (Knipling, 1970; McCree, 1971). There is very little absorptance, and a high reflectance of NIR radiation by vegetation. This is both because it is of little value for photosynthesis and it is also not absorbed by water, like wavelengths below the visible and above the NIR ranges (Knipling, 1970). Between 750 and 1300 nm, that is the NIR, the amount of radiation reflected remains relatively constant, and is less dependent on plant condition, and can, therefore, be used as a reference against which to compare the absorptance of the PAR wavelengths, which does respond to changes in the physiological condition of the plant. This response is in the form of increased reflectance (Jackson and Ezra, 1985; Myneni et al., 1995). The red wavelength band, and the transition band (red-edge) between the red and NIR in particular, have been found to react rapidly to stress (Carter, 1993; Jackson and Ezra, 1985), and can, therefore, be used as an indicator of stress. However, sensors need to be able to capture relatively narrow, hyperspectral, bandwidths to accurately correlate reflectance of a single band with plant physiological status (Kim et al., 2011; Yamada and Fujimura, 1991). The reflectance spectrum of a leaf is also dependent on environmental factors, such as temperature and CO_2 concentration (McCree, 1971). The reflectance of, for example, the red band, cannot, therefore, be used alone as an absolute value to indicate stress, except under controlled conditions, where there is no external variation over time. The reflectance values of the responsive PAR wavelength bands need to be normalised for the conditions and to create a margin of error. Numerous vegetation indices (VIs) have been devised to normalise the reflectance of the PAR and red-edge bands, as well as to highlight the reflectance of specific bands that have been found to correlate with a certain plant pigment or stress condition (Xue

and Su, 2017). Vegetation Indices are also integral to the processing of aerial imagery prior to their use as stress detectors. This is primarily due to the ease with which they enable the separation of canopy or vegetation, and non-canopy pixels (Meyer and Neto, 2008; Richardson and Wiegand, 1977).

2.3 Pre-processing of raw reflectance data

Some pre-processing is required before useful information can be acquired from the raw data from UAV mounted sensors. In the early days of remote sensing, software to accomplish these tasks had to be specially written if access to institutional software was unavailable (Berni et al., 2009b). Currently, both open source and commercial remote sensing data processing software options are readily available (Du and Noguchi, 2017).

UAVs used for agricultural remote sensing are usually flown at a relatively low altitude, therefore there tends to be an exceptionally large number of images of a single field or orchard (van der Merwe et al., 2020; Zhang and Kovacs, 2012). A significant problem with this, besides the difficulty of working with hundreds of images for a small area (Turner et al., 2012), is that only a small portion at the centre of each image represents the nadir viewing angle, or the view that is truly perpendicular to the sensor. The outer edges of each image are all a view of the surface from an angle other than the perpendicular (Berni et al., 2009b). There are also several other sources of error usually present in UAV derived images, including blurring from the motion of the platform, scattered long-wave radiation entering the sensor and the effect of particles in the air (Amigo and Santos, 2020). The first steps to creating a single usable aerial image of the site are geometric correction and orthomosaicing. Geometric correction refers to the process of ensuring that all the collected images are correctly oriented and are georeferenced, meaning that the coordinates of each pixel is true to its position on the ground, and that the images are not distorted by errors caused by the pitch and yaw motion of the vehicle (Lelong et al., 2008; Turner et al., 2012; Zhang and Kovacs, 2012). Modern UAVs have in-built instrumentation to collect GPS and inertial motion unit (IMU) data that can then be imported into processing software as part of the individual image metadata (Du and Noguchi, 2017). The geometric accuracy of images can be greatly improved by using ground control points (GCPs), these are markers of known position placed onto the ground so that they appear within some of the images. They are then used as a GPS reference to increase the accuracy of the data collected by the onboard GPS unit (Berni et al., 2009b; Turner et al., 2012).

Orthomosaicing is the process of stitching the individual images captured by the sensors into a single image covering the entire flight footprint. To be successful and accurate, images with

a significant overlap are required to ensure that no distorted image portions are used and that the entire mosaiced image represents the nadir view (Turner et al., 2012; van der Merwe et al., 2020). Orthomosaicing software uses GPS and IMU data to ensure that each pixel is in the correct position and only nadir pixels are used (Turner et al., 2012). Statistical operations may also be included in orthomosaicing software to choose an appropriate pixel value for a position from all the available options (van der Merwe et al., 2020).

When using modern remote sensing image processing software packages, the final image output can often be radiometrically corrected as a standard option, subject to the required calibration data being available as part of the sensor output (Du and Noguchi, 2017; Gago et al., 2015). Radiometric correction refers to the process of calibrating against radiation inaccuracies entering the sensor. This may be in the form of long-wave scattered light (Maes and Steppe, 2012), aerosols in the air, uneven cloud cover or radiation intensity during the duration of the flight, and the effect of slope on shadows (Suomalainen et al., 2021). Required inputs for radiometric correction are an estimation of the quality of incident radiation, which is captured in real time during the flight with a sensor mounted above the sensing platform, and an image of a calibrated reference panel by the multispectral and thermal camera. In modern systems, reference panels are usually provided when acquiring sensors, and very little expertise is required to calibrate the sensors to the conditions or correct the output images (Du and Noguchi, 2017; Maes and Steppe, 2019). Manual radiometric correction requires an excellent knowledge of the physics of radiation in the applicable wavelength. The large number of dynamic variables and the complexity of the mathematical operations involved can become significant sources of error if the proper expertise is not available (Suomalainen et al., 2021).

The first useful product of the remote sensing process is a corrected image, where the pixel values accurately represent reflectance values (Maes and Steppe, 2019; Suomalainen et al., 2021), and any artefacts in the image caused by changes in incident radiation during the flight or severe unevenness in the surface have been removed (Amigo and Santos, 2020). This image of the site can be used to detect, by the human eye, areas of lower performance of the crop (Gago et al., 2015; Lelong et al., 2008). However, the potential of a multispectral or thermal image extends far beyond this basic function. To take full advantage of the image, data related to ground conditions must be retrieved from the layers representing wavelengths outside the visible range. This is achieved most easily through VIs. They remove the inconvenience of having to deal with wavelength bands individually to extrapolate information, and are designed to normalise for differences in the conditions (Atzberger, 2013).

2.3.1 Removing Background Pixels

Vegetation indices have been used since the early days of remote sensing, and continue to be used successfully, to separate canopy from non-canopy pixels (Berni et al., 2009b; Macdonald, 1984; Pinter Jr et al., 2003). This is due to the simplicity of the process involved, and the utility of the resulting output. The output may be in the form of a raster containing only plant-material pixels, or it may be converted to a vector image that separates features at a landscape or field scale. These images may be used to quantify the area covered by various features, or to extract data about the features. Uses for this process in agriculture includes calculating the area covered by a vegetation type, field or orchard, and finding the canopy cover of a crop, which may be a row or block, or even an individual tree (Pinter Jr et al., 2003). Suitable VIs for separating plant or crops of interest from the background material, which may be soil, water, built environments, dead organic matter, or even other plant types, are those which include bands for which plants and the background have drastically different reflectance properties (Kingra et al., 2016). The oldest, and arguably most well-known of these, are the Simple Ratio Index (SRI) (equation 2.1) and the Normalised Difference Vegetation Index or NDVI (equation 2.2) (Myneni et al., 1995).

$$SRI = \frac{NIR}{Red} \quad \textbf{2.1}$$

$$NDVI = \frac{(NIR-Red)}{(NIR+Red)} \quad \textbf{2.2}$$

These VIs are effective based on the principal of differing reflectance in the near-infrared and red wavelengths. Plants have a relatively low reflectance of red light and a high reflectance of NIR radiation (Knipling, 1970), whilst soil tends to reflect red light, especially with a high iron content, while absorbing NIR radiation. Plants will, therefore, tend to have a higher SRI and NDVI value than the background. A threshold value can be chosen as the basis for separating canopy pixels. While effective, this basic version of the process known as classification does have limitations. These relate to the suitability of the VI being used, and the plant type and background involved. When using the SRI, NDVI or other red and NIR based VIs, the reflectance profile of the background may become a source of frustration (Suomalainen et al., 2021). This is well illustrated by the case of a soil containing low levels of iron, such a soil would have a low reflectance of red light, and the only distinguishing factor between the crop and the background would be the NIR reflectance. Another good example would be when

attempting to separate two plant types or separate a crop from weed covered soil. In these cases, a VI which quantifies the degree of greenness may be more useful (Meyer and Neto, 2008; Richardson and Wiegand, 1977).

2.4 Data Available from Corrected Canopy Images

With the step of obtaining a raster image consisting of only the desired canopy pixels completed, information about the crop canopies becomes available. This includes the size of the canopy (Shanmugapriya et al., 2019; Trout et al., 2008) and the spectral or thermal characteristics of the canopy (Rasmussen et al., 2016). Canopy cover is useful for quantifying the vegetation cover over a landscape (Osborne et al., 2001), the progress or health of a crop through the season (Du and Noguchi, 2017; Kingra et al., 2016) and as an input in calculating crop water use (Allen et al., 1998). The spectral characteristics of the canopy, as quantified by VIs has been used, or tested to correlate with canopy density (quantified as leaf area index) (Zheng and Moskal, 2009), plant health and nutrient status (Pinter Jr et al., 2003), various forms of stress (Berni et al., 2009b; Jackson and Ezra, 1985; Zarco-Tejada et al., 2013) and yield (Anderson et al., 2021; Dobermann and Ping, 2004).

Stress or disease factors that lead to a change in the pigment composition of crop leaves have generally been found to be good candidates for detection by remote sensing (Pinter Jr et al., 2003). The nitrogen status of a crop has been found to be particularly well suited to estimation using VIs (Bausch and Duke, 1996), likely due to the major role this nutrient plays in determining chlorophyll content, and therefore the greenness of the crop (Yamada and Fujimura, 1991). Diseases or pests that affect a crop in a patchy distribution are also easily detected using VIs (Pinter Jr et al., 2003).

2.5 Water Stress Detection by Vegetation Indices

Attempts to find direct correlations between crop water status and VIs have met with mixed success, likely due to the complexity of plants' responses to water stress that may cause reflectance changes (Jackson and Ezra, 1985). These responses can include physical changes to the canopy architecture, as a result of wilting or loss of stem turgor (Jackson and Ezra, 1985), photosynthetic pigment changes (Lin et al., 2015; Lu and Zhang, 1999) and the production of stress pigments, such as xanthophylls and anthocyanins (Zarco-Tejada et al., 2013). These responses also differ greatly by species, so that a single VI cannot be universally used for all crops (Berni et al., 2009b), in many cases, significant spectral changes only occur under extreme water stress, when symptoms are clearly displayed to the naked eye (Jackson

et al., 1983). Vegetation indices that have been found to be relatively successful at detecting water stress are the Photochemical Reflectance Index (PRI) (equation 2.3), which is sensitive to leaf xanthophyll content (Berni et al., 2009b), and the Normalised Photochemical Reflectance Index (PRI_{Norm})(equation 2.4), which has been shown to perform even better at detecting water stress, through the integration of an index sensitive to plant structure, the Renormalised Difference Vegetation Index (RDVI)(equation 2.4) and the red edge band (wavelength peak 700 nm), which normalises for chlorophyll content, into the PRI (Zarco-Tejada et al., 2013). This is useful because it has been shown that chlorophyll degrades under water stressed conditions (Lin et al., 2015).

$$\boldsymbol{PRI = \frac{(R_{570} - R_{531})}{(R_{570} + R_{531})}} \quad \textbf{2.3}$$

$$PRI_{Norm} = \frac{PRI}{RDVI * \frac{Rededge}{Red}} \quad \textbf{2.4}$$

$$RDVI = \frac{(NIR - RED)}{\sqrt{(NIR + RED)}}$$

2.4

One of the major disadvantages of the PRI is the need for an expensive hyperspectral sensor, as it requires that the red band be divided into two separate bands, with peaks at 531nm and 570nm. Most commercially available sensors have a single peak in each of the major wavelength bands (R, G, B, NIR and RE) (Puri et al., 2017), which tends to be adequate for most VIs (Shanmugapriya et al., 2019). . Direct water stress detection with various other VIs has also been attempted (Gago et al., 2015), and includes the NDVI, SR, Modified SR (MSR)(equation 2.5), RDVI, the Transformed Chlorophyll Absorption in Reflectance Index (TCARI) (equation 2.6), the Optimised Soil adjusted Vegetation Index (OSAVI) (equation 2.7), TCARI/OSAVI (Baluja et al., 2012; Bian et al., 2019; Zarco-Tejada et al., 2013).Simple indices such as NDVI and SRI have also been used to differentiate between wet and dry soil (Jackson and Ezra, 1985).

$$\boldsymbol{MSR = \frac{(NIR/RED) - 1}{\sqrt{(NIR/RED) + 1}}} \quad \textbf{2.5}$$

$$TCARI = 3 * \left[(Rededge - RED) - 0.2 * (Rededge - GREEN) * \left(\frac{Rededge}{RED} \right) \right] \quad \textbf{2.6}$$

$$OSAVI = (1 + 0.16) * \frac{(NIR - RED)}{(NIR + RED + 0.16)} \quad \textbf{2.7}$$

The NDVI, MSR, TCARI AND TCARI/OSAVI have in some cases correlated well with plant water stress measurements, such as midday stem water potential and stomatal conductance (Baluja et al., 2012), while in others only weak relationships were found (Bian et al., 2019). None have been found to be effective enough to base management decisions off of, being too easily influenced by factors other than water stress (Gago et al., 2015).

2.6 Water Stress Detection by Thermal Indices

Of all the methods tested to detect crop water stress using remote sensing, methods using canopy temperature, and indices derived from canopy temperature, have been repeatedly found to be the most effective (Bian et al., 2019; Gago et al., 2015). Canopy temperature has been used to estimate the level of water stress since the earliest days of remote sensing (Jackson et al., 1981), when the only platform options were satellites or large aircraft (Macdonald, 1984). The methods have since evolved, both to increase accuracy by adjusting for weather variables, and to take advantage of increased sensor resolution and platform availability (Maes and Steppe, 2019).

As with multispectral remote sensing, some pre-processing is required before the temperature measured by the thermal sensor accurately reflects the leaf, or canopy, temperature (Maes and Steppe, 2012). When incoming radiation in the thermal wavelengths (700 – 1400nm) is intercepted by a leaf, it may be absorbed or reflected, according to Kirchhoff's Law, as follows:

$$L_{reflected} = (1 - \varepsilon) L_{in} \quad \textbf{2.8}$$

Where $L_{reflected}$ ($W.m^{-2}$) is the reflected longwave radiation, ε is the emissivity of the system, and L_{in} ($W.m^{-2}$) is the incoming longwave radiation, which can also be taken as the power 4 of the background temperature (T_{bg}^4), in Kelvin (Maes and Steppe, 2012). All systems, including tree canopies, also emit radiation as a function of the temperature of the object, according to the Stefan-Boltzmann Law:

$$L_{emitted} = \varepsilon \sigma T_S^4 \quad \textbf{2.9}$$

Where $L_{emitted}$ ($W.m^{-2}$) is the emitted longwave radiation, ε is the emissivity of the system, σ is the Stefan-Boltzmann constant ($5.67x10^{-8}$ W. m^{-2}. K^{-4}), and T_s is the actual temperature, in Kelvin. The temperature detected by a thermal sensor above the object, the tree canopy in this case, is the sum of $L_{emitted}$ and $L_{reflected}$, and not the actual T_s, this is known as the brightness temperature (T_{br}), which is in Kelvin, to the power 4. To find the actual canopy temperature (T_s), the above equations can be written as:

$$T_S = \sqrt[4]{\frac{T_{br}^4 - (1-\varepsilon)T_{bg}^4}{\varepsilon}} \quad \textbf{2.10}$$

T_{br} is the raw temperature returned by the sensor, T_{bg} can be found by measuring the incoming radiation with the same sensor used to measure the canopy temperature, by either measuring the temperature of the sky without including the sun or measuring the temperature of a creased tinfoil reference panel with the canopy. The emissivity of a dense canopy is very close to 1, and may be taken as 0.98 or 0.99 (Maes and Steppe, 2012).

Using canopy temperature to detect or quantify the level of water stress is based on the well-established principle that under water stress, transpiration is decreased due to stomatal closure, leading to an elevation of leaf temperature, over the temperature of an unstressed leaf under the same environmental conditions (Bian et al., 2019; Hsiao, 1973). While leaf or canopy temperature alone can be used to detect areas of water stress in a single location at a single point in time (Baluja et al., 2012; Cohen et al., 2005), absolute leaf temperature cannot be accurately compared over different days, or even hours apart. This is because leaf temperature is affected by a number of environmental factors that affect the energy balance of the leaf. These factors act on the leaf simultaneously and are constantly fluctuating (Jones, 1999; Testi et al., 2008).

Besides the effects of transpirational cooling, leaf temperature is directly affected by air temperature and intercepted radiation, both direct shortwave and reflected longwave radiation (Gates, 1968). Leaf temperature at different times cannot, therefore, be compared without adjusting for the effects of, especially, the air temperature (Jackson et al., 1977). The effects of the radiation fluxes in determining leaf temperature are shown in Figure *2.2* and Figure 2.3.

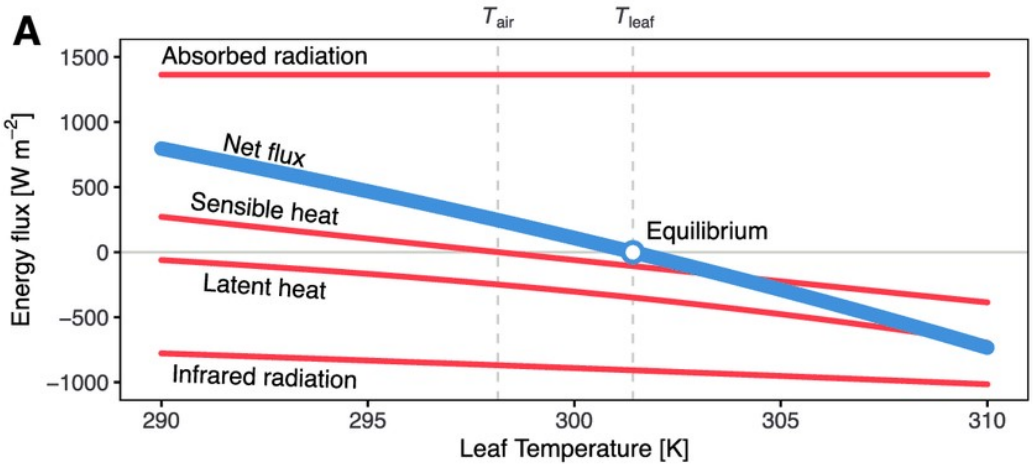

Figure 2.2 The various energy fluxes (W m^{-2}) influencing leaf temperature, the net effect of which determines the actual leaf temperature (T_{leaf}) (Muir, 2019)

When a leaf is transpiring at the potential rate, that is, when water is not limiting, the rate of transpiration is also dependent on the vapour pressure deficit (VPD) and the wind speed (Gates, 1968; Maes et al., 2011). VPD affects the rate of transpiration by determining the water vapour gradient between the saturated interior of the leaf and the air. Under high VPD, or low humidity conditions, a leaf will lose water at a greater rate than under low VPD conditions, if the temperature is the same. Wind speed affects transpiration rate by determining the boundary layer resistance of the leaf. The boundary layer is a layer of still air surrounding the surface of the leaf that acts as a barrier to the flow of gases. For the same leaf, the higher the wind speed, the thinner the boundary layer, the lower the resistance and the greater the transpirational water loss (Gates, 1968; Maes and Steppe, 2012).

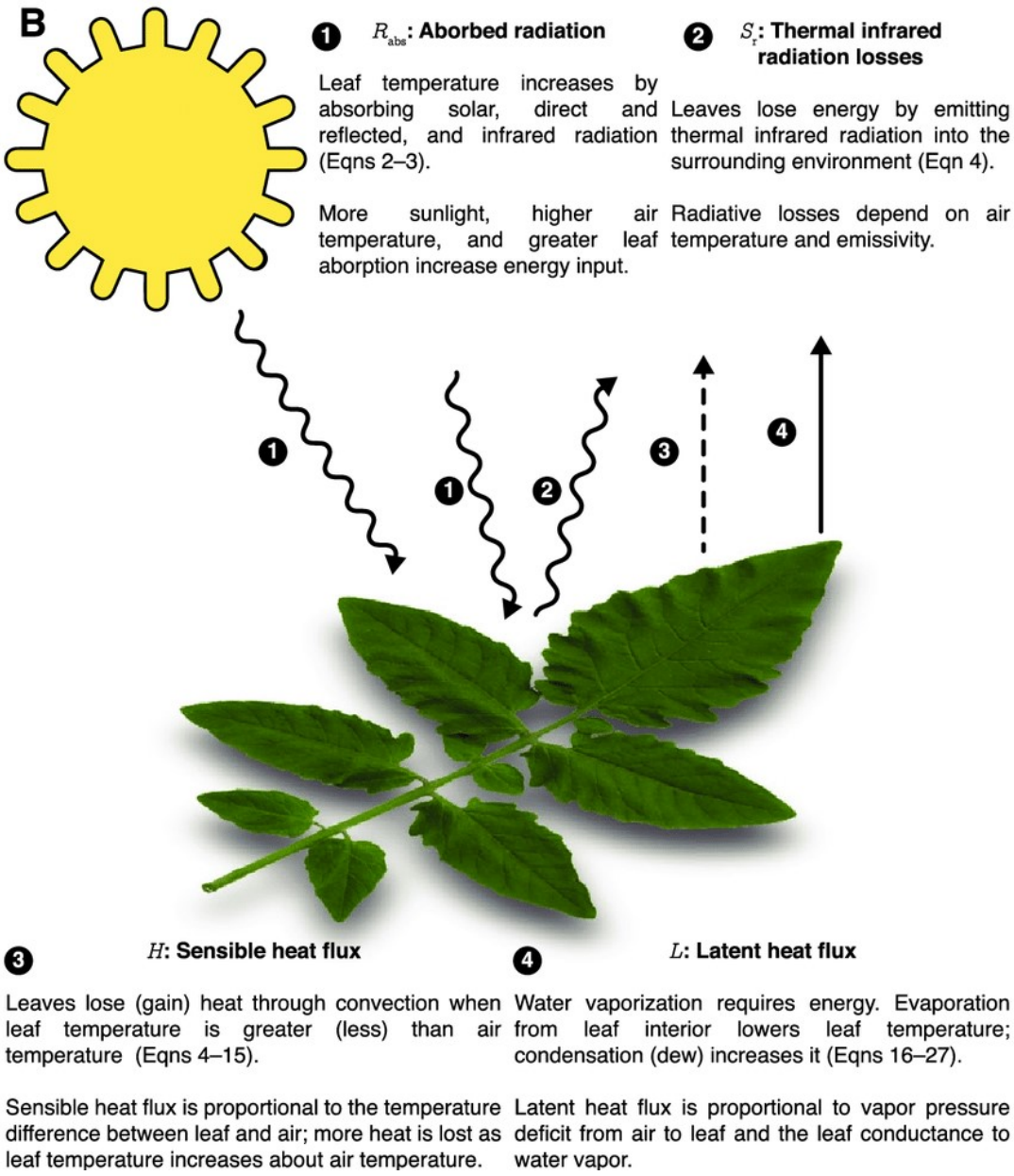

Figure 2.3 Visual illustration of the components of the energy balance equation as it applies to a leaf (Muir, 2019)

The most important of the above factors that need to be corrected for before leaf temperature can be meaningfully used as a measure of water stress are air temperature and VPD (Idso, 1982). Leaf or canopy temperature can be corrected for air temperature to allow comparison of the level of stress using a concept known as the Stress Degree Day (SDD). This is the difference between the canopy and air temperature in degrees Celsius, usually expressed as T_c-T_a. The more negative the value, that is; the lower the canopy temperature is than the air temperature, the greater the effect of transpirational cooling, therefore, the lower the level of

water stress (Jackson et al., 1977). It was, however, found that, when comparing the SDD values of completely unstressed leaves, the greater the VPD, the more negative the T_c-T_a. This means that if using the SDD alone to compare the level of water stress on different days, differences in VPD could result in large differences in Tc-Ta for the same level of stress (Idso, 1982). It is therefore necessary to correct for both air temperature and VPD. This is achieved using a crop thermal index known as the Crop Water Stress Index (CWSI), with the formula shown in equation 2.11 (Idso et al., 1981).

$$\boldsymbol{CWSI = \frac{(T_c - T_a) - (T_c - T_a)_{LL}}{(T_c - T_a)_{UL} - (T_c - T_a)_{LL}}} \qquad \textbf{2.11}$$

(T_c-T_a) is the difference between the actual canopy temperature and the air temperature at the time, $(T_c\text{-}T_a)_{LL,}$ or the “lower limit” is the difference between the canopy and air temperature of a crop transpiring at the potential rate, the temperature of such a canopy reflects the maximum cooling effect possible for the crop under the conditions. $(T_c\text{-}T_a)_{UL}$ is known as the upper limit of the CWSI. This is the T_c-T_a at which no transpiration takes place, when stomata are closed and transpirational cooling does not affect the canopy temperature at all (Idso et al., 1981). This value is invariably positive, as without any transpiration, the temperature of the canopy rises above the temperature of the air. The CWSI has been devised to easily reflect the level of stress relative to the two extremes, known as limits, while correcting for the effects of air temperature and VPD, and indirectly, the other environmental variables, depending on the method used to estimate the potential T_c-T_a, known as the lower limit of the CWSI (Idso et al., 1981).

2.6.1 The Non-Water-Stressed-Baseline

The first step in this process is determining the T_c-T_a values of a completely unstressed leaf or canopy of the crop over the complete VPD range, to be able to estimate the lower limit under any conditions. This serves as one reference point against which the Tc-Ta of the crop can be compared, while correcting for VPD and air temperature. The resulting plot is expressed as the equation known as the Non-Water-Stressed- Baseline (NWSB), where the x-axis is VPD and the y-axis is T_c-T_a (Idso et al., 1981). Using this equation, the standardised T_c-T_a of a completely unstressed crop for the VPD conditions on the day can be found. The NWSB can be expressed in the form shown in equation 2.12 (Howell et al., 1986).

$$(T_c - T_a)_{LL} = a - b\,VPD \qquad \textbf{2.12}$$

$(T_c\text{-}T_a)_{LL}$, or lower limit $T_c\text{-}T_a$, is the difference between canopy and air temperature of the crop if it were transpiring at the potential rate under the VPD currently being experienced, “a” is the intercept of the NWSB; it represents the $T_c\text{-}T_a$ of the crop when VPD is zero (saturated vapour pressure for the temperature). “b” is the slope of the NWSB, and VPD represents VPD at the time of the stress measurement, which is the determinate variable, this equation is shown graphically as the “Baseline” curve in Figure 2.4

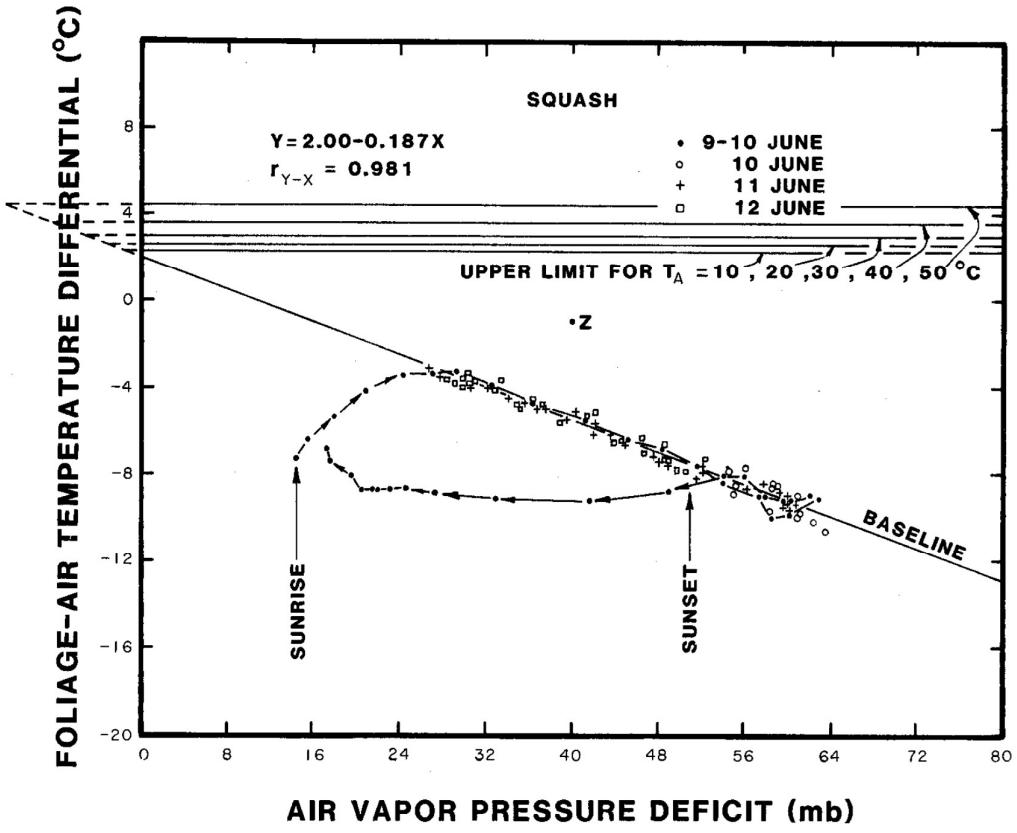

Figure 2.4 Non Water Stressed Baseline (NWSB) plot (the difference between canopy and air temperature ($T_c\text{-}T_a$)as a function of vapour pressure deficit) showing both the lower limit of the Crop Water Stress Index from the canopy temperature(T_c) of a well-watered crop and the upper limit calculated using the negative VPD method, as well as the effect of stomatal opening and closing and the effect of temperature on the upper limit (Idso et al., 1981).

It would be expected that in a saturated atmosphere, there would be no water vapour exchange between the interior of the leaf and the atmosphere, however, this is not the case; there is still a transpirational cooling effect, resulting in “a” being a negative T_c-T_a value and not zero (Idso, 1982), this is used to find the Upper Limit, as shown in Figure 2.4 .

The NWSB is crop specific, and may even be cultivar specific in some cases, as it relates to the unique stomatal control regimes of different species. Leaf size has also been proposed as an explanation, with smaller leaves being more exposed to the atmosphere, with a lower boundary layer resistance, leading to more water loss at the same VPD (Berni et al., 2009a; Idso, 1982). The effects of cultivar, however, need to be evaluated by species, as a single NWSB may be found to be suitable for all cultivars (Bellvert et al., 2016). There are several requirements, without which the NWSB cannot be found. The first is access to a completely unstressed crop for a duration of time sufficient to capture a wide range of VPD conditions, as well as the means to measure canopy or leaf temperature consistently for relatively long periods of time. The second is access to air temperature and VPD data for the duration of the measurement period. The third is the ability to collect a large number of canopy temperature measurements during the time of day when the crop is transpiring at the potential rate (Idso et al., 1981). The number of data points required for a consistent and accurate NWSB may take between a large part of a season (Howell et al., 1986) to several seasons to collect (Garrot et al., 1993). Canopy temperature data point collection times must correspond with the air temperature and VPD collection times. Care should also be taken that no data points are collected before full stomatal opening in the morning and after the onset of stomatal closure in the afternoon (Egea et al., 2017; Idso et al., 1981; Testi et al., 2008) This also ensures that no data is collected during the times of day when radiation interception is low, that is, during the times of day the heating effect of radiation flux is not at a maximum (Berni et al., 2009a). It has been found that the best time of day to collect data for a NWSB is the hours either side of midday, during this time of day the canopy is most consistently sunlit or shaded due to the sun angle, depending on the sensor view (Testi et al., 2008). Inconsistency in the time of day and sensor angle during measurement are known to be a major source of error in the NWSB (Garrot et al., 1993).

The theoretical basis of the T_c -T_a and therefore the NWSB as well, which is invariably found to be linear relationship between T_c-T_a and VPD when created empirically, can be explained using the Monteith energy balance approach by Jackson et al. (1981) as shown in equation 2.13. In this equation, for the purposes of determining the T_c-T_a of a canopy, soil heat flux is assumed to be negligible, and canopy temperature is only affected by radiation heat flux, latent heat flux from evaporating water and sensible heat flux (Howell et al., 1986; Jackson et al., 1981; Maes and Steppe, 2012).

$$T_c - T_a = \frac{r_a R_n}{\rho C_p}\left(\frac{\gamma(1+{}^{r_c}/_{r_a})}{[\Delta+\gamma(1+{}^{r_c}/_{r_a})]}\right) - \left(\frac{(e_a^* - e_a)}{[\Delta+\gamma(1+{}^{r_c}/_{r_a})]}\right) \quad \textbf{2.13}$$

where, , r_a is the canopy aerodynamic resistance (s m^{-1}), R_n is the net radiation flux (W m^{-2}), ρ is air density (kg m^{-3}), C_p is the specific heat of air at constant pressure, γ is the psychrometric constant (kPa °C^{-1}), r_c is the canopy diffusion resistance (s m^{-1}), e_a^* is the saturated vapour pressure (kPa) at the current temperature, e_a is the current vapour pressure; (e_a^*- e_a) would, therefore, be the current VPD and Δ is the slope of the curve when saturated vapour pressure is plotted against the difference between canopy and air temperature (kPa ˚C^{-1}) so (e_c^*-e_a^*)/(T_c-T_a) (Jackson et al., 1981). If an attempt is made to calculate the $(T_c-T_a)_{LL}$ using equation 2.13, that is, the potential T_c-T_a at maximum transpiration for the conditions, canopy resistance (r_c) can be taken as zero, to get equation 2.14.

$$(T_c - T_a)_{LL} = \frac{r_a R_n}{\rho C_p}\left(\frac{\gamma}{\Delta+\gamma}\right) - \left(\frac{(e_a^* - e_a)}{\Delta+\gamma}\right) \quad \textbf{2.14}$$

However, this assumes that the canopy behaves like a free water surface, which is inaccurate. For real accuracy, and to take into account crop characteristics, data would have to be collected over a well-watered crop to determine the unique canopy resistance of the particular crop transpiring at the potential rate (Berni et al., 2009a). When the equation is run repeatedly using a range of temperature inputs, a curve approximating the NWSB can be created from the endpoints of each temperature line, it differs, however, in being an upward facing curve with a negative slope rather than a straight line with a negative slope like a NWSB from actual non-stressed crop data (Howell et al., 1986; Jackson et al., 1981).

It is therefore, evident, that although the NWSB does have a theoretical basis, for the purposes of practical use, it is easier and less error prone to use a real NWSB or an artificial reference surface rather than try to calculate it using equation 2.13 (Maes and Steppe, 2012). This does not mean that the theoretical formula (equation 2.14) has not been used to find the lower limit, as it has the advantage of being able to be calculated whenever the CWSI is needed without any previously calculated NWSB (Baluja et al., 2012). Some have gone as far as calculating the entire CWSI using the theoretical formula as given by Jackson (1981) when instrumentation to collect the parameters required to use the energy balance equations (equation 2.13), was available (Berni et al., 2009a).

The measured NWSB tends to take into account a large amount of variation in the conditions, without becoming overly complicated, especially if the required data is collected over a

sufficiently long period (Idso, 1982). The great disadvantage of the NWSB is found when it is used under conditions, or in a region, differing from the those it was created under, or the method of canopy temperature collection differs. For example, when creating NWSBs for pecan, collecting canopy temperatures consisting of only sunlit leaves (Sammis et al., 1988) as opposed to a wider angle view containing more of the canopy with both sunlit and shaded areas (Garrot et al., 1993) yielded NWSB equations that differed in both slope and intercept. In pistachios, the intercept of the NWSB changed depending on the time of day that canopy temperature data was collected, primarily due to the sun angle relative to the sensor (Egea et al., 2017; Testi et al., 2008). The difference in NWSB between sunlit and shaded leaves has similarly been shown for a wide variety of crops (Idso, 1982). The slope of the NWSB has also been shown to correlate to average wind speed during data collection to create the NWSB, however, this effect is not as important as that of radiation, and may not be a source of significant error if the conditions change (Testi et al., 2008). The effect of shading and wind on the NWSB can be explained by the theoretical basis for the NWSB (equation 2.14). The reason why the same crop may need a different NWSB depending on the region can also be explained by examining the equation, as in a region with a higher average radiation flux, at any given VPD, the latent heat flux remains the same, but there is a greater heating effect from intercepted radiation, and therefore a more negative T_c-T_a, and a steeper slope overall (Howell et al., 1986). From the first term of the equation, it is quite obvious that both radiation and aerodynamic resistance affect the T_c-T_a of a crop transpiring at the potential rate, with wind speed a major factor in aerodynamic resistance (Testi et al., 2008). For the same reason, data for the NWSB should not be collected on cloudy days, as radiation flux is limited (Nielsen, 1990). The NWSB is also specific to a phenological stage for many crops, particularly those that have a distinct vegetative growth stage and a reproductive phase, such as cereal crops (Howell et al., 1986; Idso, 1982). Different NWSB equations have also had to be developed and used during different parts of the year in olive trees for CWSI values to correlate well with other stress measurements (Egea et al., 2017). In peach, separate NWSB equations had to be developed for each phenological stage, which is explained by an increase in transpiration when the trees are carrying a crop (Bellvert et al., 2016). Better results were also achieved when new NWSBs were created every season (Bellvert et al., 2016). The same effect was not observed in pecan (Garrot et al., 1993) or pistachio (Testi et al., 2008), where a single NWSB created using data from a single full season resulted in an accurate CWSI. These factors, together with improvements in the resolution of thermal sensors, allowing smaller objects to be found in the image, has led to the use of artificial reference surfaces and wetted leaves becoming increasingly popular to find the lower limit (Maes et al., 2016; Meron et al., 2010).

2.6.2 Artificial Reference Surfaces

The use of an artificial reference surface to determine the potential T_c-T_a under a particular set of conditions has the great advantage of not requiring any historical data, or crop specific equations, such as the NWSB, which may not accurately reflect the conditions on the day (Maes et al., 2011). All that is required, in addition to canopy and air temperature, is the temperature of a wet surface that resembles the canopy or a leaf (Maes et al., 2016; Meron et al., 2010) and the acquired temperature is generally referred to as T_{wet}. Using an artificial reference surface automatically takes into account all the environmental factors affecting the temperature of the canopy on the day with no extra effort on the part of the operator, this is not the case with the NWSB, where only the VPD on the day is taken into account, all other factors are assumed to be equal to the composite of conditions reflected by the NWSB (Jones, 1999; Meron et al., 2010). This is important, as it has been shown that intercepted radiation and wind speed do have a significant impact on canopy temperature, even though the effect may not be as great as air temperature and VPD (Maes and Steppe, 2012; Testi et al., 2008). Of the various types of wet reference surfaces used, leaves wetted immediately prior to thermal image collection (Irmak et al., 2000; Jones, 1999; Jones et al., 2002), or wet artificial surfaces resembling the leaves of the crop in both size and shape have been found to be extremely accurate (Jones et al., 2002; Maes et al., 2016).

However, these types of reference surfaces are impractical when thermal data is collected using UAV mounted sensors. Artificial leaves are too small to be picked out of an orchard scale orthomosaic (Meron et al., 2010). A wetted canopy has also been used to find T_{wet} of field crops with a UAV mounted sensor, but attempting to wet a complex tree canopy may not be possible in the field. For a reference surface to be suitable for use with large scale crops and UAV mounted sensors, it needs to be large enough relative to the full extent of the crop to be easily detected and have data extracted, which limits the type of surface that can be used (Cohen et al., 2005). Choices are limited to relatively large panels covered in an absorbent material, either floating in a pan of water or being constantly wetted (Meron et al., 2010). These do not resemble real leaves or canopies in any way, which may be a problem, as it has been found that there is some correlation between leaf size and shape, and leaf temperature (Maes and Steppe, 2012). They also have a tendency to act as a free water surface, unlike real leaves, which do not, even when transpiring at the potential rate (Jackson et al., 1981; Maes and Steppe, 2012). Nevertheless, they perform reasonably well when used to calculate the CWSI (Meron et al., 2010).

2.6.3 Reference Temperature from Cold Pixels

A more recent method of determining T_{wet} on the day canopy temperature is measured has been borne out of the widespread availability of UAV mounted thermal sensors and easy to use image analysis software. This method does not require any reference surfaces, previous weather or canopy temperature data or a wetted canopy, it has therefore become known as the simplified method (Bian et al., 2019). All that is required is for relatively unstressed canopies to be included in the thermal image of the orchard in question. The average temperature of the coldest pixels of the thermal image are then designated as T_{wet} and used to calculate the lower limit, by subtracting the air temperature. The methods of finding the coldest pixels, as well as the proportion of the coldest pixels used relative to the size of the image, have varied, but all methods have yielded a CWSI that performs better as a measure of water stress than when the NWSB or the reference surfaces have been used (Baluja et al., 2012; Bian et al., 2019). When using this method, it is extremely important to ensure that the canopy is separated from the soil before finding the coldest pixels, as wet soil may mistakenly be taken as cold canopy pixels.

2.6.4 The Upper Limit

The third requirement when using canopy temperature to quantify water stress, besides the actual T_c-T_a of the canopy and an estimate of the T_c-T_a of the crop transpiring at the potential rate (the lower limit), is an estimate of the T_c-T_a of a severely stressed crop that has stopped transpiring, known as the upper limit, or $(T_c\text{-}T_a)_{UL}$ (Idso et al., 1981). The T_c-T_a of the crop will usually lie between one of these two extremes.

The upper limit is a constant value across the VPD range since it represents a plant temperature value that is not affected by water vapour loss, only air temperature. It has been found that the higher the air temperature, the greater the $(T_c\text{-}T_a)_{UL}$ (Idso et al., 1981). The upper limit is also dependent on radiation interception, as can be deduced from the energy balance equations, and when conditions are the same it accounts for the difference in upper limits observed between shaded and sun leaves, (Idso, 1982; Sammis et al., 1988). Nevertheless, using a standard upper limit across conditions different to those it was originally measured under has been shown to yield a CWSI that is a good indicator of water stress (Alderfasi and Nielsen, 2001; Zarco-Tejada et al., 2013).

The fact that there is no transpiration means that latent heat flux is not a factor in the upper limit, therefore the only parts of the energy balance equation which are relevant are the radiation and sensible flux terms. The upper limit Tc-Ta value can then be obtained by solving the radiation and sensible heat flux equations for T_c-T_a. Another approach would be to set the canopy resistance (r_c) in equation 2.14 to an infinite value (Jackson et al., 1981), with the result of both approaches the same, namely equation 2.15 (Howell et al., 1986; Maes and Steppe, 2012).

$$(\boldsymbol{T_c - T_a})_{UL} = \frac{\boldsymbol{r_a R_n}}{\boldsymbol{\rho C_p}} \qquad \textbf{2.15}$$

This method of finding the upper limit is limited to situations where R_n and the parameters required to calculate r_a are available whenever the CWSI needs to be calculated. The equipment required to obtain the data needed to calculate these parameters is both complicated and expensive, and is usually not available in a commercial situation.

The upper limit of the CWSI for a particular crop can also be derived from the NWSB of that crop. In a saturated atmosphere (VPD =0), there should theoretically be no water vapour gradient between the interior of the leaf and the outside air, there should, therefore, be no transpirational water loss or cooling effect either. This is no different to a situation where the stomata are closed due to water stress, where there is no transpirational water loss or cooling (Idso et al., 1981). Since the upper limit is the T_c-T_a value at which no transpirational cooling takes place, it should also be equal to the T_c-T_a value in a saturated atmosphere. The value at which there should be no cooling effect can be found by extending the NWSB back into an imagined negative VPD range and finding the theoretical VPD value at which no transpirational cooling takes place, as explained by equation 2.16 (Howell et al., 1986). Figure 2.4 provides a good illustration of this method (Idso et al., 1981).

$$(\boldsymbol{T_C - T_a})\boldsymbol{UL} = \boldsymbol{a - b\,VPG} \qquad \textbf{2.16}$$

Vapour Pressure Gradient (VPG) refers to the negative VPD where there is no water vapour gradient at the ambient air temperature, with T_a and the saturated vapour pressure at T_a, required for the calculation of VPG as described in equation 2.17.

.

$$VPG = e^*(T_a) - e^*(T_a + a) \quad \textbf{2.17}$$

where a is the intercept of the NWSB on the T_c-T_a axis.

Using this approach to find the $(T_c\text{-}T_a)_{UL}$ may be accurate enough for many crops, including wheat (Howell et al., 1986), various vegetable crops (Idso, 1982), pistachio (Testi et al., 2008), and grapevine (Zarco-Tejada et al., 2013), where it has been found that using an upper limit calculated in this way yields a CWSI that correlates well with other methods of water stress detection. The advantage of this method is that no extra data or effort is required if an accurate NWSB is available. It would be expected to work well for most crops due to the inherent simplicity, however, for some crops, including pecan, the upper limit has been found to be higher than that calculated by regressing the NWSB, meaning that canopy temperature rises much higher above air temperature when transpiration stops than would be expected from the slope and intercept of the NWSB (Sammis et al., 1988).

2.6.5 Empirical Upper Limit

Since the $(Tc\text{-}Ta)_{UL}$ is the difference between canopy and air temperature at which no transpiration takes place, the most empirical method to find the value would be to measure the temperature of leaves that are not transpiring (Jones, 1999; Maes and Steppe, 2012). Methods of finding or creating such leaves have included coating leaves in petroleum jelly (Jones, 1999), measuring the canopy temperature of a severely stressed crop (Irmak et al., 2000) and severing branches and measuring their temperature when stomatal conductance becomes negligible (Sammis et al., 1988). Dry artificial reference surfaces have also been used, usually artificial leaves (Jones et al., 2002; Maes et al., 2016), but rectangular plastic panels have also been used (Egea et al., 2017). The problem with these is that they are too small to be used at an orchard scale when the thermal sensor is UAV based, making them impossible to find in a high enough resolution to extract a clean temperature value from the surface (Meron et al., 2010). The simplified method, as described for finding T_{wet} in section 2.6.3, has also been used to find the upper limit, by finding the average temperature of the warms pixels in the image, designated T_{dry} (Bian et al., 2019). This very easily solves the problems described above, but it cannot be ensured that the warmest pixels actually represent leaves that are not transpiring, rather than heavily stressed leaves that are still transpiring at some level.

It would appear that the accuracy of the upper limit is not essential to the ability of the CWSI to detect water stress, as it is, after all, a static reference value that should not influence the CWSI as long as all actual crop T_c-T_a values remain below it. This is evidenced by the fact that good results have been achieved using the negative VPD method (Idso, 1982; Testi et al., 2008), the energy balance method (Howell et al., 1986), the real dead leaf method (Sammis et al., 1988), the petroleum jelly method (Jones, 1999) and the artificial leaf method (Maes et al., 2016). Some have gone as far as setting the upper limit to be a somewhat arbitrary value of T_c-T_a = +5˚C, and have achieved good results (Meron et al., 2010). This last approach, which has seen an increase in popularity in more recent work, is based on the findings of a number of studies which have experimentally, with a dry crop or reference surface, shown that the upper limit is usually around five degrees above zero (Cohen et al., 2005; Irmak et al., 2000).

2.7 Application of the Crop Water Stress Index

Irrespective of the methods used to determine the baselines of the CWSI, the CWSI has been found to correlate very well with actual measured plant stress, quantified by measuring stomatal conductance (g_s), stem water potential (ψ_{stem}), leaf water potential (ψ_{leaf}), crop coefficients (K_c) and transpiration rate. It is easily understood why g_s and transpiration rate would be reflected by the CWSI, as the CWSI is a measure of the transpirational cooling effect, and this has been proven in many field crops including cotton (Bian et al., 2019) and soybean (Nielsen, 1990). Other measures of water stress that do not directly quantify the rate of water vapour loss from the leaf, such as ψ_{stem} and ψ_{leaf} have been used even more widely to validate the CWSI, including crops such as wheat (Howell et al., 1986) and cotton (Meron et al., 2010). In pecan, the CWSI has been shown to correlate with g_s and K_c (Sammis et al., 1988). In pistachio, the CWSI correlated well with ψ_{leaf} (Testi et al., 2008), in grapevine it was tested against g_s, ψ_{stem} (Baluja et al., 2012), and ψ_{leaf} (Cohen et al., 2005). In olive, the CWSI compared favourably with g_s, ψ_{stem}, ψ_{leaf}, and transpiration rate (Egea et al., 2017), in peach; correlation with g_s and ψ_{leaf} was shown (Bellvert et al., 2016). The CWSI has similarly been proven to be an accurate estimate of stress in many other crops. An interesting phenomenon observed in certain crops, such as soybean and olive, when regressing the CWSI against ψ_{leaf}, is what has been termed a two stage or curvilinear relationship, where at low stress levels; the slope of the curve is flatter than at higher stress levels (Egea et al., 2017; Nielsen, 1990). Incidentally both these crops can be considered oil-storing crops. One explanation is that at low stress levels, according to ψ_{leaf}, there is less stomatal control, causing a smaller leaf temperature change, while at higher stress levels, stomata close quicker, leading to a faster increase in leaf temperature, and higher CWSI (Egea et al., 2017). In peach, the regression

equation between CWSI and ψ_{leaf} had a different slope in the pre and post-harvest stages, which was attributed to the crop having a higher transpiration rate while carrying the crop, and therefore, a greater cooling effect at the same stress level (Bellvert et al., 2016). Such differences have not been noted in pecan, although less work has been done on this crop than the more common horticultural crops (Garrot et al., 1993). The conclusion that can be drawn from all the above is that when designed for the crop in question, and the reaction of the CWSI to the specificities of the crop is understood, the CWSI can be a very convenient tool for scheduling irrigation, requiring much less physical work than other stress measurements. When calculated using remote sensing, it allows the water status of trees of an entire orchard to be quickly understood, instead of just a sample. The CWSI has been used to schedule irrigation in pecan (Garrot et al., 1993), as well as many other crops (Nielsen, 1990). It has been found that the CWSI relates well with soil water content (Baluja et al., 2012), and pecan nut yield correlated well with the CWSI threshold chosen to trigger irrigation (Garrot et al., 1993). The use of UAV mounted thermal sensors to create a CWSI of an orchard also opens the possibility of precision irrigation, that is, irrigating areas differently based on stress level, which can lead to significant water savings (Baluja et al., 2012; Bian et al., 2019).

2.8 Yield Estimation by Remote Sensing

Another practice often associated with precision agriculture is yield estimation. When a good estimate is available early enough in the season, low and high yielding areas can be treated differently, to avoid wasting inputs on areas that will not provide the returns aimed for with those inputs (Ballesteros et al., 2020). Traditional manual yield estimation methods usually involve sampling part of the orchard, which may be in the form of a transect, random sample, or walk through by an expert; and extrapolating the data to the entire area under the crop. These methods are notorious for inaccuracies in estimation due to variability in the field, which has to be countered with a larger sample size, or a more creative sampling method, both of which add time and complexity to an already time-consuming exercise (Anderson et al., 2021). A solution that has grown in popularity for use in field crops, and has been refined over a few decades, is yield estimation by remote sensing (Ferencz et al., 2004). Using remote sensing to estimate the yield of horticultural crops has only in the very recent past started to be evaluated (Anderson et al., 2021).

The most basic approach that has been taken to estimate yield has been direct regression with vegetation indices, usually indices that quantify the greenness of the crop (Yang et al., 2019). These, however, tend to correlate poorly with yield, except in cases where yield loss is

as a result of disease or nutrient deficiency, where the difference in the greenness of high and low yielding trees are dramatic (Chen et al., 2022). Thermal indices such as T_c-T_a and the CWSI have also been used to estimate yield. The average of these indices over the season correlate well with yield where water is the main limiting factor controlling yield, this has been shown in pecan as well (Garrot et al., 1993). This method is of little use in well managed orchards, where major water stress is prevented. Another complicating factor is that it also requires regular thermal and meteorological measurements throughout the season.

Success in estimating yield using VIs has been achieved in grapevine when a multiple linear regression was used to combine VI values for various dates throughout the season (Ballesteros et al., 2020), with similar results found for other crops (Anderson et al., 2021). The problem with this method is that the regression equation obtained cannot be carried over to other seasons as it inherently reflects the condition of the crop in that specific season. A possible use is to develop the equation in a representative orchard or block and then apply it to a wider area during the same season (Anderson et al., 2021). The more complex remote sensing yield estimation approaches that reliably deliver good results involve either modelling, or machine learning, or both. Crop estimate models tend to estimate yield by attempting to quantify the total potential photosynthetic assimilation, or primary production, during the season. They use the meteorological data that affects crop productivity as input parameters, which include parameters such as radiation interception during the season, total rainfall and irrigation, and heat accumulation. They may use remote sensing tools to find the value of parameters such as canopy size, photosynthetically active radiation above the canopy that can potentially be absorbed or LAI (Ferencz et al., 2004; Maselli et al., 2012). These models need large datasets of both yield and meteorological data to calibrate and validate and in some studies a decade or several of historical data from a single area have been used (Maselli et al., 2012), which may not always be available for the crop and the area of interest. They have, nevertheless been used extensively for decades on field crops (Ferencz et al., 2004; Prasad et al., 2006). Using total production as a proxy for yield is problematic in perennial crops, as the potential production does not usually translate to harvestable yield. In such crops, yield is affected not only by the conditions of the current season, but factors such as the carbohydrate reserves of the tree after the production of the previous season's crop and the number of fruit bearing sites, as a result of the growth pattern or pruning. This is true for pecan in particular, which is known for alternate bearing (Wood et al., 2003). Conditions during early phenological stage, such as flowering and fruit set in pecan, can also limit yield even if all other factors promise a high yield (Anderson et al., 2021; Sparks, 2005). Despite these arguments, a total production model has been successfully used to predict yield in olive, however, a very large area and nine seasons of data were used to calibrate the model (Maselli et al., 2012).

A simpler approach to estimating yield using remote sensing in tree crops is the use of machine learning. However, even machine learning needed datasets consisting of more than just VI data to predict yield. Work on apple showed that best results were achieved when the algorithm used was trained using both VI data and crop architecture parameters, such as crop height, fractional interception of radiation by the canopy, relative to the space allocated to the canopy, and canopy volume (Chen et al., 2022). The same study also found that crop architecture parameters from multispectral data could not accurately quantify three-dimensional canopy characteristics, with LiDAR being the better choice to find canopy height and volume. A machine learning option available to large colourful fruit, such as citrus and mangoes, that is not available to pecan, is to train the algorithm to count actual fruit that stand out from the green canopy (Anderson et al., 2021). In pecan, any machine learning algorithm will have to be trained to estimate yield using more indirect methods, using both VIs and canopy architecture, such as described for apple. The challenge is to collect a large enough dataset of both yield data and remote sensing data to train and validate an artificial intelligence model.

3 GENERAL MATERIALS AND METHODS

3.1 Study Site Description

The study was carried out at two sites, the water stress trial in the pecan orchard on the University of Pretoria's Experimental farm (Innovation Africa@UP) shown in Figure 3.1 and the second being the instrumented pecan water use trial site at the Groen Boerdery Pecan orchard on the Vaalharts Irrigation Scheme. The UP pecan orchard (25°4'55.85" S, 28°15'3.88'' E) is located in South Africa's summer rainfall region at an altitude of 1372 masl with an average annual rainfall of 675 mm. January is usually the wettest month of the year. The pecan orchard is 3 ha in size, divided into two sections, a high-density orchard, planted to a spacing of 5 x 10 m, and an orchard planted at the industry standard spacing of 10 x 10 m. The orchard consists of two main pecan cultivars, 'Wichita' and 'Western Schley', in alternating rows, for the purpose of optimal pollination. A single mixed cultivar row is planted between the two orchard sections. 'Ukulinga' is the rootstock used throughout the orchard.

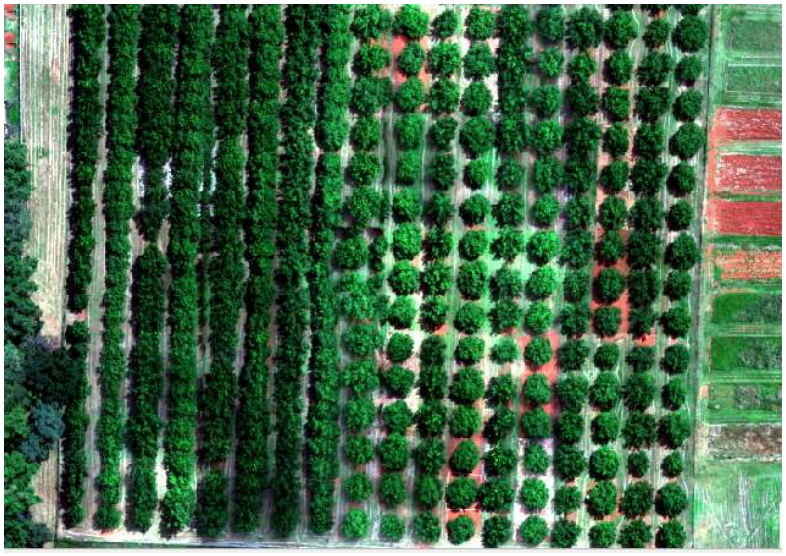

Figure 3.1 The pecan orchard at Innovation Africa@UP, showing both high density (5 x 10 m) and industry standard (10 x 10 m) orchards.

The water stress trial has been run in the 10 x10 m orchard since 2018, with only the "Wichita" in this section of the orchard being part of the trial. The water stress trial is made up of five treatments and four replicates of each treatment, arranged in a randomised complete block design. Each rep consists of three trees in the row, with data collected from the centre tree only. Pressure compensated drip irrigation is installed in the orchard, with emitters spaced 0.6 m apart, each delivering 1.6 $L.h^{-1}$. Three drip lines are installed per row, one in the centre, and one on either side, a metre from the trees. The irrigation is designed so that each treatment can be turned on independently. The five treatments are: a control, which is never intentionally

stressed, and four treatments which are stressed according to the phenological stages of pecan trees, that is, at flowering and nut set, nut sizing, nut filling, and shuck dehiscence. Stress is imposed on the treatment relevant to the phenological stage by not irrigating and attempting to exclude rainfall with a 10 m wide section of plastic sheet covering all three trees of each rep. Irrigation on the unstressed trees is scheduled using Chameleon gypsum block soil water sensors and Chameleon card readers (Virtual Irrigation Academy, Australia), as well as midday and predawn stem water potential. The orchard was fertilised according to industry advice using lime ammonium nitrate, superphosphate and potassium chloride, all in the granular form. Fertiliser was not applied timeously in the 2020–2021 season, and the essential micronutrient for pecans, zinc, was not applied. Many trees showed a variety of obvious deficiency symptoms as a result. Fertiliser was applied on time at the start of the 2021-2022 season, zinc was also applied directly to the soil as a drench. No deficiency symptoms were observed, and the trees appeared healthy throughout the season.

Hourly meteorological data (rainfall, air temperature, relative humidity, vapour pressure deficit wind speed and solar radiation) was available from a weather station situated 230 m from the UP orchard. A second weather station, measuring air temperature, relative humidity, wind speed and solar radiation was installed inside the high-density section of the orchard at the end of November 2021 to be able to obtain higher resolution weather data (20 minutes), and due to concerns about the accuracy of the main weather station. Radiation data from this weather station was not used because it was partly shaded by the canopy.

The study site on the Vaalharts irrigation scheme (28°4'11.01"S, 24°37'54.79"E) has an average annual rainfall of 590 mm and is situated in a 16-year-old 10.37 ha mixed cultivar orchard planted at a 10 x 10 m spacing. A single 150 L. h^{-1} sprinkler is installed in the row halfway between all the trees. Irrigation was scheduled using a capacitance probe installed in the row halfway between the tree and the sprinkler. An Open Path Eddy Covariance (OPEC) system (Campbell Scientific Inc., Logan, UT, USA) is installed on a lattice tower above the tree canopy (10m). Above canopy meteorological variables measured include net radiation, air temperature, relative humidity and windspeed. Data from a weather station 1 km from the orchard was also available, this included solar radiation, air temperature, relative humidity, windspeed and rainfall at hourly intervals. In February 2020, two SI-121 infrared radiometers (Apogee Instruments, North Logan, Utah, USA) were installed on a tower facing the top of two tree canopies. One was directed to the tree to the southeast of the tower and the other towards a tree in the next row to the west of the tower. Canopy temperature data from the IR radiometer facing the southeast during the 2021/2022 season was found to be much higher than the other

radiometer, and much higher than the leaf temperature could plausibly be expected to be. Upon further investigation, it was observed that a leafless branch was within the field of view of the thermometer, the temperature readings were then not from leaves, but rather bare bark.

3.2 Remote Sensing Data Collection

A UAV was available from the beginning of February 2021. The platform was a DJI Matrice M210 (SZ DJI Technology Co., Ltd. Shenzhen, Guandong, China) with a Micasense Altum Multispectral and Thermal Sensor attached (Micasense, Inc., Seattle, WA, USA). The device has a sensor for each of the five wavelength bands: Blue, Green, Red, Red-edge and Near Infrared, the centre and band width of each band is presented in Table 3.1 A radiometric thermal band is also available.

The thermal and multispectral bands are synchronised and captured simultaneously. The Altum sensor was radiometrically calibrated using a Calibration Panel before each flight. Thirteen flights were conducted between February and April 2021, when the leaves on the trees began to senesce. Flying resumed at the end of September 2021 with bud break and continued until senescence began in April 2022, 26 flights were conducted during this season. Images captured before full canopy cover was achieved were not used in the water stress detection section of this study. Trees were in full leaf by the end of October, when plant-based water stress measurements began. While an attempt was made to fly weekly, this was not always possible due to the availability of the UAV operator, as well as the weather conditions. Table 3.2 UAV data collection flights, and available plant water stress measurements. Rows highlighted in grey indicate the days selected for data analysis.

gives all dates and times that flights were conducted, with the field water stress data available for each date. Flights lasted an average of seven minutes, to capture the entire low-density section of the orchard. Dates where collected data was used is highlighted in Table 3.2 UAV data collection flights, and available plant water stress measurements. Rows highlighted in grey indicate the days selected for data analysis.

, 6 images were used from the second half of the 2020/2021 season, and 10 images were used from the 2021/2022 season.

Table 3.1. Wavelength bands available from the Micasense Altum Multispectral and thermal sensor with band centres and bandwidth (https://support.micasense.com/hc/en-us/articles/360010025413-Altum-Integration-Guide#h.5ow085yb2oll)

Band	Centre	Band width
Blue	475 nm	32 nm
Green	560 nm	27 nm
Red	668 nm	14 nm
Red-edge	717 nm	12 nm
Near-Infrared	840 nm	57 nm
Thermal	11 µm	6 µm

The data from several flights were not included in the final data due to complete cloud cover or uneven cloud cover, causing the orchard to be partially shaded. It was found to be exceptionally difficult to separate canopies from the background of images collected on cloudy days, data from these images could also not be confidently compared with the rest of the data collected on sunny days, as observed by Gago et al. (2015)

Flight paths were planned on the DJI ground-station to cover the entire orchard, with about 10 m on each side as a buffer. A flight height of 40 m, with an image overlap of 70% was chosen, as this provided an optimal balance between battery life and image resolution. These parameters yielded a ground resolution, in the form of Ground Sampling Distance (GSD) of 1.725cm per pixel for the multispectral images, and 27.119cm per pixel for the thermal images.

Days with clear skies were chosen for the weekly flights where possible, some flights did take place on overcast days, and there were several weeks, in both seasons, where no flight took place due to prolonged inclement weather, primarily in December and January. It was found early on that data from flights on cloudy days were significantly more difficult to process and could often not be used. Ideally flights should have been conducted at midday, although this was not possible on most days.

Table 3.2 UAV data collection flights, and available plant water stress measurements. Rows highlighted in grey indicate the days selected for data analysis.

Date	Ψ_{midday}	g_s	Flight Start Time
10-Feb-21	Yes	Yes	10:39
17-Feb-21	Yes	Yes	10:58
02-Mar-21	Yes	Yes	11:42
04-Mar-21	Yes	Yes	11:27
10-Mar-21	Yes	Yes	10:41
19-Mar-21	Yes	Yes	10:21
07-Apr-21	Yes	Yes	10:57
14-Apr-21	Yes	Yes	10:44
29-Sep-21	Yes	No	10:35
06-Oct-21	No	No	10:30
13-Oct-21	No	No	10:43
18-Oct-21	No	No	10:29
29-Oct-21	Yes	No	10:23
09-Nov-21	Yes	No	10:50
11-Nov-21	No	No	10:43
17-Nov-21	Yes	No	10:39
24-Nov-21	Yes	No	10:41
07-Dec-21	Yes	No	10:31
17-Dec-21	No	No	10:56
28-Dec-21	No	No	10:59
03-Jan-22	No	No	10:41
05-Jan-22	No	No	10:31
22-Jan-22	Yes	No	10:19
26-Jan-22	Yes	No	10:32
09-Feb-22	Yes	No	10:45
23-Feb-22	No	No	10:39
24-Feb-22	Yes	No	10:35
03-Mar-22	Yes	No	10:33
10-Mar-22	Yes	No	10:59
14-Mar-22	Yes	No	10:55
24-Mar-22	Yes	No	10:45
06-Apr-22	No	No	11:45
13-Apr-22	Yes	No	10:42
21-Apr-22	Yes	No	10:43

3.3 Remote Sensing Data Processing

Raw multispectral images from the Altum sensor were stitched into orthophotos after flying using Pix4D fields. All geometric and radiometric corrections were completed automatically by the orthomosaicing software using the metadata collected from the calibration panel image, and data from the radiation sensor installed at the top of the UAV. The application produced five separate images for each of the available bands. Further processing was performed in QGIS. The first step was to create composite Vegetation Index (VI) images, using the available bands. Details of the VIs used are included in Table 3.3.

Table 3.3 Vegetation Indices created using the multispectral images of the UP Pecan orchard.

Name	Abbreviation	Formula (Band)
Normalised Difference Vegetation Index	NDVI	$\frac{\text{NIR} - \text{Red}}{\text{NIR} + \text{Red}}$
Simple Ratio Index	SRI	NIR/Red
Red-edge Simple Ratio	ReSR	Rededge/Red
Red-edge NDVI (Red-edge Index)	RNDVI	$\frac{\text{NIR} - \text{Rededge}}{\text{NIR} + \text{Rededge}}$
Green NDVI	GNDVI	$\frac{NIR - Green}{NIR + Green}$
Renormalized Difference Vegetation Index	RDVI	$\frac{\text{NIR} - \text{Red}}{\sqrt{\text{NIR} + \text{Red}}}$
Optimized Soil Adjusted Vegetation Index	OSAVI	$(1 + 0.16)\ \frac{NIR-Red}{NIR+Red+0.16}$
Transformed Chlorophyll Absorption Ratio	TCARI	3((RE-Red)-0.2(RE-Green) ($\frac{Re}{Red}$))
Modified Chlorophyll Absorption Ratio Index	MCARI	((RE-Red)-0.2(RE-Green)) ($\frac{Re}{Red}$)
MCARI 1	MCARI 1	1.2(2.5(NIR−Red) − 1.3(NIR−Green))

An unsupervised classification into 10 classes was then performed on the SRI using the in-built facility in QGIS (Figure 3.2). The insights from this process and the SRI raster histogram were used to choose a threshold value to separate pecan tree canopies from the soil and interrow vegetation. The SRI raster histogram for the orchard showed two distinct frequency

spikes, a larger spike representing the background, which is the larger part of the image, and a smaller normal curve being the pecan canopy. The value at the upper edge of the background curve was used as the threshold value and was found to be satisfactory at separating out the background. A sample of the SRI histogram is given in Figure 3.3.

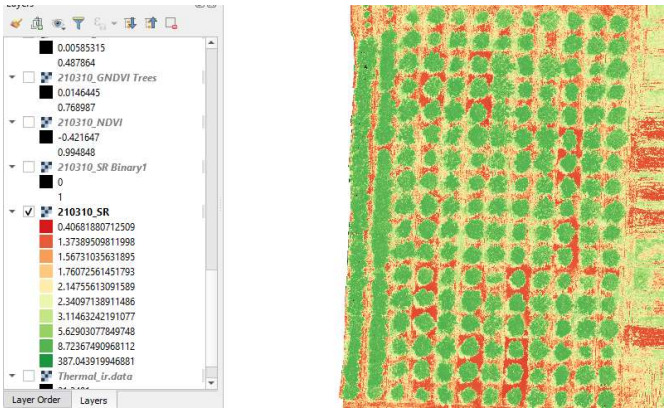

Figure 3.2 Classified Simple ratio index (SRI) orchard image used to separate pecan canopies from background soil and vegetation, the image was classified into 10 bands as observed in the key on the left of the image.

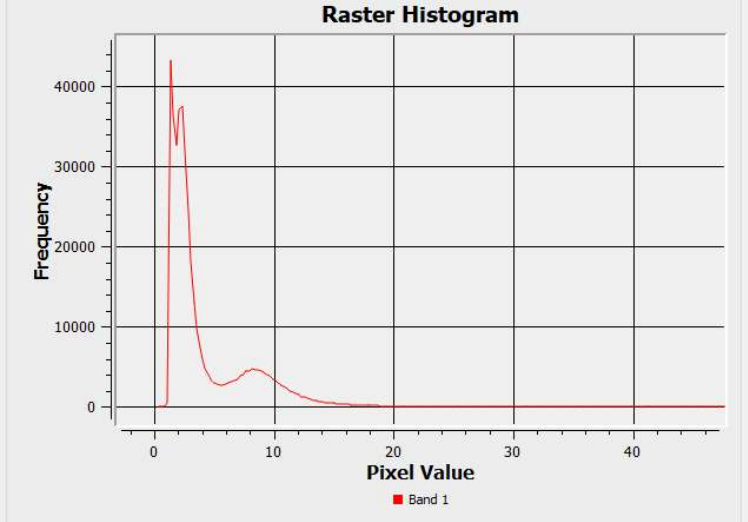

Figure 3.3 Raster histogram of the simple ratio index (SRI) used to decide on a background-separation threshold value, showing a large background spike and normal distribution for the canopy. The threshold in this case is an SRI value of approximately 5.

At first, this process was followed for all VIs, however, it quickly became apparent that certain VIs were better at separating out pecan canopies than others. Many of the VIs placed the cover crop in the same class as the tree canopies, due to highlighting specific reflectance

properties by design. Several of the VIs, including NDVI (Figure 3.4), had a very small range of values between bare soil and the pecan canopy, making the selection of a threshold value tediously sensitive. Some of the VIs also could not differentiate between shadows and pecan canopy, with shadowed background and lit pecan canopy having the same value. This was a problem as many flights were conducted before the sun was directly overhead. The best and most practical of the VIs for separating pecan canopies was found to be the Simple Ratio Index (SRI), (Figure 3.5), having both a simple formula (NIR/Red), and a large range of values between bare soil and pecan tree canopies. This gave a large margin of error when selecting the threshold value without fear of leaving out a large amount of canopy or including the background. However, even this VI performed poorly when the data was collected under overcast conditions or the interrow vegetation was too tall.

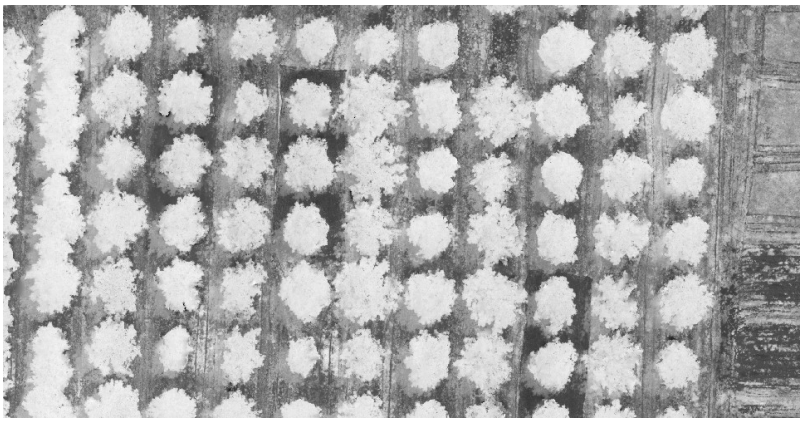

Figure 3.4 Normalised difference vegetation index (NDVI) Image of pecan orchard showing little differentiation between shadows and the pecan canopy.

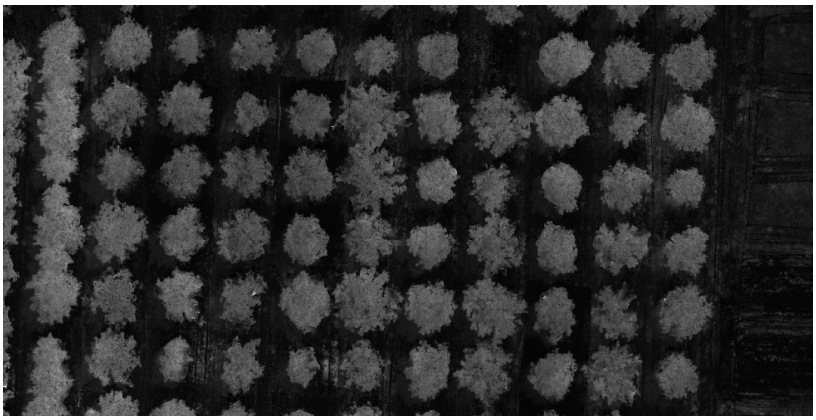

Figure 3.5 Simple ratio index (SRI) image of the pecan orchard showing clear differentiation between pecan canopy and the background.

Once a threshold value was chosen, a threshold raster was created (Figure 3.6). This is an image where all pixels have a value of either 0 or 1 (that is, black and white). All pixels that were above the threshold value (i.e., the canopy) in the VI are designated 1, while all others are 0. This can be used directly to find canopy area by imposing a vector grid that corresponds to the tree spacing on the image and finding the percentage of each block that is covered by pecan canopy. By dividing the VIs by the threshold image, new VI layers are created that include only the canopies, with all else removed or "cut out". However, this is a tedious way of extracting data from the VIs, as only one VI layer can be processed at a time, though it can be a visually appealing way to display the VI when overlain on an RGB image of the orchard.

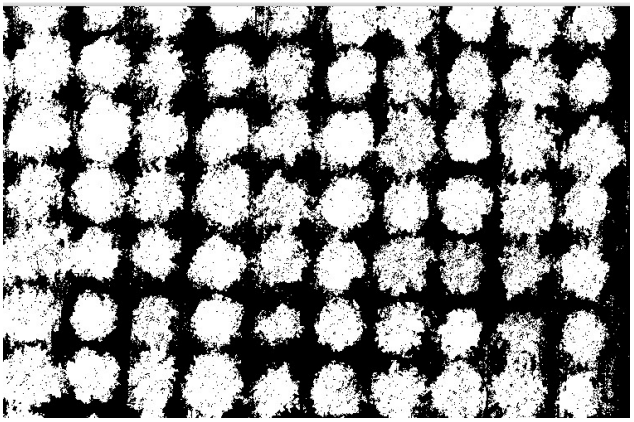

Figure 3.6 Threshold raster created using threshold value of the SRI.

The method used to extract the VI values of the canopies in the 2020 – 2021 season, and the early part of the 2021-2022 season used a vector layer containing polygons corresponding to the "1" values on the threshold image. Therefore, each polygon covered one pecan canopy (Figure 3.7). The polygons were used to visually validate the threshold value by ensuring that each polygon corresponded well to the canopy it represented. If the polygons included parts of the background, or removed parts of the canopy, a new threshold value was chosen to create a new threshold raster, and the process was repeated until the polygons satisfactorily represented the tree canopies.

Figure 3.7 Individual canopy polygons created using threshold value of simple ratio index (SRI)

Since the canopy of the low-density orchard had only just started to close, this method could be used successfully to derive data from individual canopies. Some work was required to separate polygons where trees had started to grow into each-other or the cover crop was too tall. Many of the weekly polygon layers also needed to have their geometries fixed, as ground control points were not used, to ensure the coordinate integrity of the images. By the middle of the 2021-2022 season, a large proportion of the canopies had grown into each other, likely due to the correct nutrition available to the trees in this season. As a result, the canopy polygon method of extracting canopy VI and thermal values became impractical. This was due to the large number of canopies that could not be turned into an individual polygon. For the remainder of the trial, the threshold raster images were used to create canopy only images of each VI image (Figure 3.8).

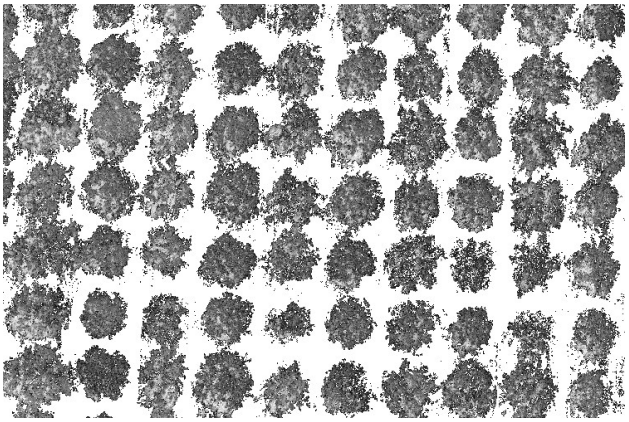

Figure 3.8 Normalised difference vegetation index (NDVI) orchard image with all non-canopy pixels removed.

A grid polygon layer was then aligned to the canopies (Figure 3.9). Due to the orchard not being planted in completely straight rows, some trees violated the 10 x 10 m spacing. Some trees at the edges of the orchard did not, therefore, align with the grid. Since the VI image contained nothing besides pecan canopy, most grid blocks contained only data from a single canopy and empty space. Blocks that contained parts of other tree canopies were removed.

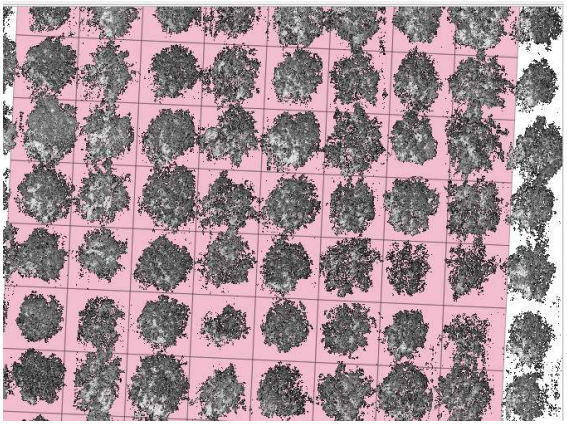

Figure 3.9 Grid aligned to individual canopies, used to extract average vegetation indices (VI) and thermal canopy values.

The average VI value of each canopy was found using the “Raster Statistics for Polygons” function in QGIS, with the polygon layer as the specifying grid for the earlier images and the aligned grid for the later images, and all the VI layers as the inputs. In this way all the VI layers could be processed at once with a single shapefile layer. The output was a single new shapefile layer with the VI value of each tree for each VI listed in the Attribute Table of this new layer in QGIS. Each tree on the original shapefile layer was previously given a label as a new attribute, this carried over to the output shapefile to allow identification of individual trees. The attribute table of the output shapefile was copied to a Microsoft Excel spreadsheet (Microsoft Corporation, Redmond, WA, USA), where the labels, which corresponded to the water stress trial tree identification, allowed VI and thermal data to be matched with individual canopies.

The thermal layer captured by the Micasense Altum was also processed in Pix4D. Pixel values of thermal image corresponded to degrees Celsius. It was assumed that software provided an accurate radiometric correction of the thermal data for background temperature and atmospheric absorption and scattering. The final thermal data was, therefore, not manually corrected. The average temperature of each canopy was extracted using the same process, threshold image and polygons as for the VIs.

Each weeks’ image was processed separately from beginning to end, threshold images and polygon layers were not carried over. Had ground control points been used, this would not be

as critical. This process of creating a threshold raster would, however, still need to be conducted several times during each season to account for canopy growth and the effects of the crop load on the canopy structure.

An alternate, and possibly simpler, approach to separating tree canopies from the background would have been the use of a Digital Elevation Model (DEM), which would have allowed canopies to be easily distinguished based on height. However, a DEM with a high enough resolution could not be generated with the software available. The tall grass and weeds that were present in the orchard at some points during the season would also have proven a complicating factor.

3.4 Field Water Stress Data Collection

Field data was collected from the trees of the UP pecan water stress trial on the same days as the remote sensing data was collected. To assess the water stress status of the trees and provide a possible reference point for the remote sensing data, both Ψ_{Midday} and stomatal conductance (g_s) at midday were measured. Measurement trees during the first season of data collection were the well-watered control, and the current stress treatment trees of the water stress trial (these trees change with each phenological stage) to provide a range of stress values. During the second season, because a second operator was available to collect Ψ_{Midday}, the centre tree of every treatment and replicate were able to be measured for Ψ_{Midday} within approximately an hour. Midday SWP was collected by covering three selected leaves on each tree with a foil covered plastic bag half an hour before measurement, which was conducted with a Scholander type pressure chamber (PMS Model 600, PMS instrument company, Albany, OR, USA). Stomatal conductance was measured on five leaves of each tree using the LI-600 combination porometer/fluorometer (LICOR, Lincoln, NE, USA) during the first measurement season only, as it was decided at the start of the second season to collect Ψ_{Midday} data of all treatment trees in the orchard. Had g_s been measured as well, the time difference between the first and last measurement would have been large enough for environmental conditions to change significantly, preventing measurements from being directly compared. The instrument also measured leaf temperature and photosynthetic pigment fluorescence. However, the parameters of interest were g_s and leaf temperature. It was not always possible to collect accurate T_{leaf} with the LI-600 due to changes in the sun angle during the period it took to measure all trees.

4 WATER STRESS DETECTION BY VEGETATION INDICES

4.1 Introduction

Vegetation Indices (VIs) have been found to be critical to the processing of remote sensing data, primarily for their use in separating the vegetation or crop in question from the background. However, most VIs were designed to highlight or quantify a specific property of the target vegetation (Xue and Su, 2017) by a sensitivity to specific sections of the reflectance spectrum relevant to vegetation, or the relationships between different sections of the spectrum. This gives them a greater utility than just a processing aid. Amongst the more indirect plant properties that quantification by VIs has been applied to is water stress. However, the results have been largely inconclusive. The ability of a VI to detect water stress depends to great degree on the physiological and physical response of the crop to water stress, because there is no way in which a VI can directly measure water stress, it therefore, detects the response of the plant. The most success has been achieved in crops which show a dramatic response to water stress that causes a change in the VI value of the crop. An example includes the ability of the NDVI, which is sensitive to plant health and photosynthetic rate, by quantifying the reflected red light, to detect water stress in almond (Zhao et al., 2017b). Another is the ability of VIs which are sensitive to canopy structural properties to detect stress in grapevine (Zarco-Tejada et al., 2012), a crop which wilts under water stress. Some VIs are also sensitive to chlorophyll content, which declines in some plants under water stress (Pirzad et al., 2011). Since pecans do not wilt under water stress, VIs which are sensitive to canopy structure are not expected to be able to detect water stress. VIs which are sensitive to the absorption of photosynthetic radiation, or chlorophyll content are expected to be better able to detect water stress, although chlorophyll probably only declines under long term stress (Wells, 2017). Canopy reflectance is known to be affected by a number of factors external to the plant, or dependent on the structure of the specific canopy (Jackson and Huete, 1991), this has been shown to be important in almond, where NDVI could only detect differences in the water status of canopies that were captured in an image at the same time and when data from different days was compared, scatter made it impossible to find a trend (Zhao et al., 2015). This would not be unexpected from this study, where there was a high variability in both canopy structure and daily conditions.

The aim of this section of the study is to determine whether any correlation exists between any of the VIs correlate with field measured water stress in pecan, in the form of Ψ_{Midday} or g_s, and if any of the VIs tested will relate well enough to water stress to reliably allow their use to detect water stress for the purpose of scheduling irrigation. It is hypothesised that at least

some of the VIs will correlate with water stress, most likely NDVI or indices derived from it, or indices based on the chlorophyll adjusted red-edge indices. These promise the best results after a study of the literature (Zarco-Tejada et al., 2013; Zhao et al., 2017b).

4.2 Materials and Methods

The VI values for each individual canopy, obtained as described in chapter 3.3, were plotted against the corresponding average midday stem water potential (Ψ_{Midday}) and stomatal conductance (g_s) for that tree, obtained as described in chapter 3.4. Separate plots were created for each measurement season, due to the differences in the nutritional status of the trees between the two seasons. No g_s data was collected during the 2021/22 season, to accommodate a greater number of Ψ_{Midday} measurements within a reasonable duration of midday. All data from all measurement dates were plotted together, to give only two plots in total for each VI, one for each season. The 2020/21 plot only included data collected between February 2021 and April 2021 as the UAV only became available in February. The correlation coefficient (r^2) of the plots were used to determine whether a relationship exists between each VI and Ψ_{Midday}.

4.3 Results and Discussion

The results of the attempts to detect water stress using common VIs have reaffirmed previous findings to a large degree, which found a large variability in the ability of VIs to detect water stress, with most VIs tested being unsuccessful on grapevine, olive and almond (Baluja et al., 2012; Zarco-Tejada et al., 2013; Zhao et al., 2017b). No meaningful correlation was found between any of the VIs and the plant-measured water stress indicators, ψ_{midday} and g_s. This was observed during both seasons of data collection, as can be seen in Figure 4.1, Figure 4.2 and Figure 4.3.

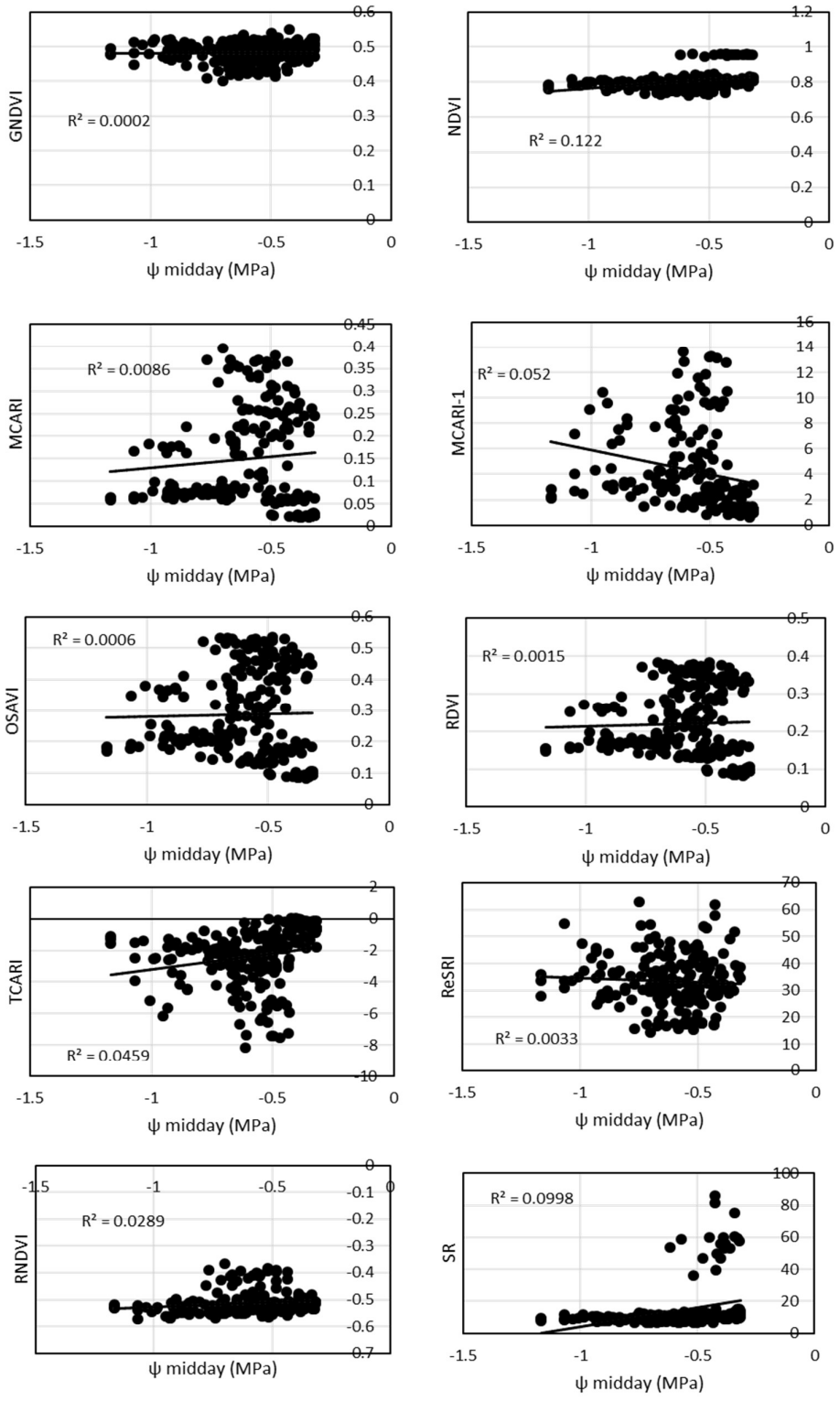

Figure 4.1 Relationships between vegetation indices and midday stem water potential (ψ_{midday}) collected during the 2020/2021 season. Data was collected from 20 trees on 6 days.

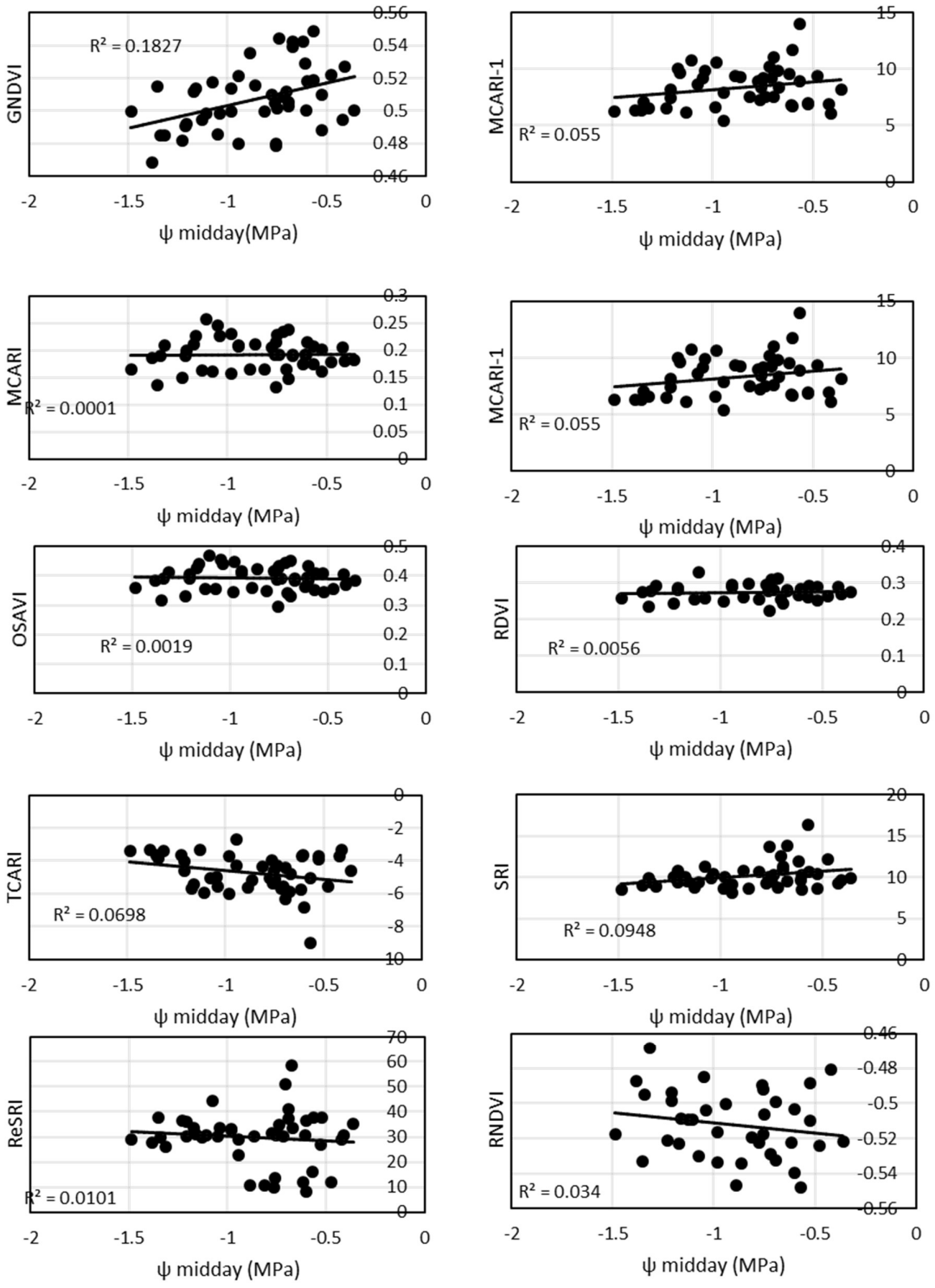

Figure 4.2 Relationships between vegetation indices and midday stem water potential (ψ_{midday}) collected during the 2021/2022 season. Data was collected from 8 trees on 12 days

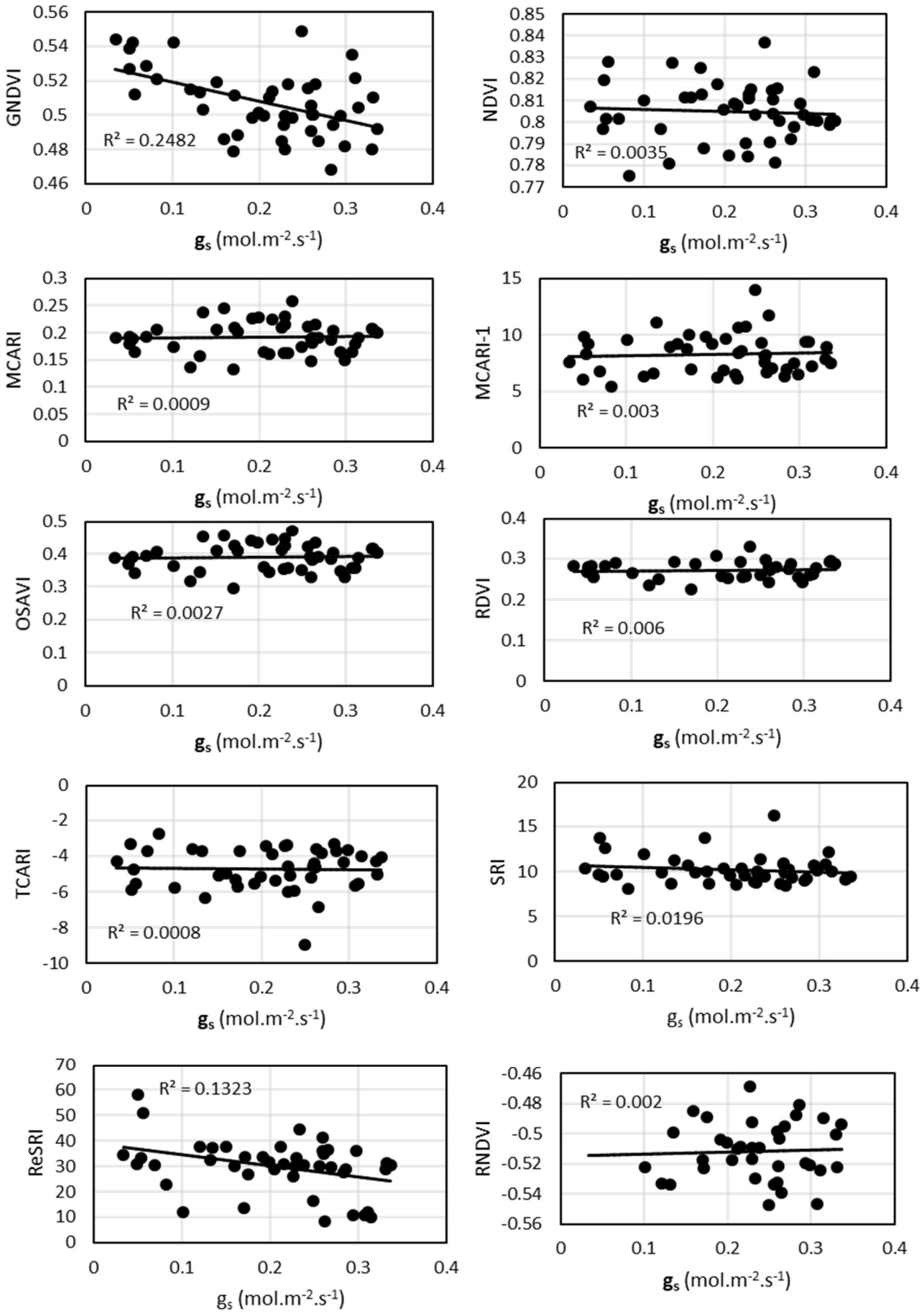

Figure 4.3 Relationships between vegetation indices (VIs) and stomatal conductance (g_s) collected during the 2020/2021 season. Data was collected from 20 trees on 6 days.

If taken in isolation, data collected between February and April 2021 (Figure 4.2), suggests that there may be some correlation between the VIs; GNDVI and ReSR, and ψ_{midday} and g_s. However, when considering the larger dataset collected during the 2021/2022 season, it was evident that no real relationship existing between VIs and ground measurements of plant stress, as the R^2 values for these relationships were very low. This agrees with what has been found in other crops, where some correlation was observed between specific VIs and water stress, with most other VIs showing very little correlation with stress. In cotton, a slight relationship was found between water stress and NDVI (Bian et al., 2019). In grapevine, promising VIs included GNDVI, SRI, MCARI, NDVI and TCARI (Baluja et al., 2012), while another study found only NDVI to have a moderate relationship with water stress, and the other VIs to be ineffective (Zarco-Tejada et al., 2013). NDVI was also found to be a good predictor of water stress in almond (Zhao et al., 2017b), but only for individual flights. An absolute NDVI value was found to have a weaker relationship with water stress when canopy NDVI and water stress data collected at different times of day were tested together (Zhao et al., 2017a). The relatively poor performance in pecan of many of the VIs that were found to be effective in other crops may be explained by the morphological response to water stress of pecan trees. It was observed early on that mature pecan leaves do not wilt under water stress, nor do they drop their leaves unless water stress is very severe (Sparks, 1989). Thus, water stress generally causes no structural change to pecan canopies. Therefore, as expected, VIs which indicate structural changes in canopies, such as the RDVI and OSAVI (Broge and Leblanc, 2001), did not correlate well with water stress in pecan, while they may have been found to be effective in crops which do wilt, such as grapevine (Baluja et al., 2012). While not causing any changes to the structure of the canopy, water stress has been found to reduce the chlorophyll content of pecan leaves (Wells, 2017). It would, therefore, be expected that VIs which are sensitive to leaf chlorophyll content, such as TCARI and MCARI, and those that quantify photosynthetic activity, like NDVI, would be sensitive to water stress. However, this was found not to be the case (Pirzad et al., 2011). It has been found in several species that there may actually be an increase in chlorophyll content under a low level of water stress, while chlorophyll only decreases significantly under severe water stress (Pirzad et al., 2011). Indices that respond to chlorophyll, would, therefore, not show a linear relationship with the level of water stress. Some indication of this can be observed in Figure 4.3, on the OSAVI, TCARI, RDVI and RNDVI plots. Importantly, due to unusually high rainfall in both seasons, a high level of water stress (Ψ_{midday} <1.5 MPa) was not achieved, which could have created sufficient contrast between well-watered and stressed trees to find a reasonable correlation between VIs and measurements of plant stress. Despite this, it seems unlikely that VIs could detect mild stress in pecan orchards that would ordinarily trigger irrigation events.

Vegetation indices are affected directly by environmental factors external to the target vegetation, which include solar radiation intensity, aerosols in the air, longwave or diffuse radiation and illumination angle, that is, the angle of the sun incident on the canopy (Jackson and Huete, 1991; Suomalainen et al., 2021). Some of these sources of error, such as incoming solar radiation intensity, can be corrected for during pre-processing (Kingra et al., 2016). If not adequately corrected, the only way to reliably use multispectral remote sensing data would be to only compare data collected at a single point in time, to ensure that all environmental variables are the same. To test whether inadequate atmospheric correction was responsible for the large scatter and lack of correlation observed in some of the VI plots in Figure 4.1, Figure 4.2 and Figure 4.3, data from a single flight was plotted independently against ψ_{midday} (Figure 4.4). The day chosen was 24 February 2021 as there was a large variation in the water stress values observed, including both heavily stressed and unstressed trees. Poor correlations were found between the VIs tested and water stress, indicated by ψ_{midday}, even though all atmospheric variables were constant. A significant challenge with this approach is the collection of sufficient data to be able to test the assumptions. All water stress data must be collected within a short space of time, as it is known that both canopy reflectance and plant water stress parameters can change within a period of time as short as an hour (Ishihara et al., 2015). It is possible that the small number of data points may be responsible for the lack of correlation observed, if more data points were to be collected at the same time, relationships between VIs may become apparent.

A major weakness of this study is the variability in the times of remote sensing data collection. Differences in flight times result in differences in solar zenith angle during the flights. This means that during each of the flights during the season, the tree canopies were illuminated from a slightly different angle. This results in changes in the reflectance of light from the canopy detected by the camera, and ultimately the value of any VIs calculated (Ishihara et al., 2015; Jackson and Huete, 1991). The effect of illumination angle on the VI value is further complicated by diffuse radiation incident on the leaves (Ishihara et al., 2015). Due to the high rainfall during the 2021/22 season, some flights were conducted on overcast days, data from which were not used, or when there was partial cloud cover. Data from canopies that were visibly shaded were not used, however, it is likely that longwave radiation interception varied greatly between flights and even between canopies at the same time, due to intermittent cloud cover during the flight. It has also been found that the effect of illumination angle on VI values is affected by the amount of diffuse radiation present, and that the effect is not the same for all VIs (Emmel et al., 2020; Ishihara et al., 2015).

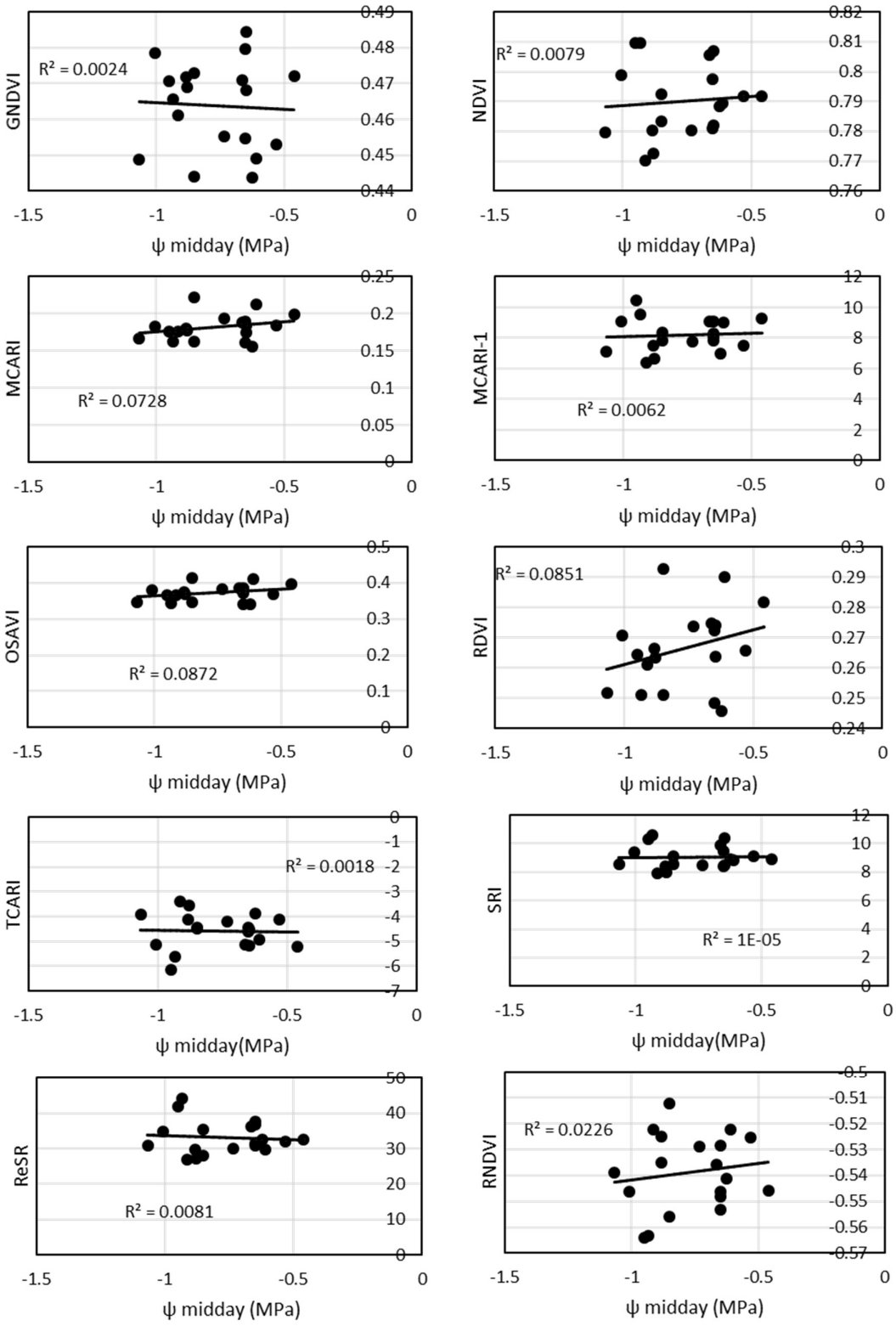

Figure 4.4 Relationships between vegetation indices (VIs) and midday stem water potential (ψ_{midday}) collected on 24 February 2022

Canopy properties, including architecture and leaf area index (LAI), also have an impact on the average canopy reflectance, and therefore the VI values calculated from the reflectance (Emmel et al., 2020). There are two factors that affect light reflectance from a canopy. The first is light scattering within a canopy (Emmel et al., 2020), and the second is the amount of soil reflectance transmitted through the canopy to the sensor above (Zhao et al., 2017b). The more heterogenous a canopy is, the greater the scattering of incident radiation within the canopy before being reflected back to the sensor. This allows for greater absorption of photosynthetically active radiation (Emmel et al., 2020), changing the ratio of red to near infrared (NIR) light reaching the sensor (Jackson and Huete, 1991), which will affect VIs that use these bands. A more vertically oriented canopy will also scatter more of the incoming radiation horizontally, and less directly towards the sensor directly above, changing the average reflectance of the canopy in most bands (Jackson and Huete, 1991). Many VIs have also been found to be exceptionally sensitive to LAI, indeed, VIs like those derived from the Soil Adjusted VI and the RDVI are used primarily to detect canopy density and biomass, often quantified by the LAI (Broge and Leblanc, 2001). Since the canopies making up a pecan orchard are usually not completely homogenous, especially in a canopy that has not closed into a hedgerow, they can be expected to vary greatly in both architecture and density. Such canopies cannot, therefore, be realistically expected to show correlations between VIs and an external factor such as water stress. Some of these problems can be solved by comparing the change in the VI value of individual canopies to measured water stress, rather than the absolute VI value. This will automatically take into account the properties of each canopy, and allow them to be compared with each other across different days without the properties of the canopy having too big an effect. To use this method, VI values are required that are of a high enough quality that they can be compared across days, which was not the case in this study.

Besides the canopy properties that affect the ability of the VIs to detect water stress, the intrinsic quality of the data may also be to blame. It was assumed that the commercial software used to convert the radiation entering the multispectral sensor into reflectance values for each pixel was accurate, and that the quality of the incoming radiation and atmospheric distortion was taken into account using data from the calibration panel image and UAV-mounted radiation sensor. It is possible that this was not the case and that the reflected radiation was distorted on the way back to the sensor (Amigo and Santos, 2020), or there was some error in the preprocessing that did not accurately render the reflectance values.

4.4 Conclusions

Considering the above, it is not surprising that no correlations could be found between any of the VIs and water stress. The VI value of an individual canopy depends on too many factors that cannot be easily corrected for, or accounted for statistically (Broge and Leblanc, 2001; Zhao et al., 2017b). Factors that prevent VI values being compared across different dates or times of day include the angle and the quality of the incoming radiation (Emmel et al., 2020; Ishihara et al., 2015). These can be mitigated to some extent by ensuring that the conditions under which data collection flights take place remain as constant as possible. The two main, controllable factors to consider are illumination angle and predominant radiation type. The illumination angle is made constant by choosing a solar zenith angle to use throughout the measurement period, ideally solar noon, to minimise shadows (Ishihara et al., 2015). The solar azimuth angle cannot be controlled, as it changes through the year. Controlling radiation type would imply choosing either cloudless days, or complete cloud cover, to collect all data under. Both have their advantages; on cloudless days, there is better reflectance back to the overhead sensor and better canopy illumination overall, while on overcast days, illumination angle does not have to be considered (Ishihara et al., 2015). The best way to minimise individual canopy differences that prevent canopies being confidently compared even when data was collected together, is to choose data collection trees that are as similar as possible with regards to canopy size, LAI and architecture. The relative success of VIs at detecting water stress in field crops and grapevine may possibly be attributed to the homogeneity of these crops (Baluja et al., 2012; Bian et al., 2019).

Besides tree properties and atmospheric conditions, removal of background pixels also plays a role in the accuracy of average canopy VI values. It was found in almond that the correlation between water stress and NDVI was related to the threshold value chosen to exclude the background (Zhao et al., 2017b). A looser threshold allowed interference from soil pixels, when these were removed by using a tighter threshold, water stress was able to be detected using the NDVI (Zhao et al., 2017b). It is likely that a similar effect could have occurred in this study. Due to the height of the interrow vegetation on many of the data collection days, setting a threshold to completely remove the background, necessitated removing pixels within the pecan canopy. This would have introduced the bias of the thresholding VI into all the VI data. Differences in illumination angle on different days also meant that portions of the canopy were removed, or background pixels included on some days, and not on others. The differing LAI of the canopies chosen was also further complicated by the effects of soil moisture on soil reflectance. For the same LAI value, different amounts of soil reflectance is transmitted through the canopy depending on both soil moisture and illumination angle, where the soil is

lit differently (Broge and Leblanc, 2001). The plastic sheets used to exclude rainfall from the stressed treatment trees also most likely had a very different reflectance to the soil and weedy backgrounds of the rest of the orchard, adding further complexity.

5 WATER STRESS DETECTION BY THERMAL REMOTE SENSING

5.1 Introduction

Under water stress, amongst the first responses of plants is stomatal closure to reduce transpirational water loss (Hsiao, 1973). This results in an increase in leaf temperature, due to the absence of transpirational cooling. The temperature of a leaf can, therefore, be used to quantify water stress (Idso et al., 1981). However, leaf temperature (T_c) is also heavily influenced by atmospheric variables, the most important of these being the air temperature (T_a) and vapour pressure deficit VPD (Idso, 1982; Maes et al., 2011). The canopy temperature is corrected for air temperature using the stress degree day, which is the difference canopy and air temperature (T_c-T_a) (Idso et al., 1981). This parameter can be effective at detecting water stress in areas where there is very little variation in VPD throughout the season (Idso et al., 1981; Testi et al., 2008).

Since leaf temperature is dependent on both T_a and VPD, in addition to the level of water stress, there can be no meaningful direct relationship between canopy temperature and water status of the tree when compared over different days. The crop water stress index (CWSI) was therefore developed (Jackson et al., 1981). This index uses the difference between the canopy and air temperature adjusted for VPD using the following formula (equation 2.11 in chapter2):

$$\mathbf{CWSI} = \frac{(\boldsymbol{Tc} - \boldsymbol{Ta}) - (\boldsymbol{Tc} - \boldsymbol{Ta})\boldsymbol{LL}}{(\boldsymbol{Tc} - \boldsymbol{Ta})\boldsymbol{UL} - (\boldsymbol{Tc} - \boldsymbol{Ta})\boldsymbol{LL}}$$

The lower limit ((T_c-T_a)$_{LL}$) is the difference between canopy and air temperature of a canopy transpiring at the maximum rate over the range of VPD conditions. The upper limit ((T_c-T_a)$_{UL}$) is the difference between canopy and air temperature when no transpiration takes place. It should be a constant value across all atmospheric conditions.

The methods used to determine (T_c-T_a)$_{LL}$ and (T_c-T_a)$_{UL}$ can be divided into the non-water-stressed-baseline (NWSB) and the empirical methods. The NWSB is a plot of the T_c-T_a as a function of VPD, with the lower limit on the day being the T_c-T_a found from the NWSB using the VPD at the time. Empirical methods of finding the (T_c-T_a)$_{LL}$ at the time depend on the temperature of a representation of a fully transpiring canopy being available at the time. This can be in the form of the temperature of a wet reference surface measured with the same instrument used to measure T_c (Maes and Steppe, 2012), or the temperature of the coolest of the pixels of the thermal image of the crop on the day (Baluja et al., 2012). The empirical

methods must fully take into account all the conditions affecting T_c on the day, not just T_a and VPD, as is the case with the NWSB. A further problem with the NWSB is that the bias of the conditions under which the data for the NWSB was first collected are introduced into the CWSI. The empirical methods can, therefore, be expected to perform better when used to calculate the CWSI, even though the protocols to collect the empirical lower limits are not yet fully developed using UAV remote sensing (Maes and Steppe, 2019). The accuracy of the empirical lower limit depends, to a large extent, on the accuracy of the thermal sensor used and the methods of extracting the canopy temperature from the orchard thermal data.

The upper limit value is temperature dependent, but it is not critical to account for this as long as actual T_c-T_a of the crop falls below this value, it is, therefore, in practice, often taken as a constant value (Maes et al., 2016). Methods often used to calculate $(T_c\text{-}T_a)_{UL}$ of a crop include the negative VPD method (Idso, 1982), the artificial reference surface method (Maes et al., 2016), the stressed canopy method (Sammis et al., 1988), and the thermal histogram method (Bian et al., 2019). The negative VPD method tends to perform well for some crops (Testi et al., 2008), but yields an upper limit that is far too low for many others, which is likely to be the case in pecan, as was found with most tree crops {Sammis, 1988 #68}. The other methods are more empirical, directly measured from pecan leaves or canopies, so will likely perform better when used to calculate the CWSI. An arbitrary positive T_c-T_a may also be used, so long as all data points fall below it, which has been shown to be successful (Maes and Steppe, 2012), which will probably be found here as well.

The aim of this section of the study is to determine whether water stress, as measured using ψ_{midday}, can be detected in pecan using the remotely sensed thermal indices, T_c-T_a and the CWSI. The best method of collecting the relevant data and calculating the CWSI will also be determined. It is hypothesised that the CWSI will correlate well enough with water stress, when using any of the empirical methods to calculate it, to be used to schedule irrigation. The NWSB will likely have a weaker relationship with water stress, as will T_c-T_a. This is due to the failure to incorporate the effects of all environmental conditions in real time.

5.2 Materials and Methods

5.2.1 Finding the lower limit of the CWSI

The measured non-water-stressed-baseline was created using hourly canopy temperature data from the tower mounted IR radiometers in the Vaalharts orchard study site, and air temperature and VPD data from the nearby weather station. Only canopy temperatures between the start of October and the end of March were used during both seasons of measurement, to ensure that data was collected only from trees in full leaf, and no soil or other background temperature was included. It was assumed that due to good farm management and measurements of $\Psi_{predawn}$ every 4-6 weeks that the trees were not water stressed. Initially, all data collected in full daylight (8:00 to 4:00) was used to create the non-water stressed baseline (NWSB) plot. A second plot using only data collected between 11:00 and 14:00 was created. This was to comply with best practice mentioned in the literature to remove error caused by dramatic changes in sun angle (Garrot et al., 1993; Testi et al., 2008). This ensured that the pattern of sunlight incident on the canopy within the footprint of the IR radiometers remained relatively constant. Hourly T_c points where rainfall was recorded were removed. The equation of the linear regression line of each season's plot was taken as the NWSB for that season. The NWSB of each season was used individually to calculate the CWSI for that season; and tested against the field measured water stress data. A combined NWSB using data from both seasons was also tested by comparing the CWSI against the plant stress data. This was to determine if accuracy was improved when considering the unique conditions of the season or if including as much variation as possible through the data of two seasons would yield better results.

The lower limit of the CWSI was found by using the temperature (T_{wet}) of an artificial reference surface placed just outside the UP pecan orchard within the UAV flight path as the T_c component of the $(T_c\text{-}T_a)_{LL}$. The wet reference surface consisted of a thin polystyrene sheet, covered in white cloth, floating in a pan of water. The cloth wicks water from the tray as water evaporates from the cloth. The temperature value extracted from the thermal image of the cloth covered board was taken as T_{wet} on the day. The T_a component of the lower limit value was obtained from the second automatic weather station placed in the orchard which logged data every 20 minutes.

The statistical histogram of the thermal raster image was also used to determine T_{wet}. As with the artificial wet reference surface method, the process was conducted separately for each thermal image. The T_{wet} value was taken as the lower edge of the normal distribution of the

thermal images which contained only pecan canopies, with the background removed, to prevent wet soil or free water temperatures being used. An example of the thermal histogram is shown in Figure 5.1. Air temperature was taken from the in-orchard weather station.

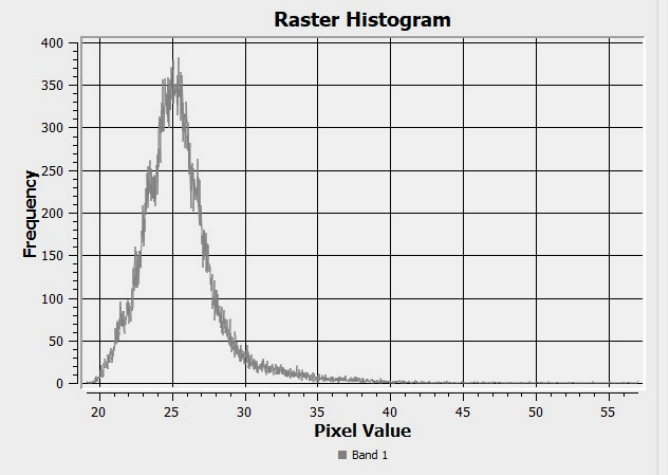

Figure 5.1 Raster histogram of thermal pecan canopy images, showing a normal distribution, used to derive the limits of the crop water stress index (CWSI)

5.2.2 Finding the Upper Limit of the CWSI

Several methods were attempted to find the UL, including the negative VPD method (Idso, 1982), the artificial reference surface method (Maes et al., 2016), the stressed canopy method (Sammis et al., 1988), and the thermal histogram method (Bian et al., 2019).

The negative VPD method used the NWSB created using data from the IR radiometers at the Vaalharts study site. The upper limit equation from the NWSB requires the T_c-T_a intercept of the NWSB and the saturated vapour pressure at air temperature, and T_a plus the intercept, which is negative (equations 2.14 and 2.15). Two approaches can be used to find the upper limit on a particular day when the CWSI will be calculated. Either the actual air temperature on the day can be used, or an arbitrary high temperature can be used to derive a static upper limit that will be applied as a constant value. Both approaches were considered. The CWSI was calculated using the NWSB upper limit calculated using the temperature on the day, and 50˚C was chosen as the arbitrary temperature for a constant upper limit. This value was chosen as it is sufficiently high to encompass the highest air temperatures experienced in Pretoria, while still being a realistic temperature.

An attempt was also made to calculate the upper limit using a highly stressed pecan canopy, that has stopped transpiring. In August 2021, six trees in the high-density part of the orchard were selected, and the ground was covered with plastic to exclude rain. Irrigation was completely withheld. These trees are not part of the water stress trial, but they were included in the flight path of the weekly flights so that thermal data was available from them. However, due to the high rainfall experienced during the season, the required level of stress was not achieved at any point during the season, as shown by both weekly Ψ_{midday} and g_s measurements.

Trees in the high-density orchard section were also used for destructive upper limit measurements. This entailed severing a leafy branch at the terminal point of the previous year's growth during the hottest part of the day, to ensure that transpiration stopped as fast as possible. The branch was then hung back in the canopy in the approximate original position using heavy duty adhesive tape, to simulate the effects of all other environmental conditions on the leaves. Two cut branches were used on each measurement day. The LI-600 porometer was used to measure the g_s and leaf temperature of three leaflets on separate leaves on each branch at 10-minute intervals, starting immediately after the branch was cut, until two successive g_s measurements of zero were recorded. The temperature of the leaflets at this point were taken as an approximation of the temperature of non-transpiring leaves (T_{dry}). It, however, quickly became apparent that the measured g_s and T_a values of the individual leaflets showed extreme variation, likely due to the position in the canopy and the differences in behaviour of sun and shade leaves. Because only individual leaflets were measured, this variation could not be confidently combined into a single T_{dry} value for each branch on each measurement day. It was also found that the sun angle changed significantly during the period from branch cutting to zero g_s, this resulted in part of a severed branch or the whole branch becoming completely shaded before transpiration stopped. Using the T_{dry} from these branches would not accurately take into account the effect of direct solar radiation on the temperature of the non-transpiring leaf. A handheld IR thermometer would likely have yielded a better result by aggregating the temperature of the entire severed branch, including the tiny environmental variations experienced by each individual leaflet.

The raster histogram method was used on each thermal image to calculate the upper limit as well, by finding T_{dry} and using T_a from the weather station. The method used was identical to that used to find T_{wet}, except that the maximum normally distributed thermal pixel value was used instead of the minimum.

The published upper limit for pecans was also tested. The values found by Sammis (1988) using the severed branch method and a handheld IR thermometer was $(T_c\text{-}T_a)_{UL}$ equals 6˚C for a branch fully exposed to the sun, and 4 ˚C for a branch tied back into a closed canopy. Since it has become common to use 6˚C as an arbitrary upper limit (Baluja et al., 2012), and the canopies in UP pecan water stress trial orchard had only just begun to grow into each other, $(T_c\text{-}T_a)_{UL}$ = 6˚C was used to calculate the CWSI.

5.2.3 Testing the CWSI

The CWSI was calculated for each day where both thermal data and field data was available. The CWSI was then plotted against Ψ_{midday} for both seasons and g_s for the first measurement season. All data collected during each season was plotted separately, a combined plot of both seasons data was also created. This gave one Ψ_{midday} vs CWSI plot for each season, a g_s vs CWSI plot for the 2020-2021 season and a combined Ψ_{midday} plot. These plots were created for each of the methods used to calculate the CWSI. The combinations of the lower and upper limits used to calculate the CWSI are summarised in Table 5.

Table 5.1 Methods used to calculate the CWSI

Lower Limit	**Upper Limit**
NWSB	$(T_c\text{-}T_a)_{UL}$ = +6˚C
T_{wet} from Artificial Reference Surface, T_a from weather station	$(T_c\text{-}T_a)_{UL}$ = +6˚C
T_{wet} = coolest pixel, T_a from weather station	T_{dry} = warmest pixel, T_a from weather station

The 2020-2021 plots only included data collected between February 2021 and April 2021 as the UAV only became available in February. The correlation coefficients (R^2) of the plots were used to determine whether a relationship exists between the CWSI and the field measurements of stress.

5.3 Results and Discussion

5.3.1 T_c-T_a

The importance of taking T_a and VPD into account when determining the level of water stress using canopy temperature is illustrated by Figure 5.2**Error! Reference source not found.** Beside the low correlation between water stress, as quantified by ψ_{midday}, and canopy temperature alone, it can also be observed that leaf temperature data points collected on certain days are grouped together. This suggests that there are factors apart from water stress alone that influences the temperature of the individual leaves and the canopy as a whole. The relationship between the stress degree day (T_c-T_a), which attempts to correct for the effect of air temperature on canopy temperature, and ψ_{midday} is not particularly strong, as shown in Figure 5.3. T_c-T_a typically only relates well to water stress in areas where VPD remains stable throughout the season, which is not the case in Pretoria. Therefore, T_c also has to be corrected for VPD at the time of measurement before being used as a detector of water stress.

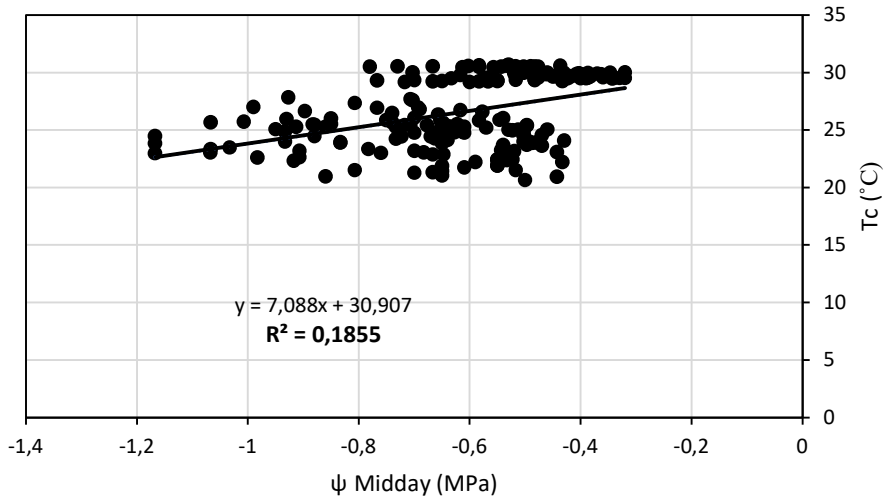

Figure 5.2The relationship between canopy temperature (T_c) and midday stem water potential (ψ_{midday}), showing the problems with using leaf temperature alone to detect water stress. Data was collected from 18 trees over 10 days during the 2021/22 season.

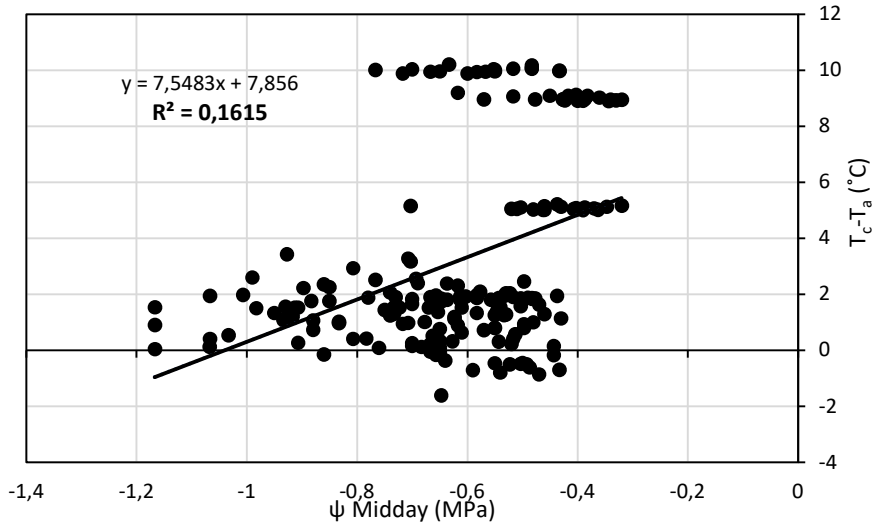

Figure 5.3 Relationship between the difference between canopy and air temperature (T_c-T_a) and midday stem water potential (ψ_{midday}), showing that correcting for T_a alone is not sufficient for detecting water stress. Data was collected from 18 trees over 10 days during the 2021/22 season.

In Figure 5.3 it is evident that there are several groups of points where the canopy temperature is far higher than the air temperature at the same ψ_{midday}. These correspond to days with unusually low VPD compared to the rest of the season, 29 October 2021 (VPD = 0.81 kPa) and 22 January 2022 (VPD = 1.29 kPa) . Under low VPD, there is a low rate of gaseous exchange, and therefore cooling, due to a smaller vapour pressure gradient between the interior of the leaf and the atmosphere, even under low water stress and open stomata (Idso et al., 1981; Maes and Steppe, 2012). The thermal sensor was also found to be overestimating canopy temperatures, an issue that was encountered throughout both seasons of measurement, which skewed the data. This could be related to the relatively low resolution of the thermal camera compared to the multispectral camera that was used to separate trees from the background. This likely resulted in many mixed pixels at the edge of the canopies, so that background temperature was included in the canopy temperature. It could also be related to an error in the calibration or processing software of the sensor.

Figure 5.3 shows several data points collected under non-stressed conditions having a negative T_c-T_a, that is, the canopy temperature is lower than the air temperature, this is exactly what is expected (Idso, 1982). However, there are several points that fall within the stressed range. These points were collected on a day with a very high VPD, 10 March 2022, which had the highest VPD of all the days that data was used. Under high VPD, atmospheric demand is

so high that enough transpiration takes place even with a degree of stomatal closure for there to be a leaf cooling effect (Maes and Steppe, 2012). It may also be linked to a quirk of the pecan stomatal control regime (Andersen and Brodbeck, 1988) . It has been found that summer flush pecan leaves have more stomata and a greater stomatal conductance under the same conditions than spring flush leaves. As the leaves get older, higher water stress and VPD is needed before stomatal closure occurs (Andersen and Brodbeck, 1988). This would mean that, later in the season, there would be a greater transpirational cooling effect, and lower T_c-T_a, under the same set of conditions, than earlier in the season. It is, thus, apparent that some method is required to correct for VPD, in addition to air temperature, to allow for the detection of water stress using canopy temperature.

5.3.2 The Non-Water-Stressed-Baseline (NWSB)

The oldest method used to correct the canopy temperature for both the air temperature and the VPD is the NWSB. The individual NWSB plots from each season are presented in Figure 5.4 and Figure 5.5.

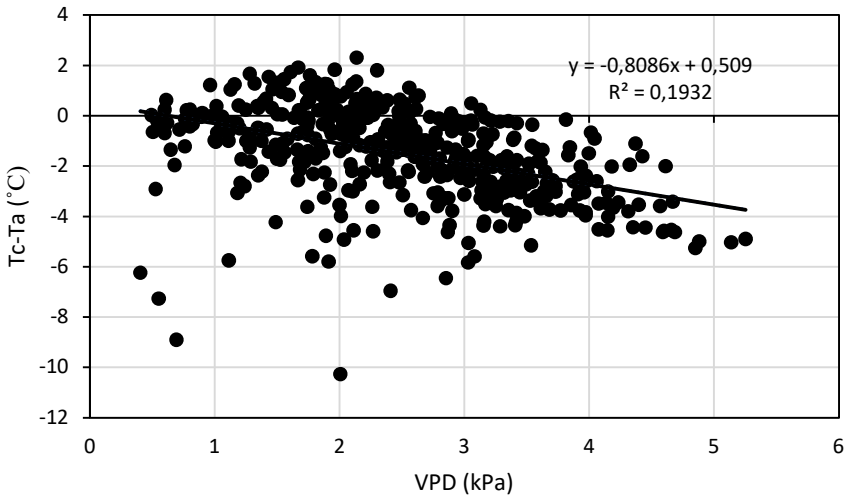

Figure 5.4 Non water stressed baseline (NWSB) plotted from data collected during the 2020/21 season at the Vaalharts site. T_c-T_a is the difference between canopy and air temperature. Canopy temperature data was measured using infrared radiometers.

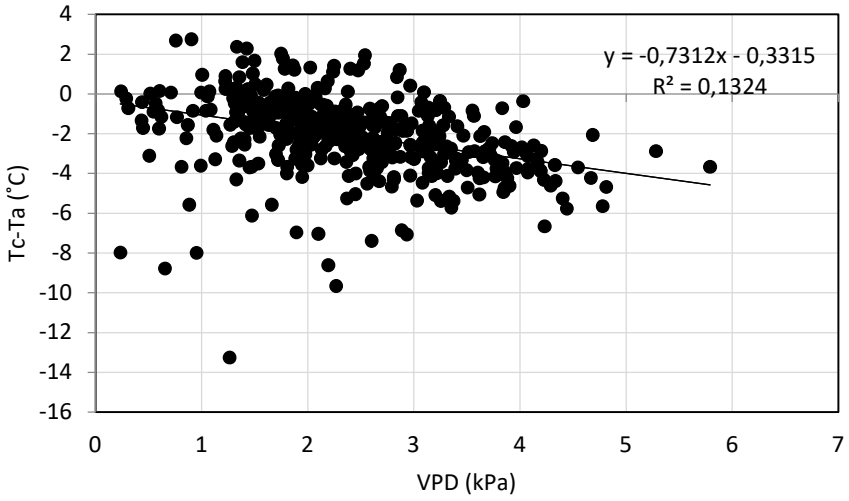

Figure 5.5 Non water stressed baseline (NWSB) plotted from data collected during the 2021/22 season at the Vaalharts site. T_c-T_a is the difference between canopy and air temperature. Canopy temperature data was measured using infrared radiometers.

The data in both Figure 5.4 and Figure 5.5 was only from between 11:00 and 14:00 during the part of the season when the canopy was in full leaf. This was to ensure that only leaf temperatures were measured, and not the soil or bare bark, and to ensure that were no extreme changes in solar angle or intensity in the measurement period. It can, therefore, be assumed that the NWSBs represent the canopy transpiring at the maximum rate for the conditions. The intercept of the 2020/21 NWSB was slightly positive, while the 2021/22 NWSB was slightly negative. This may be explained by the prevailing conditions during the season. The intercept of the NWSB is the T_c-T_a at a VPD value of zero, or a completely saturated atmosphere, at which very little gaseous exchange takes place between the interior of the leaf and the atmosphere (Idso et al., 1981). A negative intercept means that, under a saturated atmosphere, the air temperature is higher than the canopy temperature, so there is still a slight cooling effect. If the intercept is positive, it means that, in a saturated atmosphere, gaseous exchange is so low that canopy temperature rises above air temperature, even without any water stress. This may be due to the effects of solar radiation and wind. With a higher wind speed, boundary layer resistance is lower, and there may still be a significant amount of transpiration, even in a saturated atmosphere. The higher the solar radiation, the more transpiration is required to lower the canopy temperature below the air temperature, an effect which is magnified in a saturated atmosphere, where VPD is no longer a consideration (Maes and Steppe, 2012). This means that if many data points were collected under such conditions,

they have the potential to change the gradient of the NWSB, making it slightly inaccurate under all conditions. The NWSB is also not the best method of correcting for T_a and VPD under saturated conditions due to this effect. Figure 5.6 is a combined NWSB using data from both seasons, where the intercept is almost zero. This supports the assumption that the differences in slope and intercept are due to the effects of seasonal conditions and are not characteristic of the crop. Many crops do have a NWSB intercept that is not zero (Idso, 1982), however, the pecan NWSB has been shown to be very close to zero (Garrot et al., 1993; Sammis et al., 1988), which supports the results found in this study.

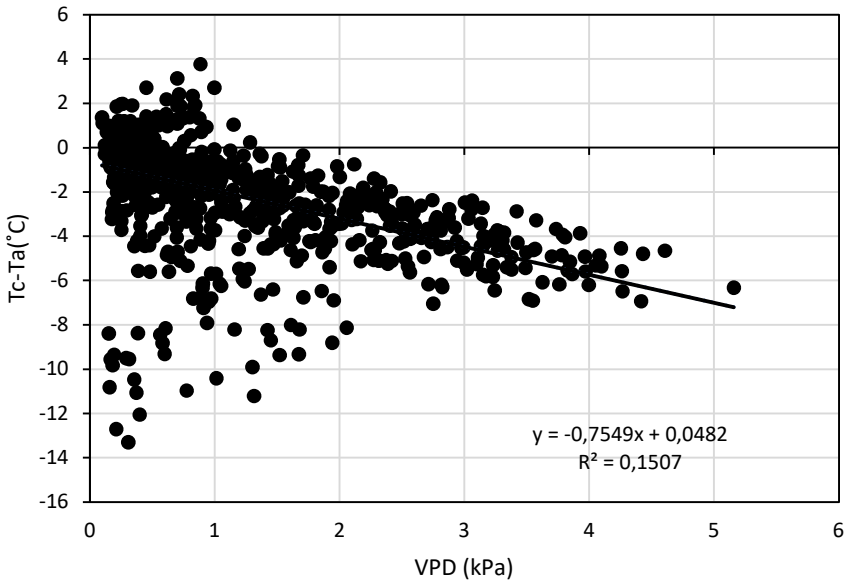

Figure 5.6 Combined non-water stressed baseline (NWSB) from both measurement season.

It can be seen in the NWSB plots from both seasons that there a number of points where the T_c-T_a is much lower than the majority of the points. It was found that most of these points represent measurements collected later in the season, when pecan leaves are known to have a much higher stomatal conductance, this effect is greater close to leaf senescence (Andersen and Brodbeck, 1988). A higher stomatal conductance, therefore, caused a greater cooling effect than would have been experienced under the same conditions at a different point during the season. There are two points during the season when the majority of leaves were relatively older, these are before the summer flush and towards the end of the season, when most of these data points were collected. Closer examination also revealed that several of these points were collected in the afternoon, when a sudden drop in VPD occurred, relative to the rest of the day. This could be the result of sudden, short, afternoon rainfall events that cooled the

canopy, but were too small to register on the weather station. No half hourly data points where rainfall was recorded were included in the final dataset.

To give a better understanding of the effects of insufficient attention to detail when creating the NWSB, Figure 5.7 and Figure 5.8 are presented. In Figure 5.7, only data from the morning and evening is used, when the solar zenith angle is large, and the stomata have not yet opened. The most obvious difference between Figure 5.7 and the correctly created NWSB in Figure 5.6 is the greater slope. This means that for every VPD value, the canopy temperature is much lower than the air temperature. However, this is not as a result of more efficient cooling by transpiration, but rather, a decreased solar heating effect. It therefore, does not reflect the conditions of the majority of the day, and such data should not be included in a NWSB used to quantify water stress.

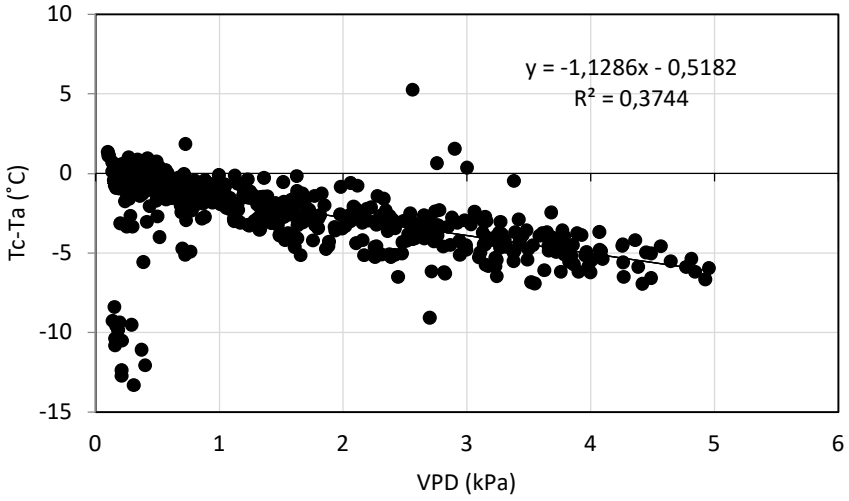

Figure 5.7 Non-water stressed baseline (NWSB) from the 2020/21 season using only data from the two hours after sunrise and two hours before sunset

The group of points observed in the low VPD range, having an extremely low T_c-T_a, were mostly collected in the evening, just before sunset. On these days, the air temperature remained high late into the day, above 34˚C on average between 17:00 and 18:00. The canopy cooled down at the usual rate as the sun set. The observed T_c-T_a was driven not by an exceptional level of canopy cooling, but rather by exceptionally high air temperature. Several of the group of points were also collected on unusually cool mornings. This suggests the possibility of dew, especially as VPD was close to zero. This provides further evidence against the inclusion of early morning and late afternoon data in a NWSB. Besides dew on the leaves

at these times of day, condensation on the sensor in the early morning may have resulted in a temperature reading that was much lower than what is possible for a plant leaf.

The impact of inaccurate estimates of canopy temperature on the NWSB due to the measurement of background temperatures (bark or soil) is presented in Figure 5.8. Data from two IR radiometers are plotted together, with one of them (open circles) measuring the temperature of a bare branch that was within the target canopy area. If this NWSB were to be used in the CWSI, the lower limit would have been above the actual canopy temperature.

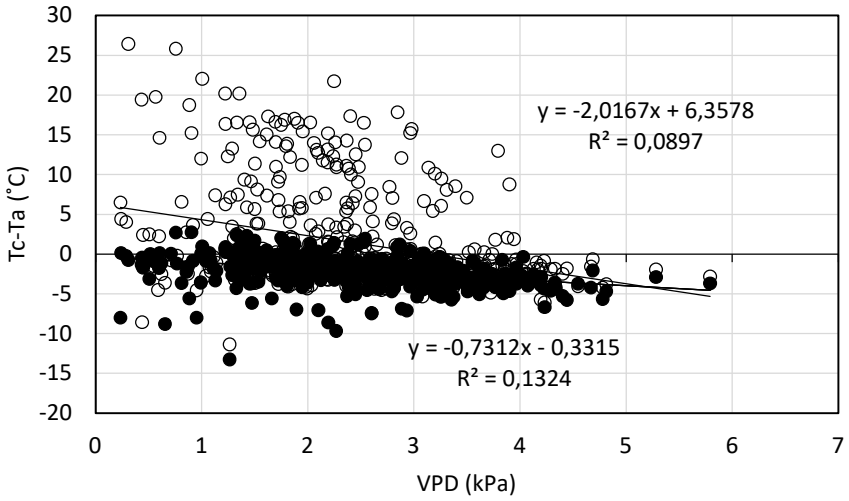

Figure 5.8 Non water stressed baseline (NWSB) from the 2021/22 season including data from the infrared radiometer detecting the temperature of a bare branch within the canopy (indicated by open circles)

The above figures may provide an explanation for many of the outliers that are to be found in the NWSBs that were used, which ultimately impacted on the NWSB equations that were used in the CWSI. In future, it may be useful to statistically remove outliers, as they are very likely not the result of temperatures measured from dry leaves transpiring at the potential rate. A method which may be used successfully is the DBSCAN method, this categorises the data according to the distance from the trend and clustering of the rest of the data. It is appropriate as it does not assume a normal distribution of the data, or categorise outliers based on the mean, which has no relevance to the NWSB.

5.3.3 The Crop Water Stress Index

All canopy temperatures used to calculate the CWSI were collected by the UAV based thermal sensor, with orthomosaicing in Pix4D Fields and extraction of canopy temperatures in QGIS. The $(T_c\text{-}T_a)_{LL}$, or the $T_c\text{-}T_a$ of a canopy transpiring at the potential rate was calculated using the NWSB and the thermal image histogram (Bian et al., 2019). The $(T_c\text{-}T_a)_{UL}$ was found using the image histogram and a static Upper Limit of $T_c\text{-}T_a$ = +6˚C was also tested (Maes et al., 2016; Sammis et al., 1988). The negative VPD method of finding the Upper Limit yielded an Upper Limit of approximately +0.1˚C between canopy and air temperature on all the days it was tested. It was found that the thermal sensor consistently provided data that was above the plausible surface temperature for the conditions, likely as a result of the inclusion of mixed background-canopy pixels due to the low resolution of the sensor, or incorrect emissivity calibration or correction by the sensor software. Hence, all canopy temperatures, and the CWSI limits from the thermal image histograms are overestimated. The same images were used for the canopy temperatures and the histogram limits. Therefore, the error was constant, and the histogram limits were used with the canopy temperatures. The histogram Upper Limit could not be used with the NWSB, and the Histogram Lower Limit could not be used with the static limit to calculate the CWSI. Therefore, the CWSI was calculated using data from the 2020/21, 2021/22 seasons and the two seasons' combined NWSB and $T_c\text{-}T_a$ = 6˚C as the upper limit. The CWSI was also calculated using both limits from the thermal image histogram. While not ideal, the thermal sensor canopy temperatures were used in all cases.

The CWSI was calculated for each measurement tree, using the data from each day. All the data collected throughout the 2021/22 season was used to calculate the CWSI and all CWSI from the entire season was plotted together against the corresponding ψ_{midday} (Figure 5.9).

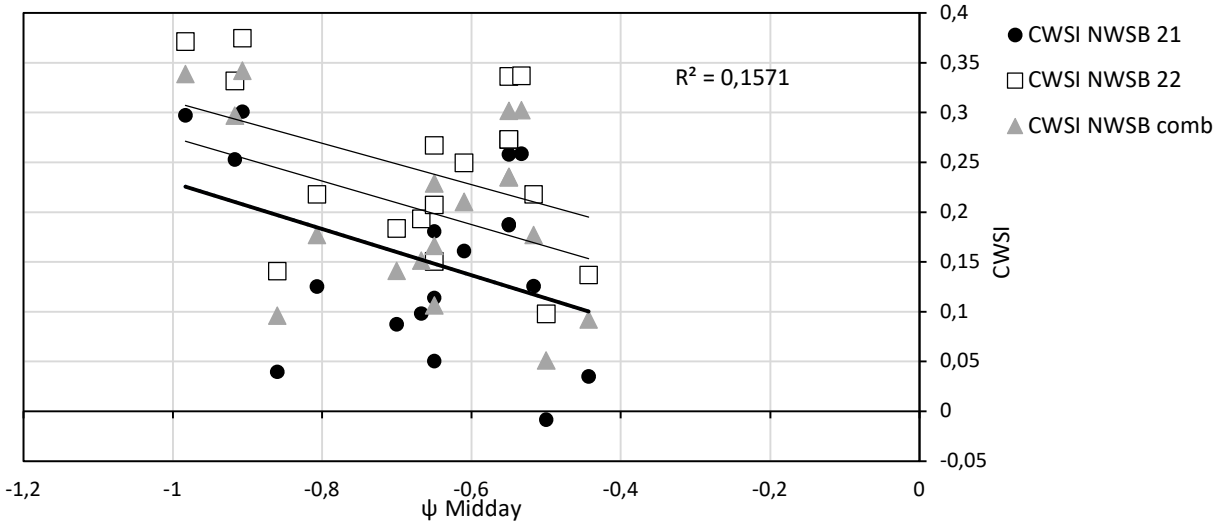

Figure 5.9 Relationship between the crop water stress index (CWSI) calculated using the non-water stressed baseline (NWSB) and the static Upper Limit for each season, and the midday stem water potential (ψ_{midday})

The NWSB created from data from each season were similar enough that they caused little difference in the ability of the CWSI to detect water stress, even though the actual value of the CWSI differed (Figure 5.9). In this case, the CWSI using the NWSB was found to be mostly unable to detect water stress. This may be due to an inherent inaccuracy in the thermal sensor, discussed earlier in this section. It may also be as a result of the variability in both time-of-day and environmental conditions during data collection. These include cloud cover and solar angle, which affect the temperature of the leaf without taking air temperature and VPD into account.

The CWSI calculated using the reference surfaces and the image histogram limits would be expected to perform better, if the problem with the NWSB method is the effect of factors such as radiation and windspeed on the day of water stress measurement are different to the conditions under which the NWSB was created. This was, however, not found to be the case when the entire season was plotted together, as Figure 5.10, Figure 5.11 and Figure 5.12 show.

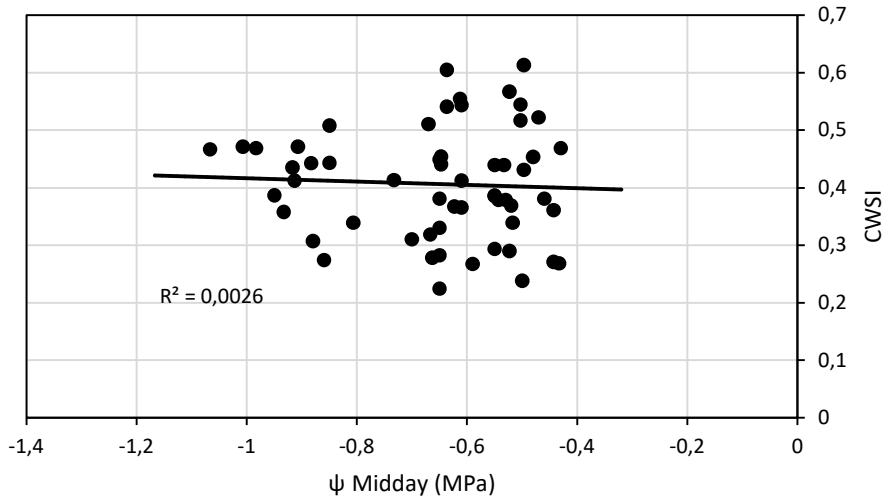

Figure 5.10 Relationship between the crop water stress index (CWSI) with a lower limit found from a wet reference surface and an upper limit of 6˚C, and midday stem water potential (ψ_{midday})

A possible explanation of the low correlation between the reference surface CWSI and ψ_{midday} is the difference in the illumination of the reference panel on different days, which the sensor system could not correct for. This is supported by data in Figure 5.11, which shows a slightly better correlation between the reference surface CWSI when a single day's data is plotted compared to several days in Figure 5.12.

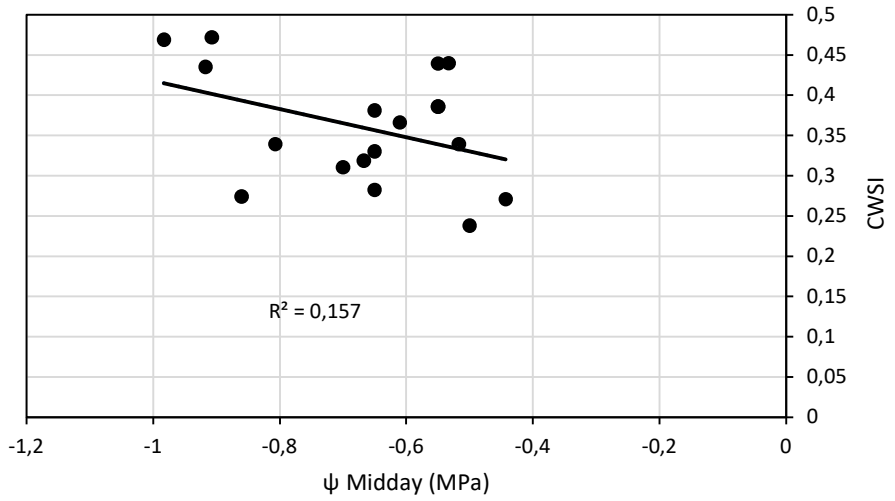

Figure 5.11 Relationship between the CWSI with a lower limit found from a wet reference surface and an upper limit of 6˚C on 13 April 2022, and midday stem water potential (ψ_{midday})

A very similar pattern was observed when the CWSI calculated using the thermal image histogram was tested for all data days (Figure 5.12), where a very low correlation was found, as opposed to a single day, where the correlation between ψ_{midday} and the CWSI was slightly better (Figure 5.11). Plotting the day from each measurement day individually may provide an opportunity to find the conditions under which a high correlation is achieved, and replicate these in future measurements. Plotting all data together may possibly nullify any correlation that is present between an individual day's water stress and CWSI data, in this study it is unlikely, as correlation appears to be low for all the data.

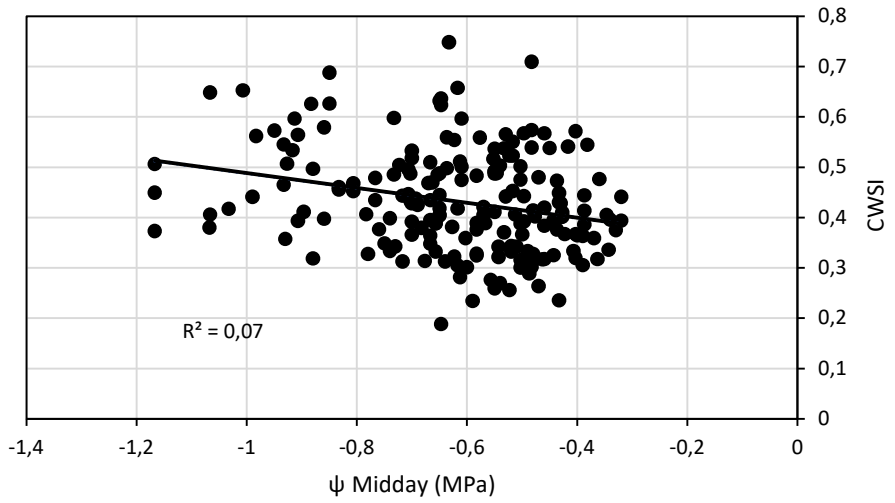

Figure 5.12 Relationship between the crop water stress index (CWSI) calculated using the thermal image histogram for both limits, and midday stem water potential (ψ_{midday})

The image histogram method does not use an external reference surface or NWSB to correct for the atmospheric differences at the time of data collection, accounting for VPD and other atmospheric parameters is achieved by directly using the extremes of the canopy temperature data (Bian et al., 2019). Therefore, there can be only two possible sources for the high variability observed in the temperature data. The first is a high variability amongst the trees that were tested, so that they responded differently to water stress in terms of the regulation of water loss and leaf temperature. The differences in canopy density would also have played a large part in the actual temperatures recorded by the thermal camera. Less dense canopies would have allowed more radiation reflected from the soil to reach the sensor than more dense canopies. Since soil, especially when dry, can have a much higher temperature than vegetation (Gago et al., 2015), this would have been a large source of variability in the data. A possible solution would be to use a thermal index, such as the Water Deficit Index (WDI) that accounts for the density of the canopy when using temperature to estimate water stress (Maes and Steppe, 2012). The other is inaccuracy in the sensor or the pre-processing software or methodology, so that environmental differences are able to influence the surface temperature recorded. This is more likely to be the cause of the inaccuracy observed in the thermal data. It was trusted that the preprocessing and conversion of the at-sensor brightness temperature (T_{br}) was accurately converted to true surface temperature by the commercial software, using data from the UAV-mounted radiation sensor and calibration panel. This is not the case. It would have been prudent to retrieve T_{br} from the thermal camera and process this data using background temperature (T_{bg}) data that was collected from an aluminium foil-covered reference panel imaged with the canopy. This would not have been too complicated,

as the canopy was closed and an emissivity of 0.98 or 0.99 could have been used. Using the canopy temperatures calculated using this T_{bg} may have yielded thermal water stress indices that correlated better with actual field-measured water stress. As the data cannot be corrected due to this data not being collected during flights, this approach should be used in future. Scattering and atmospheric absorption of the radiation reflected back to the thermal camera may also have distorted the data and provided an inaccurate T_{br} to begin with. When a commercial sensor is used in future, it would be prudent to manually correct for this using the air temperature, humidity and distance to the object (Maes and Steppe, 2012), although there are some that contend that these corrections are not needed when working with UAV data due to the short distance between the sensor and the surface (Berni et al., 2009b). This would have required the acquisition of additonal data and thus it is not possible to re-process the data. It is possible that, on a single day, not enough data was collected for any relationship to become apparent when all external conditions are the same. The fact, however, remains that no CWSI method could be found which was able to provide an indication of water stress under all atmospheric conditions, which is the purpose of the CWSI, particularly the more empirical methods, which do not rely on the NWSB.

5.4 Conclusion

Even though the NWSB performed marginally better than the empirical methods when the entire seasons' data was tested together, all the methods of calculating the LL yielded a CWSI that performed poorly as an indicator of water stress. When the CWSI data from individual days were tested against ψ_{midday}, they performed better than when the season's data was combined. This is evidence that there were factors that were not taken into account when correcting the thermal data, or the thermal data was not collected in a consistent manner over the season. The most likely explanation for this is that thermal data collection flights did not consistently take place when the sun was at the same angle relative to the trees and the reference surface. The flight times shown in chapter 3 support this. Canopy temperature was also, therefore, affected, in addition the reference surface temperature. This could explain the poor performance of the NWSB derived CWSI. Not enough data was collected on individual days to test the CWSI on a single day, to negate the effect of changing conditions.

Evidence that there is good potential to detect water with the CWSI using these methods is the fact that trends are present in all regression plots between the CWSI and ψ_{midday}, even though correlation was weak. To prove this, better quality data will be required, as well as better attention to the conditions under which data is collected.

6 YIELD ESTIMATION

6.1 Introduction

Various methods have been used to attempt to estimate yield by remote sensing. Attempts have been made to estimate yield directly from canopy characteristics, such as size, or change in size (Sarron et al., 2018). It is both logical, and well established, that the potential yield of a tree depends on the canopy size (Sarron et al., 2018; Zaman et al., 2006). Canopy size is often defined by the area of soil covered by the canopy, the height of the canopy, and the volume of the canopy. Alternatively, leaf area index (LAI) and canopy porosity may be used to quantify the density of the canopy. These parameters can assist with determining the amount of bearing wood present on the tree, and the carbohydrate production potential of the tree. It, therefore, makes sense to attempt to predict yield using canopy size. Some have taken a more indirect approach, relating the photosynthetic production potential available during the season, calculated from climatic data and historical records, to potential yield (Maselli et al., 2012). However, this approach does not take photosynthate partitioning into account, as yield may not necessarily correlate with the carbohydrate fixed over several seasons. Different proportions of photosynthate may be partitioned to vegetative growth than yield in different years. Pecans, in particular, are notorious for this, being alternate bearers (Wood et al., 2003). Alternate bearing can also prevent canopy characteristics being related directly to yield. A canopy of a particular size may not yield the same in an “off” year compared to an “on” year. Vegetation Indices (VIs) have also been used to estimate yield (Rahman et al., 2018; Robson et al., 2017b). They have been used to estimate yield directly, by quantifying changes to the overall reflectance of the canopy, caused by large bright-coloured fruit, such as oranges or mango (Robson et al., 2017b), but it is unlikely to be possible with pecan, due to pecans having shucks that remain green. Vegetation indices have also been shown to indirectly relate to yield in crops that are green when ripe, such as avocado and macadamia (Robson et al., 2017a), however, it is hypothesised that VIs are related to the health or the density of the canopy and nor directly to yield. The same might be true of pecan. Whichever the method attempted, alternate bearing, and conditions or events that have a drastic effect on yield, such as physiological disorders, weather events, and diseases, are likely to play an important role in the realised yield of pecan trees in any particular year. This will prevent the development of a simple relationship between yield and canopy characteristics or VIs for pecan.

The aim of this section of the study was to attempt to predict yield using remote sensing methods. Two methods were tested to this end. An attempt to predict yield using VIs, and an attempt to predict yield using a measure of canopy size. A further aim was to find and test a method of quantifying canopy size using UAV remote sensing. It is hypothesised that fractional

canopy cover will be a convenient metric of canopy size and will have a limited correlation with yield. Some of the VIs tested are expected to correlate with yield, particularly those that are sensitive to leaf chlorophyll content, as nuts are a different shade of green from a healthy pecan canopy.

6.2 Materials and Methods

Trees in the Innovation Africa@UP pecan orchard were harvested, during May and June of each season, when shuck dehiscence was complete, and leaf drop was nearly complete. Trees were harvested individually by shaking onto nets spread under the canopy. Nuts that dropped before shaking were collected by hand and added to the shaken nuts for each tree. The yield of each tree was collected individually and weighed. A total of 80 individual tree yields were collected for the 2020/21 season, and all of the trial trees during the 2021/22 season, for a total of 120, half the trees were 'Wichita', and half 'Western Schley'.

Three clusters of nuts were marked on each of the 60 trial 'Wichita' tree early in the season, soon after pollination. The number of nuts on each cluster were counted at least once during each of the pecan phenological stages (Sparks, 2005) to obtain an estimate of nut set and fruit drop during each stage.

The parameters used to attempt to estimate yield were fractional canopy cover (the fraction of the area allocated to the tree covered by the canopy), and the average canopy vegetation index (VI) value. Both these parameters were obtained as described in Chapter 3 for March and April 2021, and the entire 2021/22 season. Data from four days in the 2020/21 season (4 Mar, 10 Mar, 19 Mar and 14 Apr) and 10 days evenly distributed throughout the 2021/22 season (29 Oct, 17 Nov, 22 Jan, 09 Feb, 24 Feb, 10 Mar, 14 Mar, 24 Mar, 06 Apr, 13 Apr, 21 Apr) were plotted against the individual tree yield for the whole orchard, including both Wichita and Western Schley trees, for that season. Factional interception data from individual days were plotted separately. The correlation coefficient (R^2) was used to determine whether a relationship exists between fractional canopy size and yield for each date. The correlation coefficient was calculated for the relationship between the VIs and yield for each date individually, this was then used to find any relationships between VI and yield.

6.3 Results and Discussion

6.3.1 Canopy size as a predictor of yield

Since fractional canopy cover, that is, the proportion of the area of soil allocated to the tree that is covered by the canopy, was already available for the entire UP pecan orchard at regular intervals during both measurement seasons, an attempt was made to find a relationship between yield and fractional canopy cover. Various dates throughout both seasons, for which there was data available, were plotted separately against yield to find the point in the season at which canopy cover best relates to yield.

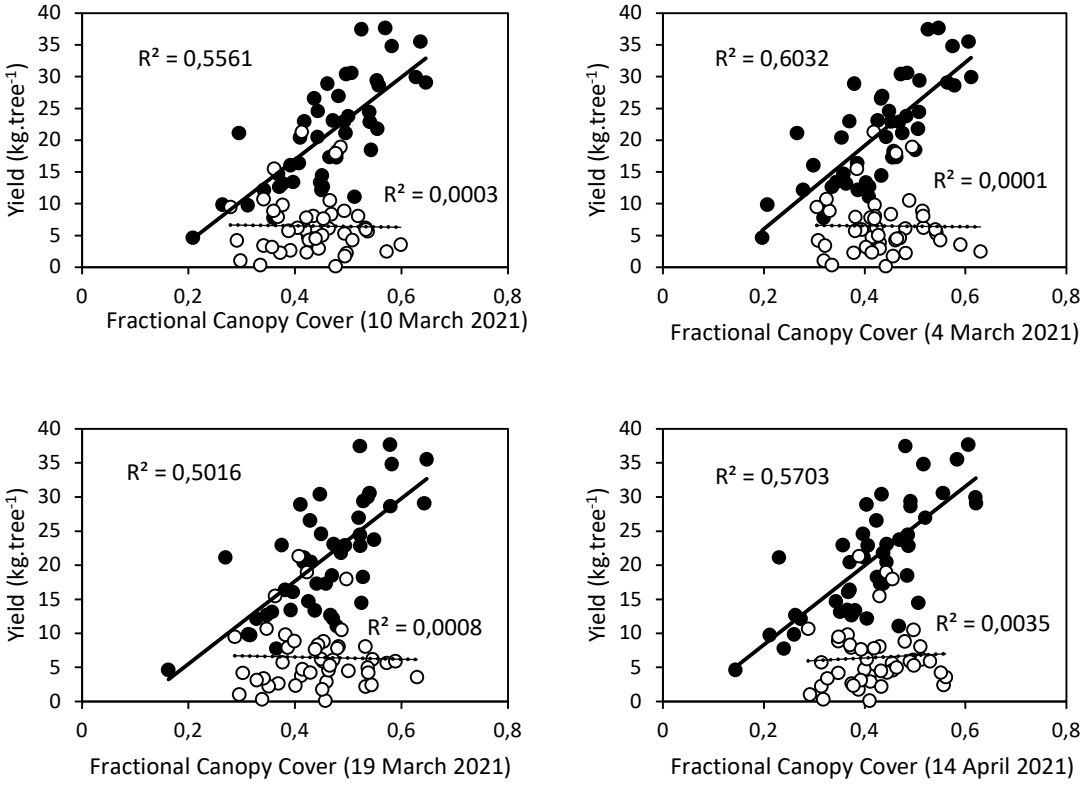

Figure 6.1 Relationship between individual tree yield (kg tree^{-1}) at the end of the 2020/2021 season and canopy fractional cover on four dates during the 2020/2021 season. Solid dots are for 'Western Schley' trees and open circles are for 'Wichita' trees.

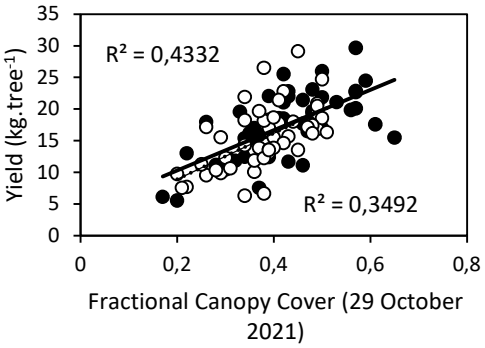
R² = 0,4332
R² = 0,3492
Yield (kg.tree-1)
Fractional Canopy Cover (29 October 2021)

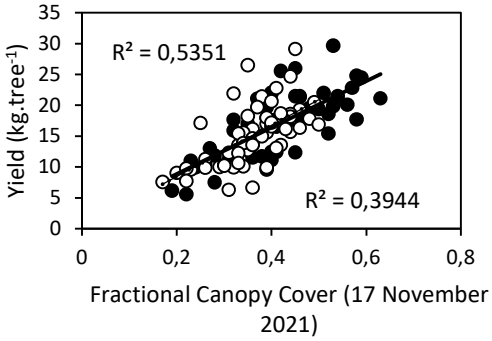
R² = 0,5351
R² = 0,3944
Yield (kg.tree-1)
Fractional Canopy Cover (17 November 2021)

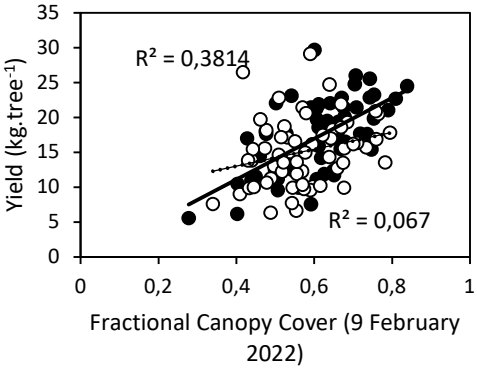
R² = 0,3814
R² = 0,067
Yield (kg.tree-1)
Fractional Canopy Cover (9 February 2022)

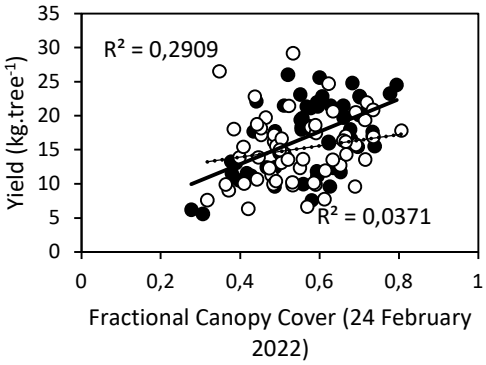
R² = 0,2909
R² = 0,0371
Yield (kg.tree-1)
Fractional Canopy Cover (24 February 2022)

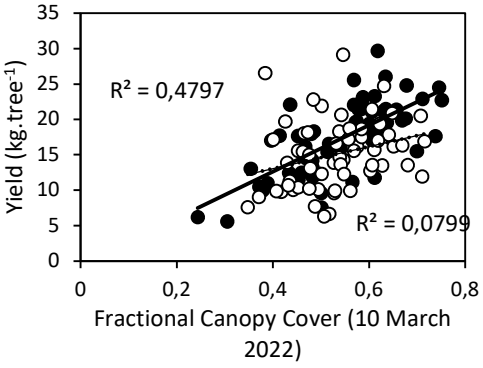
R² = 0,4797
R² = 0,0799
Yield (kg.tree-1)
Fractional Canopy Cover (10 March 2022)

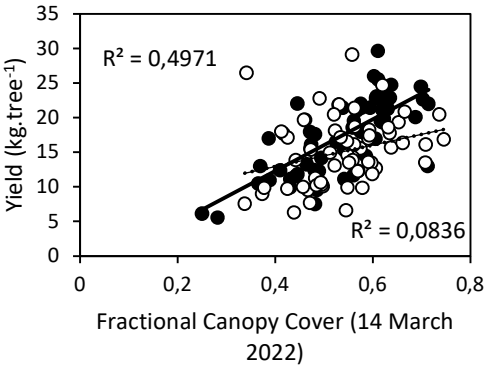
R² = 0,4971
R² = 0,0836
Yield (kg.tree-1)
Fractional Canopy Cover (14 March 2022)

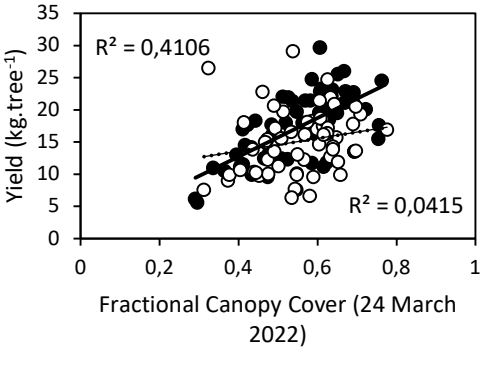
R² = 0,4106
R² = 0,0415
Yield (kg.tree-1)
Fractional Canopy Cover (24 March 2022)

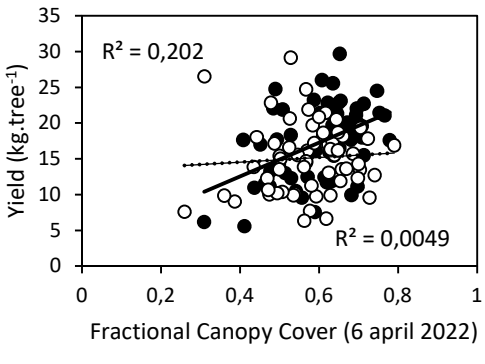
R² = 0,202
R² = 0,0049
Yield (kg.tree-1)
Fractional Canopy Cover (6 april 2022)

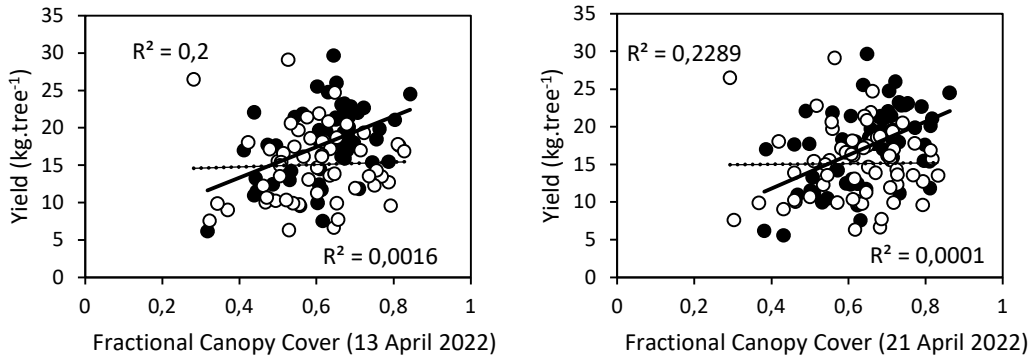

Figure 6.2 Relationship between individual tree yield (kg.tree^{-1}) at the end of the 2021/2022 season and canopy fractional cover on 10 dates during the 2021/2022 season. Solid dots are 'Western Schley' and open circles are 'Wichita'.

The most obvious observation from Figure 6.1 , in particular, is the large difference in the correlation between canopy fractional cover and yield between the two cultivars. In the 2020/21 season, the 'Western Schley' trees approached the potential yield for the size of the tree and it appears that the main determining factor for yield in this season, for 'Western Schley', is the size of the tree. Had other tree size parameters, such as canopy height and volume been taken into account, in addition to fractional canopy cover, tree size would likely have been found to be even better at predicting yield, as was found in mango (Sarron et al., 2018). However, it is very seldom that trees reach the potential yield for canopy size. This is due to both internal tree factors, and external management or environmental factors. The 'Wichita' trees during the 2020/21 season is a good example of this, as shown in Figure 6.1 , many large trees had a very low yield, or, at least, a much lower yield than a similarly sized 'Wester Schley' tree during the same season. This discrepancy in yield between the cultivars in Figure 6.1 are largely due to external factors, with some influence from internal factors. In such a case, tree size, or fractional canopy cover, cannot be used to predict yield with any accuracy, as yield is not determined primarily by the size of the tree.

The cause of the exceptionally low yield of the 'Wichita' trees in the 2020/21 season, on average 6.28 kg.tree^{-1}, that prevented the use of fractional canopy cover as a predictor of yield, was due to a physiological disorder known as water stage nut spilt. 'Wichita' is known to be highly susceptible to this disorder, while 'Western Schley' remains unaffected (Wood and Reilly, 1999), which was again shown in this study. Water stage split occurs when there is an influx of water into the kernel just as the shell of the nut begins to harden (Wood and Reilly,

1999). In this case, a heavy rainfall event was experienced in the week preceding shell hardeneing, which is highly typical of this disorder. The green shuck splits and the nut usually abscises (Figure 6.3). Evidence that water stage split was the main cause of yield loss in the 'Wichita' trees was provided by a nut count conducted on marked clusters on every tree that was part of the trial, before and after the shell hardening phase. Three nut clusters on each of the 60 measurement 'Witchita' trees in the orchard were monitored. Clusters consisted of, on average, 1.77 nuts before the event, while the average number of nuts on the same clusters afterwards was 0.84. This represents a decrease of 52% in the number of nuts in the sample clusters..

Figure 6.3 Water stage showing split and senescence, and eventual nut drop, all examples are 'Wichita' during the 2020/2021 season.

The 'Wichita' trees also showed both macronutrient and zinc deficiencies during the 2020/21 season. Unfertilised pecan trees are known to experience consecutive low yielding years until internal nutrient reserves are built up, when the tree then carries and ripens a crop very close to the potential yield for the size of the tree (Sparks, 2005). Adequate fertilisation every season

reduces the incidence of irregular bearing to some degree. However, pecans are known for alternate bearing, that is, alternate high and low yielding years (Wood et al., 2003), which was evident in the relationship between yield and fractional canopy cover for the 2021/22 season (Figure 6.2). In this season, the 'Wichita' trees show a relatively higher yield following the low-yielding 2020/21 season, while the 'Western Schley' trees had a reduced yield. The differences in the yields between the two seasons of both cultivars are presented inTable 6.1.

Table 6.1Average yield per tree (kg) of the two cultivars, 'Wichita' and 'Western Schley' in the UP pecan orchard during the two measurement seasons, and the percentage change in yield between the seasons

Cultivar	Average Yield (kg tree^{-1})		Average % Change/tree
	2021	2022	
Wichita	6.278	15.119	140.8
W. Schley	21.064	17.37	-17.5

The differences in the yields of the two cultivars can possibly be explained by the carbohydrate reserves of the trees (Smith and Samach, 2013; Sparks, 2005). During the 2020/21 season, the carbohydrate reserves of the 'Western Schley' were depleted due to a heavy crop load. An unusually heavy crop is known to induce an alternate bearing cycle in pecans, due to the high carbohydrate requirement to ripen the oil rich nuts (Sparks, 2005). Due to the oil-rich, carbohydrate intensive, nature of the product, a much lower crop weight, 21 kg.tree^{-1} in this case (Table 6.1), can induce alternate bearing than in a crop such as apple, where the fruit consists mostly of simpler carbohydrates (Anderson et al., 2021) This leaves the carbohydrate reserves of the tree depleted by the end of a high-yielding season, such as 2020/21. The 'Western Schley' trees, therefore, did not have the reserves to produce many female flowers at the start of the 2021/22 season, or set many of the female flowers that were produced. The 'Wichita' trees on the other hand were able to build up reserves, because there were very few nuts to be filled due to nut drop prior to the nut filling stage. This allowed them to set, and ripen, more nuts during the 2021/22 season, as proven by the nut count data from the 'Wichita' at the start of the seasons. In November 2020, the average number of nuts per sample cluster on unstressed trees was 2.2, while in November 2021, an average of 3.8 nuts per cluster was counted.The yield during the 2021/22 was, therefore, less affected by an external factor, and tree size played a greater role in determing yield. This was observed as a greater correlation between canopy fractional size and yield in 'Wichita' trees during the 2021/22 season. Even in an "off" year, however, the canopy size of the 'Western Schley' trees still correlated better with yield than that of the 'Wichita' trees. This would suggest that, in the Pretoria area at least, 'Witchita' has a lower yield to canopy size ratio than 'Western Schley', and any succesful prediction equation or model would need to treat cultivars separately.

One approach that can be used to take take into account the effects of alternate bearing and cultivar characteristics is the use of an adjustment factor to adjust the yield predicted from canopy size in years when ratio of yield to canopy size is lower than in years when the trees yield close to the potential for the size of the trees. This factor would adjust the yield predicted from canopy characteristics when an “off” year is expected, or based on the cultivar in question. This approach has been successfully used in mango (Sarron et al., 2018) and olive (Anderson et al., 2021; Maselli et al., 2012), where in a low yielding year or for a low potential cultivar, the y-intercept intercept of the regression curve developed in a high yielding year, or for a high yielding cultivar, is adjusted downwards, so that a tree of the same size will be predicted to yield less. An alternate bearing cycle is often synchronised by a major yield loss event (Anderson et al., 2021; Smith and Samach, 2013; Sparks, 2005), which was the case with the ‘Wichita’ trees in this study. This can be used to predict an “off” year, and the regression curve developed can be adjusted downwards to predict yield in the “off” year. Another approach would be to estimate or sample the crop load early in the season, and adjust the regression equation up or down based on the estimated crop to canopy size ratio, relative to that under which the regression equation was developed (Sarron et al., 2018).

Alternate bearing and cultivar are not the only factors that alter the canopy to yield ratio of an individual tree or orchard. Soil characteristics and microclimate also change the potential yield for a particular canopy size. This is a known phenomenon in pecan (Sparks, 2005), and is related to the heat accumulation, and temperatures at the start and end of the season, which are known to affect both the timing of bud break, and the start of the season, as well as the length of each phenological stage (Sparks, 2005). The water and nutrient holding capacity of the soil can also greatly affect the size of the crop that can be expected from a particular sized tree. This was well illustrated in the University of Pretoria’s pecan orchard during the 2020/21 season, as shown by the yield map of the orchard for that season (Figure 6.4).

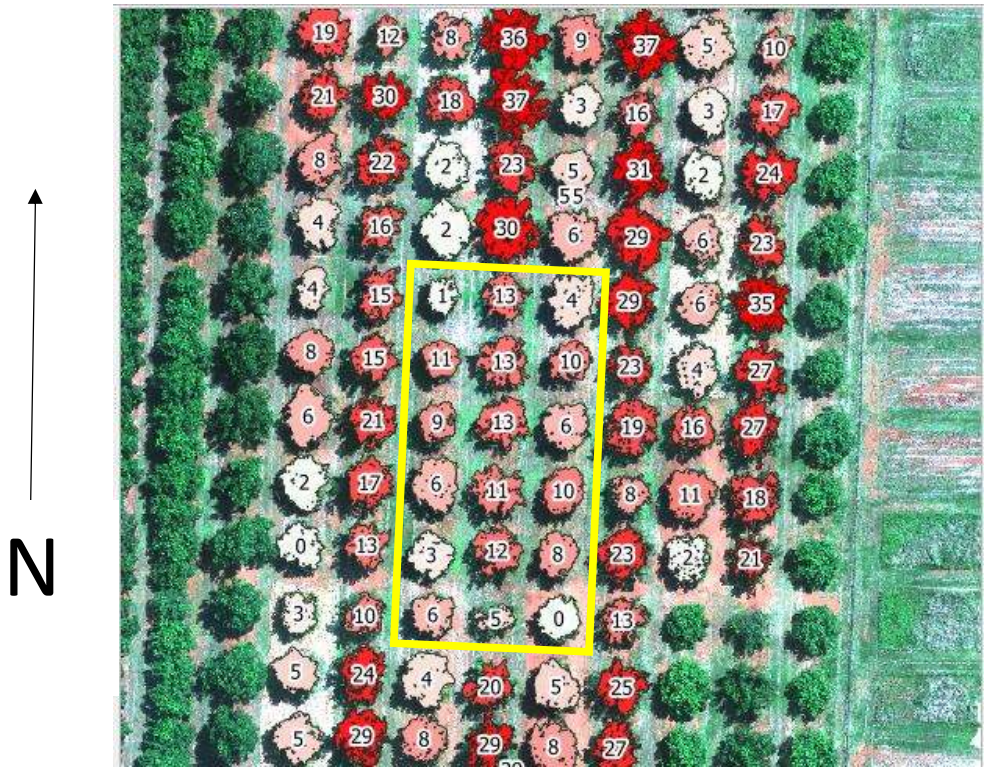

Figure 6.4 Yield map of the UP pecan orchard from the 2020/2021 season, rows of 'Wichita' and 'Western Schley' alternate, with the first labelled row on the right-hand side (Eastern side) of the image being 'Western Schley'. Labels are in kilograms harvested from the tree, and intensity of shading corresponds to yield.

The first observation from Figure 6.4 is the visual difference in yield between the alternating rows of the two cultivars, due to the reasons explained above. The yield loss caused by water stage split is easily understood when a high yielding canopy of the same size is found next to a tree which had a good yield. The effect of soil type is shown by the large section in the centre of the orchard (the area in the yellow block in Figure 6.4), where the 'Western Schley' trees in this section of the orchard had a lower yield than the 'Western Schley' trees on the edges of the orchard. These two yield zones correspond almost exactly to subsoil type. The edges on the orchard have a uniform red soil from just below the top horizon up to at least a metre deep, while the lower soil horizons in the low yielding centre of the orchard consist of a stoney yellow soil. The potential yield for canopy size, is therefore, lower in this area than the edges of the orchard, and this has to be taken into account, and treated separately when making a yield estimation. Reasons for the yield disparity between the soil types may be related to the drainage characteristics of the soil, or barriers to root penetration (Sparks, 2005). It is of interest that the 'Wichita' trees were not as affected by water stage split in the area where the 'Western Schley' trees were low yielding. This suggests that the central area of the orchard had a greater water holding capacity or worse drainage than the rest of the orchard. It has

been found that water stage split is greater when trees on a drier soil experience an influx of water, such as a heavy rainfall event (Wood and Reilly, 1999). This area of the orchard was, therefore, likely wetter before the heavy rain. The ‘Wichita’ trees had a greater yield in this area due to a reduced incidence of nut split, while the ‘Western Schley’ yield could have been reduced because of an intolerance to water logging (Sparks, 2005).

In order to successfully estimate yield using canopy size, there must be a proper understanding of the various factors that affect the potential crop that a particular canopy size can carry, both in general, and in a specific season (Anderson et al., 2021). In this study, the effects of a major yield loss event, alternate bearing, cultivar, and soil variability were experienced in just two seasons. It is, therefore, imperative that a sufficiently large dataset be available to capture the variability, and allow an understanding of its effect on yield, before canopy size can be used to predict yield. The expertise of an individual with an understanding of the crop is also beneficial when deciding on an adjustment factor, for the prediction equation to be used in the season in question, to account for the canopy size to yield ratio in a particular year (Sarron et al., 2018).

Both Figure 6.1 and Figure 6.2 show that the best time of the season to capture the canopy size to be used for yield estimation of ‘Western Schley’ in Pretoria is the early to middle part of March. This is what would be expected, as at this point in the season, the summer vegetative flush is complete, so the canopy is at its maximum size for the season, and senescence has not yet begun. The fact that the the summer vegetative flush and the developing nuts act as competing carbohydrate sinks may also contribute to March being the best time of year to use canopy size to estimate yield (Smith and Samach, 2013). A larger crop load should, in theory, reduce the vegetative growth during the summer flush, as it occurs during stages of high sink strength for the nut, that is nut sizing and later nut filling (Smith and Samach, 2013; Sparks, 2005). For ‘Wichita’, the canopy size in mid November, towards the end of the spring flush, was found to correlate best with yield, when water stage split was not a factor, and canopy size was the greater determinant of yield, as observed during the 2021/22 season, It is possible that trees with more carbohydrate reserves, both set more nuts and grew more at the start of the season. The discrepancy found in March probably relates to the summer flush and sink competition between nuts and vegetative growrh.

To test whether the sink competition could be used to estimate yield, the change in canopy size between the start of the 2021/22 season and the middle of March 2022 was plotted against yield (Figure 6.5). This figure shows that, as expected, the greater the yield, the less the canopy size increased during the season. Lower yielding trees had more photosynthates

to partition towards vegetative growth and therefore showed a greater increase in canopy size than higher yielding trees, which had a greater demand from the crop load. However, the relationship between change in canopy cover and yield is not particularly strong for either cultivar, and a lot of scatter was observed (Figure 6.5). This may be attributed to the fact that larger canopies have the potential to grow more, in absolute canopy cover terms, than smaller canopies. To solve this, the percantage change in fractional canopy size relative to the fractional canopy cover observed at the end of October 2021, when a full canopy was first achieved for the season, was plotted against yield, this is shown in Figure 6.6.

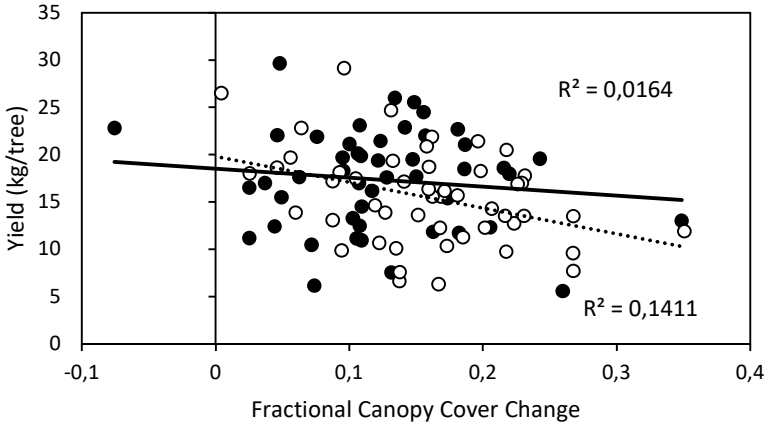

Figure 6.5 Individual tree yield (kg) of the two cultivars in the UP pecan orchard as a function of the change in fractional canopy cover. The open circles, dotted trendline and R^2 at the bottom of the figure represent 'Wichita', while 'Western Schley' is shown as the solid dots and trendline, with R^2 at the top of the figure.

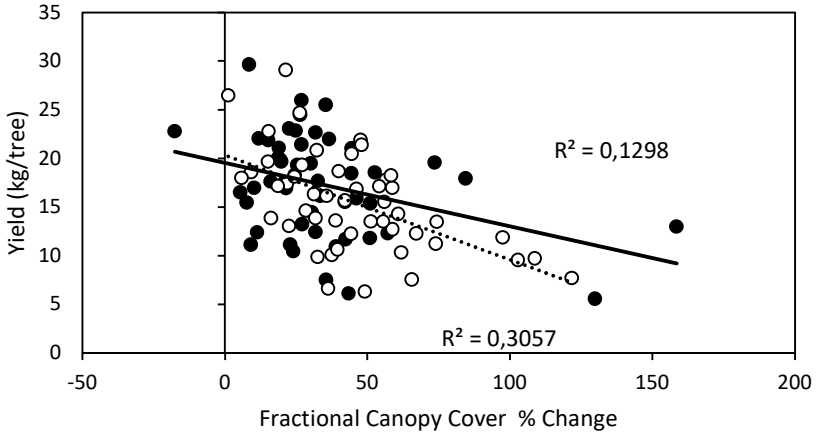

Figure 6.6 Individual tree yield (kg) of the two cultivars in the UP pecan orchard as a function of the percentage change in fractional canopy cover. The open circles, dotted trendline and R^2 at the bottom of the figure represent 'Wichita', while 'Western Schley' is shown as the solid dots and trendline and R^2 at the top of the figure.

As expected, a better correlation between the change in canopy fractional cover was observed when the percantage change in fractional canopy cover was considered (Figure 6.5 and Figure 6.6). The percentage canopy cover increase correlated better with yield for the 'Wichita' trees than the 'Western Schley'. This is explained by the alternate bearing cycle of the 'Wichita' trees. The trees were able to build up a large carbohydrate reserve during the 2020/21 season, and even though yield increased dramatically (**Error! Reference source not found.**) during the 2021/22 season, there was likely a large carbohydrate reserve for all the trees during the second season. In trees that set fewer fruit, or aborted more fruit, for reasons not due to a lack of available photosynthates, the available photosynthates were partitioned to vegetative growth, as observed by Smith and Samach (2013). This helps explain the inverse correlation between the change in canopy size and yield and why maximum canopy size in March did not correlate well with yield in 'Wichita'. High yielding trees grew less, so had a smaller canopy size after the summer flush, while lower yielding trees had a greater maximum canopy size. The 'Western Schley' trees, on the other hand, showed only a small difference in yield between "on" and "off" years. This translates to a more balanced carbohydrate reserve cycle, and less excess energy to partition to vegetative growth, resulting in a less distinct relationship between vegetative growth over the season and yield. Even though there is a relationship between yield and canopy size change in 'Wichita', the relationship is not strong enough to use as an estimator of yield. Absolute maximum canopy size for the season remains a better predictor of yield for 'Western Schley'. More seasons of yield and canopy size data will be needed for the 'Wichita', to allow the carbohydrate reserves and the relationships between the competing sinks to be normalised, and to moderate the alternate bearing cycle, before a good relationship between canopy size and yield can be found. In both cultivars, including more canopy size parameters, such as height and volume, in the form of, possibly, a multiple regression, will most likely increase the strength of the relationship between canopy size and yield, and allow accurate yield estimation.

6.3.2 Yield Estimation by Vegetation Indices

No correlation was found between most VIs tested and yield, however, several VIs did correlate with yield to some extent (Table 6**.2** and Table 6**.3**). The most promising VIs were MCARI, OSAVI and RDVI. The relationship between these VIs and yield only started to form in the second half of the season, becoming strongest in March (Table 6**.3**). No early season data was available for the 2020/21 season, so this observation is based on the data from the 2021/22 season. Nevertheless, correlation between the three VIs and yield was also observed in March 2021. There was also a cultivar effect, particularly in the 2021/22 season, where each

of the VIs that were found to correlate with yield at some point during the season performed well with only one of the cultivars and was completely insensitive to yield in the other. In the 2020/21 season, the timing of the best correlation differed between cultivars, with some VIs performing better in earlier in March, and others performing better closer to senescence in April (Table 6.**2**).

Table 6.2 Correlation coefficients (R^2) between the yield of individual trees (kg) during the 2020/2021 season and the vegetation index value of their canopies on four dates during the season for all the vegetation indices tested. The two cultivars, 'Wichita' and 'Western Schley' are shown separately.

Vegetation Index	Cultivar	04-Mar-21	10-Mar-21	19-Mar-21	14-Apr-21
GNDVI	W. Schley	0.118	0.083	0.039	0.075
	Wichita	0.011	0.001	0.071	0.030
MCARI	W. Schley	0.496	0.501	0.443	0.285
	Wichita	0.444	0.388	0.155	0.131
MCARI 1	W. Schley	0.242	0.046	0.108	0.230
	Wichita	0.074	0.067	0.075	0.145
NDVI	W. Schley	0.127	0.035	0.070	0.249
	Wichita	0.078	0.020	0.062	0.107
ReSR	W. Schley	0.329	0.144	0.054	0.355
	Wichita	0.003	0.007	0.049	0.075
RNDVI	W. Schley	0.000	0.497	0.512	0.000
	Wichita	0.000	0.099	0.075	0.000
SR	W. Schley	0.197	0.042	0.054	0.236
	Wichita	0.078	0.023	0.049	0.105
RDVI	W. Schley	0.444	0.492	0.364	0.254
	Wichita	0.471	0.399	0.152	0.114
OSAVI	W. Schley	0.432	0.489	0.362	0.272
	Wichita	0.447	0.355	0.122	0.084
TCARI	W. Schley	0.260	0.067	0.142	0.272
	Wichita	0.039	0.046	0.064	0.133

Table 6.3 Correlation coefficients (R^2) between the yield of individual trees (kg) during the 2021/2022 season and the vegetation index value of their canopies on 10 dates throughout the season for all the vegetation indices tested. The two cultivars, 'Wichita' and 'Western Schley' are shown separately.

		29-Oct-21	17-Nov-21	22-Jan-22	09-Feb-22	24-Feb-22	10-Mar-22	14-Mar-22	24-Mar-22	06-Apr-22	13-Apr-22	21-Apr-22
GNDVI	**W.Schley**	0.060	0.001	0.042	0.010	0.002	0.009	0.006	0.005	0.044	0.025	0.108
	Wichita	0.022	0.054	0.369	0.108	0.039	0.004	0.033	0.076	0.009	0.017	0.012
MCARI	**W.Schley**	0.036	0.000	0.028	0.071	0.112	0.000	0.240	0.111	0.110	0.107	0.088
	Wichita	0.102	0.173	0.080	0.007	0.323	0.009	0.400	0.302	0.367	0.111	0.300
MCARI 1	**W.Schley**	0.000	0.111	0.001	0.033	0.002	0.121	0.000	0.023	0.007	0.012	0.000
	Wichita	0.000	0.131	0.052	0.007	0.005	0.111	0.000	0.007	0.170	0.069	0.083
NDVI	**W.Schley**	0.012	0.002	0.017	0.013	0.000	0.021	0.031	0.011	0.005	0.003	0.008
	Wichita	0.046	0.055	0.021	0.006	0.020	0.027	0.002	0.004	0.169	0.073	0.017
ReSR	**W.Schley**	0.052	0.000	0.003	0.023	0.004	0.028	0.064	0.034	0.018	0.004	0.069
	Wichita	0.106	0.164	0.021	0.045	0.096	0.000	0.033	0.012	0.054	0.001	0.002
RNDVI	**W.Schley**	0.147	0.060	0.067	0.113	0.157	0.197	0.231	0.160	0.134	0.060	0.067
	Wichita	0.178	0.286	0.142	0.152	0.238	0.144	0.107	0.060	0.006	0.056	0.007
SR	**W.Schley**	0.018	0.003	0.027	0.000	0.004	0.005	0.020	0.008	0.000	0.000	0.001
	Wichita	0.037	0.065	0.006	0.004	0.026	0.025	0.007	0.000	0.124	0.039	0.003
RDVI	**W.Schley**	0.010	0.082	0.017	0.054	0.124	0.127	0.212	0.102	0.092	0.084	0.058
	Wichita	0.062	0.090	0.027	0.331	0.281	0.134	0.365	0.231	0.337	0.115	0.258
OSAVI	**W.Schley**	0.005	0.097	0.013	0.070	0.120	0.140	0.233	0.109	0.089	0.086	0.058
	Wichita	0.044	0.115	0.017	0.344	0.275	0.133	0.349	0.238	0.283	0.111	0.258
TCARI	**W.Schley**	0.000	0.000	0.003	0.036	0.004	0.001	0.050	0.026	0.011	0.006	0.001
	Wichita	0.000	0.187	0.110	0.018	0.016	0.004	0.001	0.001	0.135	0.058	0.052

The observation that only a very small number of VIs correlate with yield out of a large number tested is in line with what has been found by similar studies in other horticultural crops. In mango, RDVI and variations of NDVI correlated best with yield (Rahman et al., 2018), while in avocado, RNDVI and GNDVI performed the best (Robson et al., 2017a). In both these cases, different VIs performed the best in different years, and on different orchard blocks. In pecans, it appears that the VIs that correlated with yield were MCARI, RDVI and OSAVI. In the 2020/21 season, all three VIs correlated better with yield of the 'Western Schley' trees than the 'Wichita' trees between the middle of March and mid April, while the VIs did not correlate well with the 'Wichita' yield in March. In early March, during this season, the three VIs correlated better with the 'Wichita' yield than the 'Western Schley' yield. In the 2021/22 season, all three VIs correlated better with the yield of 'Wichita' trees, while a much weaker relationship was found with the yield of 'Western Schley' trees in February, March and April. This may be related to the density and health of the canopy, or the increase in canopy size during the summer flush.

The VIs from which MCARI and OSAVI are derived, the CARI and SAVI respectively, have been shown to be very sensitive to canopy chlorophyll density, which is a measure of both the density and greenness of a canopy (Broge and Leblanc, 2001). It is possible that MCARI, OSAVI and RDVI correlated with yield because yield may have had a slight correlation with canopy density and vegetative growth, as was shown by attempts to predict yield using fractional canopy cover and change in fractional canopy cover. The three VIs, MCARI, OSAVI and RDVI all correlated negatively with yield, that is, the greater the yield, the lower the VI value. Since they are known to be indicators of canopy density (Broge and Leblanc, 2001), it is possibble that they are able to predict yield by providing a measure of canopy density, with more dense canopies having a lower yield. This is supported by the observation that in the 2021/22 season, where 'Wichita' showed a greater percentage increase in canopy size due to more vegetative ggrowth (45%) than 'Western Schley'(34%), 'Wichita' also likely had a greater canopy density. Since the change in canopy size was shown in Figure 6.6 to correlate with yield, canopy density could also possibly correlate with yield. So, higher yielding 'Wichita' trees grew less, and were, therefore, less dense. VIs which are sensitive to canopy density, therefore, likely also correlated with yield. As there was a much lower correlation between yield and the change in canopy size for 'Western Schley' trees than 'Wichita' trees, there was also likely no correlation between canopy density and yield in 'Western Schley' trees. However, as no actual canopy density data was collected, this hypothesis could not be tested. The explanation for the correlation between the three VIs and yield may also be as simple as a sensitivity to the ratio of lighter green nuts to the darker green canopy. The reason for the decline in the sensitivity of VIs to the yield of the 'Witchita' trees earlier in the season than

'Western Schley' during the 2020/21 season is far simpler. Due to severe nutrient deficiencies, many of the 'Witchita' trees started to senesce early, changing the reflectance properties of the entire canopies.

It is important to note that the VI values used for yield prediction are the same as those used in Chapter 4, and are therefore subject to the same sources of inaccuracy mentioned in that chapter. These relate to the quality and angle of incident radiation, and differences in atmospheric conditions during data collection flights, as discussed by Jackson and Huete (1991). An indication of this is found when considering correlations between VIs and yield for the month of March 2022 (Table 6.3). The three VIs mentioned correlated relatively well with 'Wichita' yield for the majority of the month, except on 10 March, where the R^2 value was close to zero (Table 6.3). On this day, most of the orchard was subject to intense sunlight, but isolated clouds cast irregular shadows over small parts of the orchard. It cannot be expected that data from shaded and sunlit areas can be used together to generate a regression with any accuracy. All other cloudy days were left out of the final dataset, but 10 March 2022 was considered a mild case, and included, which proved to be an unsound decision. If high quality multispectral data can be collected, VIs may be able to be better used to estimate yield. The yield prediction power of VIs may also be improved by fitting an exponential curve to the data rather than a simple linear equation. This has been found to be the case with avocado (Robson et al., 2017a) and mango (Rahman et al., 2018). There are indications that this could be true for pecans and the three VIs that showed a good correlation with yield. Figure 6.7 is a good illustration of such a relationship, with this date and VI chosen because both cultivars showed a good correlation between RDVI and yield.

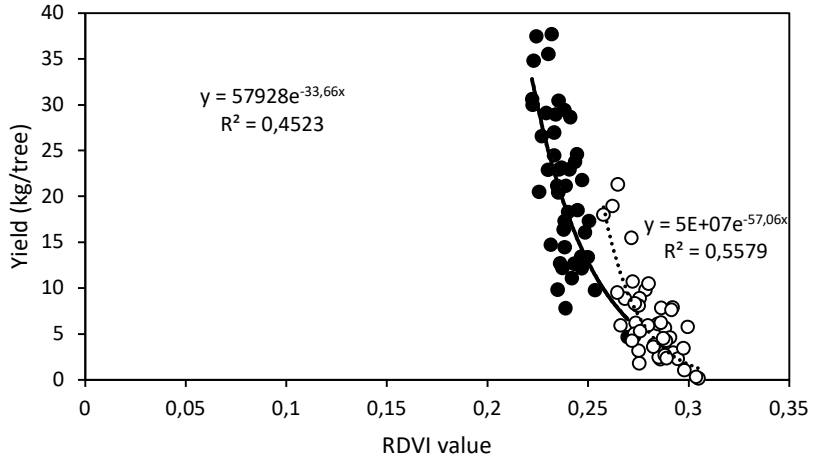

Figure 6.7 The relationship between the individual tree yield (kg) and the RDVI value of the corresponding canopy of the two pecan cultivars on 4 March 2021, showing an exponential relationship between the variables. 'Western Schley' is represented as solid dots, and 'Wichita' as open circles.

If an exponential relationship is found to be the rule between pecan yield and VI value, a method other than simple linear regression should in future be used to find the best VI to use for yield estimation. A step-wise regression has been successfully used in mango (Rahman et al., 2018). Better use of statistical regression techniques would have identified the regression patterns present in the data that were not apparent to the eye, or through the use of a simple R^2. Significance tests based on the F-test would have proven useful in identifying whether the relationships observed were as strong as they seemed. It is possible that more value can be extracted from the yield, VI and fractional canopy cover datasets by a more in-depth analysis to categorise the significance of the relationships found and find relationships that are not apparent with a linear regression. The best use of remote sensing data to estimate yield has been shown to be the use of either a model or artificial intelligence which can combine both canopy characteristics and vegetation indices (Anderson et al., 2021; Rahman et al., 2018; Robson et al., 2017a). For both of these, however, a very large sample size and several seasons of data are needed to train the AI to capture all possible variabilty in the data.

6.4 Conclusion

As expected, alternate bearing did play a major role in the success of yield estimation using canopy size, represented by fractional canopy cover. In “on” years, canopy size had a much better relationship to yield than in “off” years. This is understandable, as in the low-yielding years, only a few of the bearing sites on the tree carry nuts, causing a mismatch between the yield possible and the canopy size. In high-yielding years, most of the bearing sites carry nuts, so yield is largely determined by the number of bearing sites, and therefore, the size of the canopy. Photosynthate partitioning could also be used to advantage in determining yield during low-yielding years. When fewer nuts were set, more photosynthates were partitioned to vegetative growth as the season progressed. This could be related to yield in the form of the change in canopy size. However, this method was complicated by both cultivar, and the effect of stored carbohydrates from previous seasons, and did not therefore perform as well as the canopy size during an “on” year. The two cultivars tested seemed to have different relationships between yield and vegetative growth. If this method is taken forward, different cultivars will have to be treated individually. Trees that had consecutive low-yielding seasons, and therefore, the chance to build up carbohydrate reserves, showed high vegetative growth when they did have an “on” year. This suggests that yield can be more easily predicted using change in canopy cover in more stable, or better managed orchards, where consecutive low yields are prevented where possible.

Certain vegetation indices did relate to yield. These were mostly VIs which, from literature, are said to relate to canopy structure or density. It is likely that these VIs were sensitive to the density of vegetative growth, being indirectly related to yield. This is supported by the observation that most of the effective VIs had the best relationship with yield after the summer vegetative flush. In this respect, they work similarly to the method that relates yield to the change in canopy cover, with canopies having more vegetative growth during the season being denser, which the VIs are sensitive to. To conclusively prove this, data from more seasons will be needed, as well as ground canopy density measurements. This will also allow the exact nature of the relationship between certain VIs and yield to be determined.

7 GENERAL CONCLUSION

Unmanned aerial vehicles (UAVs) and high resolution multispectral and thermal cameras are emerging technologies that have made remote sensing accessible to a wider user base in the agricultural sector (van der Merwe et al., 2020). It has also allowed remote sensing to be used at a much smaller scale and higher temporal frequency than was previously possible when the only available remote sensing platforms were satellites, balloons or fixed-wing aircraft (Gago et al., 2015). This has allowed operators, or even producers, to collect high resolution data from individual canopies, or even parts of a canopy, almost at will. The ability and methods to turn the raw data into information that can be used to base decisions upon does seem to have lagged behind the development of the technology for many crops. While the processing methodology, and the relationships between remote sensing parameters has been developed for the more popular horticultural crops, such as grapevine (Baluja et al., 2012; Zarco-Tejada et al., 2013), olive (Berni et al., 2009a), and pome fruit (Kim et al., 2011), amongst others (Gonzalez-Dugo et al., 2013), less work has been done on applying, and calibrating, this knowledge to crops that are not as widely grown, but still have great economic importance. In South Africa, one such crop is pecans, the subject of this study.

Pecans are known to have a particularly high water requirement, when compared to most field crops, and many horticultural crops (Miyamoto, 1983). In South Africa, this may have the potential to limit their commercial production in the future, as water is increasingly being allocated away from agriculture towards industrial and domestic use, and the fact that a large proportion of total pecan plantings are not yet mature, and are using less water that they potentially will (FAO, 2016; Hedden and Cilliers, 2014). It is, thus, imperative to increase the water use efficiency of pecans in South Africa and scheduling decisions play a major role in achieving this (Ibraimo et al., 2016). Remote sensing tools have the potential to increase the ease and accuracy of irrigation scheduling, by better detection of stress, and the potential to identify situations where a variable irrigation rate over an orchard might be beneficial (Gago et al., 2015). Older remote sensing methods, using satellite and fixed wing aircraft mounted sensors have been shown to be highly successful at detecting water stress, and informing irrigation scheduling decisions (Garrot et al., 1993; Sammis et al., 1988). However, the stress detection methods have not been extensively tested using modern tools, such as UAVs and high-resolution sensors.

A remote water stress detection method in pecans that has found good success uses thermal indices to detect water stress (Garrot et al., 1993). The most widely used of these indices is the crop water stress index (CWSI). It requires the difference between canopy temperature and air temperature at the time of calculation (T_c-T_a), as well as reference T_c-T_a values that

represent both the maximum possible transpiration of the canopy under the present conditions, and the T_c-T_a of a non-transpiring canopy (Idso et al., 1981). These are known as the upper and lower limits of the CWSI. Methods tested to obtain the lower limit are the non-water-stress-baseline (NWSB), which is a plot of T_c-T_a of a non-stressed canopy as a function of VPD, included the use of a wet reference surface within the flight image of each day, and the temperature of the coolest pixels of the thermal image. A static upper limit of 6˚C was tested, as well as the use of the temperature of the warmest pixels of the thermal image on the day. Attempts to stress a pecan tree to the point of complete stomatal closure were unsuccessful due to the exceptionally high rainfall during the period of the study. All methods performed similarly, where correlation was found between the CWSI and field measured water stress, which was midday stem water potential (ψ_{midday}). However, the relationship did not provide the confidence needed to use the CWSI for irrigation scheduling decisions based on the detection of stress. This most likely was a result of inaccuracy in the thermal camera used, which consistently overestimated canopy temperature by approximately 3-4˚C, and inconsistencies in the time of day and weather conditions at the time of thermal data collection. Evidence of this is the fact that a better correlation was found between canopies on one day, than when data from different flights were pooled and tested. The T_c-T_a values calculated using the thermal images were also found to be far higher than what could be reasonably expected. A better test of the CWSI on pecans from remote sensing data will require a more accurate, and better calibrated thermal camera. The CWSI has been shown to be both a convenient and accurate method of water stress detection, in both pecans (Garrot et al., 1993), and a variety of common horticultural crops (Baluja et al., 2012; Testi et al., 2008; Zarco-Tejada et al., 2012), and this study has shown that this is potentially true in pecan as well. However, the accuracy of the equipment and consistency of data collection have been shown to be key limiting factors in this study, which prevented a proper analysis of the utility of the CWSI for detecting stress in pecans.

The use of vegetation indices (VIs) to detect water stress was also tested. These attempts were met with little success, which was not unexpected. Most of the VIs tested were found to have little potential to detect water stress in similar studies (Zarco-Tejada et al., 2013). However, there was some doubt over whether the failure of the VIs was due to the innate character of the VIs, or the quality of the multispectral data collected. A major weakness of this study is the inconsistency in both the time of day at which data collection flights were conducted, and the cloud cover at the time. The angle of incident light on the canopy depends on the time of day, and the amount of longwave radiation intercepted by the canopy is heavily affected by the cloud cover (Ishihara et al., 2015). Both of these are known to affect the reflectance of the canopy, and the therefore, the source data from which VIs are calculated.

The structure of the canopy and the groundcover in the orchard also affect the overall reflectance of the canopy, through transmittance and diffusion of light (Jackson and Huete, 1991). Pecan canopies in general, and in the measurement orchard in particular, have highly variable canopy structures. The groundcover in the orchard also varied throughout the orchard and changed as the season progressed. Despite all the shortcomings in this study, water stress detection by VI appears to have less potential than the use of thermal indices.

The two methods of remote sensing used for yield estimation were, on the whole, more successful than water stress detection. Using canopy size to predict yield was found to be highly effective when trees yielded close to their potential for their size. However, potential yield is not often achieved due to both environmental factors and the energy reserve status of the trees. Cultivar also seems to impact the potential yield for canopy size, based on the observation that the 'Western Schley' trees in the study had a greater yield to canopy size ratio than 'Wichita' during both "off" and "on" years. Suggested solutions, that have not been tested, include adjusting the estimate of the yield per canopy size up or down based on a physical inspection of the crop load, or the expectation of a low yielding year (Sarron et al., 2018). Including more canopy size parameters in the prediction model will also likely increase the accuracy of the prediction, as canopy size consists of more than just the fractional canopy cover used in this study. Canopy size estimates from late in the season before the onset of senescence were found to correlate best with yield, as maximum canopy size for the season was captured at this time. The change in canopy size during the season was also related to yield, with lower yielding trees putting out more vegetative growth during the season, as a result of more photosynthate being partitioned to nuts than vegetative growth in high yielding trees. However, this parameter also depends on the carbohydrate reserves of the tree, with trees having high carbohydrate reserves, due to a previous low yielding season, showing a lot of vegetative growth irrespective of crop load, so the use of this metric is not as reliable as absolute canopy size.

Three VIs were found to correlate relatively well with yield, having an exponential relationship. However, the performance varied greatly between seasons and cultivars. This could complicate their future use for yield estimation, because the relationship between the VI and yield may not be fully understood for the season or cultivar in question, prior to harvest, when an estimate is required. The differences observed could be as a result of differences in the vegetative growth pattern and density of the canopy, which has been shown in this study to vary between cultivars and season. If a VI estimates yield by sensitivity to these factors, it cannot be easily used to estimate yield without some sort of calibration for cultivar and seasonal effects (Broge and Leblanc, 2001). Integrating canopy size and VIs, through the use of machine learning, or a mathematical model, will likely provide a tool to accurately predict

yield in pecans, as has been found with avocado (Robson et al., 2017a), mango (Rahman et al., 2018), and apple (Chen et al., 2022).

Remote sensing allows the collection of large amounts of data in a horticultural setting. Properly understood and processed, this will give finer control and a more thorough understanding of the condition of crop properties, such as water status and crop load. To achieve this, a better understanding of the required sensor specifications for application in pecans, in particular, is needed. A better understanding of the relationship between specific cultivars and seasonal phenomena, and stress and yield is also needed.

8 REFERENCES

Abioye, E.A. et al., 2020. A review on monitoring and advanced control strategies for precision irrigation. Computers and Electronics in Agriculture, 173: 105441.

Alderfasi, A.A. and Nielsen, D.C., 2001. Use of crop water stress index for monitoring water status and scheduling irrigation in wheat. Agricultural water management, 47(1): 69-75.

Allen, R.G., Pereira, L.S., Raes, D. and Smith, M., 1998. Crop evapotranspiration-Guidelines for computing crop water requirements-FAO Irrigation and drainage paper 56. Fao, Rome, 300(9): D05109.

Amigo, J.M. and Santos, C., 2020. Preprocessing of hyperspectral and multispectral images, Data Handling in Science and Technology. Elsevier, pp. 37-53.

Andersen, P. and Brodbeck, B., 1988. Net CO2 assimilation and plant water relations characteristics of pecan growth flushes. Journal of the American Society for Horticultural Science, 113(3): 444-450.

Anderson, N.T., Walsh, K.B. and Wulfsohn, D., 2021. Technologies for forecasting tree fruit load and harvest timing—from ground, sky and time. Agronomy, 11(7): 1409.

Annandale, J.G., Stirzaker, R.J., Singels, A., Van der Laan, M. and Laker, M.C., 2011. Irrigation scheduling research: South African experiences and future prospects. Water SA, 37(5): 751-764.

Atzberger, C., 2013. Advances in remote sensing of agriculture: Context description, existing operational monitoring systems and major information needs. Remote sensing, 5(2): 949-981.

Backeberg, G.R., 2005. Water institutional reforms in South Africa. Water policy, 7(1): 107-123.

Ballesteros, R. et al., 2020. Vineyard yield estimation by combining remote sensing, computer vision and artificial neural network techniques. Precision Agriculture, 21(6): 1242-1262.

Baluja, J. et al., 2012. Assessment of vineyard water status variability by thermal and multispectral imagery using an unmanned aerial vehicle (UAV). Irrigation Science, 30(6): 511-522.

Bausch, W.C. and Duke, H., 1996. Remote sensing of plant nitrogen status in corn. Transactions of the ASAE, 39(5): 1869-1875.

Bellvert, J. et al., 2016. Airborne thermal imagery to detect the seasonal evolution of crop water status in peach, nectarine and Saturn peach orchards. Remote Sensing, 8(1): 39.

Berni, J., Zarco-Tejada, P., Sepulcre-Cantó, G., Fereres, E. and Villalobos, F., 2009a. Mapping canopy conductance and CWSI in olive orchards using high resolution thermal remote sensing imagery. Remote Sensing of Environment, 113(11): 2380-2388.

Berni, J.A., Zarco-Tejada, P.J., Suárez, L. and Fereres, E., 2009b. Thermal and narrowband multispectral remote sensing for vegetation monitoring from an unmanned aerial vehicle. IEEE Transactions on geoscience and Remote Sensing, 47(3): 722-738.

Bian, J. et al., 2019. Simplified evaluation of cotton water stress using high resolution unmanned aerial vehicle thermal imagery. Remote Sensing, 11(3): 267.

Broge, N.H. and Leblanc, E., 2001. Comparing prediction power and stability of broadband and hyperspectral vegetation indices for estimation of green leaf area index and canopy chlorophyll density. Remote sensing of environment, 76(2): 156-172.

Carter, G.A., 1993. Responses of leaf spectral reflectance to plant stress. American Journal of Botany, 80(3): 239-243.

Chen, R. et al., 2022. Predicting individual apple tree yield using UAV multi-source remote sensing data and ensemble learning. Computers and Electronics in Agriculture, 201: 107275.

Cohen, Y., Alchanatis, V., Meron, M., Saranga, Y. and Tsipris, J., 2005. Estimation of leaf water potential by thermal imagery and spatial analysis. Journal of experimental botany, 56(417): 1843-1852.
Courault, D., Seguin, B. and Olioso, A., 2003. Review to estimate evapotranspiration from remote sensing data: some examples from the simplified relationship to the use of mesoscale atmospheric models, ICID workshop on remote sensing of ET for large regions, pp. 1-18.
Dobermann, A. and Ping, J., 2004. Geostatistical integration of yield monitor data and remote sensing improves yield maps. Agronomy journal, 96(1): 285-297.
Du, M. and Noguchi, N., 2017. Monitoring of wheat growth status and mapping of wheat yield's within-field spatial variations using color images acquired from UAV-camera system. Remote sensing, 9(3): 289.
Egea, G., Padilla-Díaz, C.M., Martinez-Guanter, J., Fernández, J.E. and Pérez-Ruiz, M., 2017. Assessing a crop water stress index derived from aerial thermal imaging and infrared thermometry in super-high density olive orchards. Agricultural Water Management, 187: 210-221.
Emmel, C. et al., 2020. Canopy photosynthesis of six major arable crops is enhanced under diffuse light due to canopy architecture. Global change biology, 26(9): 5164-5177.
FAO, 2016. AQUASTAT Country Profile-South Africa, Food and Agriculture Organisation of the United Nations, Rome, Italy.
Ferencz, C. et al., 2004. Crop yield estimation by satellite remote sensing. International Journal of Remote Sensing, 25(20): 4113-4149.
Gago, J. et al., 2015. UAVs challenge to assess water stress for sustainable agriculture. Agricultural water management, 153: 9-19.
Garrot, D.J., Kilby, M.W., Fangmeier, D.D., Husman, S.H. and Ralowicz, A.E., 1993. Production, growth, and nut quality in pecans under water stress based on the crop water stress index. Journal of the American Society for Horticultural Science, 118(6): 694-698.
Gates, D.M., 1968. Transpiration and leaf temperature. Annual Review of Plant Physiology, 19(1): 211-238.
Gonzalez-Dugo, V. et al., 2013. Using high resolution UAV thermal imagery to assess the variability in the water status of five fruit tree species within a commercial orchard. Precision Agriculture, 14(6): 660-678.
Hedden, S. and Cilliers, J., 2014. Parched prospects-the emerging water crisis in South Africa. Institute for Security Studies Papers, 2014(11): 16.
Howell, T., Musick, J. and Tolk, J., 1986. Canopy temperature of irrigated winter wheat. Transactions of the ASAE, 29(6): 1692-1698.
Hsiao, T.C., 1973. Plant responses to water stress. Annual review of plant physiology, 24(1): 519-570.
Ibraimo, N.A., Taylor, N.J., Steyn, J.M., Gush, M.B. and Annandale, J.G., 2016. Estimating water use of mature pecan orchards: A six stage crop growth curve approach. Agricultural Water Management, 177: 359-368.
Idso, S., Jackson, R., Pinter Jr, P., Reginato, R. and Hatfield, J., 1981. Normalizing the stress-degree-day parameter for environmental variability. Agricultural meteorology, 24: 45-55.
Idso, S.B., 1982. Non-water-stressed baselines: a key to measuring and interpreting plant water stress. Agricultural Meteorology, 27(1-2): 59-70.
Irmak, S., Haman, D.Z. and Bastug, R., 2000. Determination of crop water stress index for irrigation timing and yield estimation of corn. Agronomy Journal, 92(6): 1221-1227.
Ishihara, M., Inoue, Y., Ono, K., Shimizu, M. and Matsuura, S., 2015. The impact of sunlight conditions on the consistency of vegetation indices in croplands—Effective usage of vegetation indices from continuous ground-based spectral measurements. Remote Sensing, 7(10): 14079-14098.
Jackson, R. and Ezra, C., 1985. Spectral response of cotton to suddenly induced water stress. International Journal of Remote Sensing, 6(1): 177-185.

Jackson, R., Slater, P. and Pinter Jr, P., 1983. Discrimination of growth and water stress in wheat by various vegetation indices through clear and turbid atmospheres. Remote sensing of environment, 13(3): 187-208.
Jackson, R.D. and Huete, A.R., 1991. Interpreting vegetation indices. Preventive veterinary medicine, 11(3-4): 185-200.
Jackson, R.D., Idso, S., Reginato, R. and Pinter Jr, P., 1981. Canopy temperature as a crop water stress indicator. Water resources research, 17(4): 1133-1138.
Jackson, R.D., Reginato, R. and Idso, S., 1977. Wheat canopy temperature: a practical tool for evaluating water requirements. Water resources research, 13(3): 651-656.
Jones, H.G., 1999. Use of infrared thermometry for estimation of stomatal conductance as a possible aid to irrigation scheduling. Agricultural and forest meteorology, 95(3): 139-149.
Jones, H.G. et al., 2002. Use of infrared thermography for monitoring stomatal closure in the field: application to grapevine. Journal of experimental botany, 53(378): 2249-2260.
Kim, Y., Glenn, D.M., Park, J., Ngugi, H.K. and Lehman, B.L., 2011. Hyperspectral image analysis for water stress detection of apple trees. Computers and Electronics in Agriculture, 77(2): 155-160.
Kingra, P., Majumder, D. and Singh, S.P., 2016. Application of remote sensing and GIS in agriculture and natural resource management under changing climatic conditions. Agric Res J, 53(3): 295-302.
Knipling, E.B., 1970. Physical and physiological basis for the reflectance of visible and near-infrared radiation from vegetation. Remote sensing of environment, 1(3): 155-159.
Lelong, C.C. et al., 2008. Assessment of unmanned aerial vehicles imagery for quantitative monitoring of wheat crop in small plots. Sensors, 8(5): 3557-3585.
Lin, C., Popescu, S., Huang, S., Chang, P. and Wen, H., 2015. A novel reflectance-based model for evaluating chlorophyll concentrations of fresh and water-stressed leaves. Biogeosciences, 12(1): 49-66.
Lu, C. and Zhang, J., 1999. Effects of water stress on photosystem II photochemistry and its thermostability in wheat plants. Journal of Experimental Botany, 50(336): 1199-1206.
Macdonald, R.B., 1984. A summary of the history of the development of automated remote sensing for agricultural applications. IEEE Transactions on Geoscience and Remote Sensing(6): 473-482.
Maes, W., Achten, W., Reubens, B. and Muys, B., 2011. Monitoring stomatal conductance of Jatropha curcas seedlings under different levels of water shortage with infrared thermography. Agricultural and Forest Meteorology, 151(5): 554-564.
Maes, W. and Steppe, K., 2012. Estimating evapotranspiration and drought stress with ground-based thermal remote sensing in agriculture: a review. Journal of Experimental Botany, 63(13): 4671-4712.
Maes, W.H. et al., 2016. A new wet reference target method for continuous infrared thermography of vegetations. Agricultural and Forest Meteorology, 226: 119-131.
Maes, W.H. and Steppe, K., 2019. Perspectives for remote sensing with unmanned aerial vehicles in precision agriculture. Trends in plant science, 24(2): 152-164.
Maselli, F., Chiesi, M., Brilli, L. and Moriondo, M., 2012. Simulation of olive fruit yield in Tuscany through the integration of remote sensing and ground data. Ecological Modelling, 244: 1-12.
McCree, K.J., 1971. The action spectrum, absorptance and quantum yield of photosynthesis in crop plants. Agricultural Meteorology, 9: 191-216.
Meron, M., Tsipris, J., Orlov, V., Alchanatis, V. and Cohen, Y., 2010. Crop water stress mapping for site-specific irrigation by thermal imagery and artificial reference surfaces. Precision agriculture, 11(2): 148-162.
Meyer, G.E. and Neto, J.C., 2008. Verification of color vegetation indices for automated crop imaging applications. Computers and electronics in agriculture, 63(2): 282-293.
Miyamoto, S., 1983. Consumptive water use of irrigated pecans. Journal of the American Society for Horticultural Science, 108(5): 676-681.

Muir, C.D., 2019. tealeaves: an R package for modelling leaf temperature using energy budgets. AoB Plants, 11(6): plz054.
Myneni, R.B., Hall, F.G., Sellers, P.J. and Marshak, A.L., 1995. The interpretation of spectral vegetation indexes. IEEE Transactions on Geoscience and Remote Sensing, 33(2): 481-486.
Nielsen, D., 1990. Scheduling irrigations for soybeans with the crop water stress index (CWSI). Field Crops Research, 23(2): 103-116.
O'Connell, M. et al., 2010. Satellite remote sensing of crop water use in perennial horticultural crops, Program and abstracts Australian irrigation conference held in Sydney in, pp. 129-130.
Osborne, P.E., Alonso, J. and Bryant, R., 2001. Modelling landscape-scale habitat use using GIS and remote sensing: a case study with great bustards. Journal of applied ecology, 38(2): 458-471.
Othman, Y., VanLeeuwen, D., Heerema, R. and Hilaire, R.S., 2014. Midday stem water potential values needed to maintain photosynthesis and leaf gas exchange established for pecan. Journal of the American Society for Horticultural Science, 139(5): 537-546.
Pinter Jr, P.J. et al., 2003. Remote sensing for crop management. Photogrammetric Engineering & Remote Sensing, 69(6): 647-664.
Pirzad, A. et al., 2011. Effect of water stress on leaf relative water content, chlorophyll, proline and soluble carbohydrates in Matricaria chamomilla L. Journal of Medicinal Plants Research, 5(12): 2483-2488.
Prasad, A.K., Chai, L., Singh, R.P. and Kafatos, M., 2006. Crop yield estimation model for Iowa using remote sensing and surface parameters. International Journal of Applied earth observation and geoinformation, 8(1): 26-33.
Prince, S., 1991. Satellite remote sensing of primary production: comparison of results for Sahelian grasslands 1981-1988. International Journal of remote sensing, 12(6): 1301-1311.
Puri, V., Nayyar, A. and Raja, L., 2017. Agriculture drones: A modern breakthrough in precision agriculture. Journal of Statistics and Management Systems, 20(4): 507-518.
Rahman, M.M., Robson, A. and Bristow, M., 2018. Exploring the potential of high resolution worldview-3 Imagery for estimating yield of mango. Remote Sensing, 10(12): 1866.
Rasmussen, J. et al., 2016. Are vegetation indices derived from consumer-grade cameras mounted on UAVs sufficiently reliable for assessing experimental plots? European Journal of Agronomy, 74: 75-92.
Richardson, A.J. and Wiegand, C., 1977. Distinguishing vegetation from soil background information. Photogrammetric engineering and remote sensing, 43(12): 1541-1552.
Robson, A., Rahman, M.M. and Muir, J., 2017a. Using worldview satellite imagery to map yield in avocado (Persea americana): A case study in Bundaberg, Australia. Remote Sensing, 9(12): 1223.
Robson, A. et al., 2017b. Evaluating satellite remote sensing as a method for measuring yield variability in Avocado and Macadamia tree crops. Advances in Animal Biosciences, 8(2): 498-504.
Sadler, E., Evans, R., Stone, K. and Camp, C., 2005. Opportunities for conservation with precision irrigation. Journal of soil and water conservation, 60(6): 371-378.
Sammis, T., Mexal, J. and Miller, D., 2004. Evapotranspiration of flood-irrigated pecans. Agricultural water management, 69(3): 179-190.
Sammis, T., Riley, W. and Lugg, D., 1988. Crop water stress index of pecans. Applied Engineering in Agriculture, 4(1): 39-45.
Sarron, J., Malézieux, É., Sané, C.A.B. and Faye, É., 2018. Mango yield mapping at the orchard scale based on tree structure and land cover assessed by UAV. Remote Sensing, 10(12): 1900.
Sepulcre-Cantó, G. et al., 2007. Monitoring yield and fruit quality parameters in open-canopy tree crops under water stress. Implications for ASTER. Remote Sensing of Environment, 107(3): 455-470.

Shanmugapriya, P., Rathika, S., Ramesh, T. and Janaki, P., 2019. Applications of remote sensing in agriculture-A Review. International Journal of Current Microbiology and Applied Sciences, 8(1): 2270-2283.
Smith, H.M. and Samach, A., 2013. Constraints to obtaining consistent annual yields in perennial tree crops. I: Heavy fruit load dominates over vegetative growth. Plant Science, 207: 158-167.
Sparks, D., 1989. Drought stress induces fruit abortion in pecan. HortScience, 24(1): 78-79.
Sparks, D., 2005. Adaptability of pecan as a species. HortScience, 40(5): 1175-1189.
Suomalainen, J. et al., 2021. Direct reflectance transformation methodology for drone-based hyperspectral imaging. Remote Sensing of Environment, 266: 112691.
Testi, L., Goldhamer, D., Iniesta, F. and Salinas, M., 2008. Crop water stress index is a sensitive water stress indicator in pistachio trees. Irrigation science, 26(5): 395-405.
Trout, T.J., Johnson, L.F. and Gartung, J., 2008. Remote sensing of canopy cover in horticultural crops. HortScience, 43(2): 333-337.
Turner, D., Lucieer, A. and Watson, C., 2012. An automated technique for generating georectified mosaics from ultra-high resolution unmanned aerial vehicle (UAV) imagery, based on structure from motion (SfM) point clouds. Remote sensing, 4(5): 1392-1410.
Usha, K. and Singh, B., 2013. Potential applications of remote sensing in horticulture—A review. Scientia Horticulturae, 153: 71-83.
van der Merwe, D., Burchfield, D.R., Witt, T.D., Price, K.P. and Sharda, A., 2020. Drones in agriculture. Advances in agronomy, 162: 1-30.
Van Niekerk, A., Jarmain, C. and Goudriaan, R., 2018. An Earth Observation Approach Towards Mapping Irrigated Area and Quantifying Water Use by Irrigated Crops in South Africa. Water Research Commission.
Wang, J. et al., 2007. Crop coefficients of open-canopy pecan orchards. Agricultural water management, 88(1-3): 253-262.
Wells, L., 2015. Irrigation water management for pecans in humid climates. HortScience, 50(7): 1070-1074.
Wells, L., 2017. Response of young pecan trees to irrigation in a humid climate. HortScience, 52(3): 457-462.
Wood, B.W., Conner, P.J. and Worley, R.E., 2003. Relationship of alternate bearing intensity in pecan to fruit and canopy characteristics. HortScience, 38(3): 361-366.
Wood, B.W. and Reilly, C.C., 1999. Factors influencing water split of pecan fruit. HortScience, 34(2): 215-217.
Xue, J. and Su, B., 2017. Significant remote sensing vegetation indices: A review of developments and applications. Journal of sensors, 2017.
Yamada, N. and Fujimura, S., 1991. Nondestructive measurement of chlorophyll pigment content in plant leaves from three-color reflectance and transmittance. Applied Optics, 30(27): 3964-3973.
Yang, Q., Shi, L., Han, J., Zha, Y. and Zhu, P., 2019. Deep convolutional neural networks for rice grain yield estimation at the ripening stage using UAV-based remotely sensed images. Field Crops Research, 235: 142-153.
Zaman, Q., Schumann, A. and Hostler, H., 2006. Estimation of citrus fruit yield using ultrasonically-sensed tree size. Applied Engineering in Agriculture, 22(1): 39-44.
Zarco-Tejada, P.J., González-Dugo, V. and Berni, J.A., 2012. Fluorescence, temperature and narrow-band indices acquired from a UAV platform for water stress detection using a micro-hyperspectral imager and a thermal camera. Remote sensing of environment, 117: 322-337.
Zarco-Tejada, P.J. et al., 2013. A PRI-based water stress index combining structural and chlorophyll effects: Assessment using diurnal narrow-band airborne imagery and the CWSI thermal index. Remote sensing of environment, 138: 38-50.
Zhang, C. and Kovacs, J.M., 2012. The application of small unmanned aerial systems for precision agriculture: a review. Precision agriculture, 13(6): 693-712.

Zhao, T., Doll, D., Wang, D. and Chen, Y., 2017a. A new framework for UAV-based remote sensing data processing and its application in almond water stress quantification, 2017 International Conference on Unmanned Aircraft Systems (ICUAS). IEEE, pp. 1794-1799.

Zhao, T., Stark, B., Chen, Y., Ray, A.L. and Doll, D., 2015. A detailed field study of direct correlations between ground truth crop water stress and normalized difference vegetation index (NDVI) from small unmanned aerial system (sUAS), 2015 International Conference on Unmanned Aircraft Systems (ICUAS). IEEE, pp. 520-525.

Zhao, T., Stark, B., Chen, Y., Ray, A.L. and Doll, D., 2017b. Challenges in water stress quantification using small unmanned aerial system (suas): Lessons from a growing season of almond. Journal of Intelligent & Robotic Systems, 88(2-4): 721-735.

Zheng, G. and Moskal, L.M., 2009. Retrieving leaf area index (LAI) using remote sensing: theories, methods and sensors. Sensors, 9(4): 2719-2745.